# GOLD BEARING SKARNS

# FROM THE

# MOINA AREA

# NORTHWEST TASMANIA

**André C. Taylor**

A thesis submitted in partial fulfilment
of the requirements of the degree of
Bachelor of Science with Honours

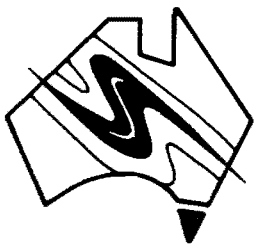

**Centre for Ore Deposits and Exploration Studies**
**Geology Department**
**University of Tasmania**

**1990**

**FRONTISPIECE:** View along the Lea River, spectacular scenery combined with great geology.

# ABSTRACT

Stormont, Fletcher's Adit and Ti Tree Creek are three mineralised, calc-silicate skarns in the Moina district, NW Tasmania. Stormont is a Au and Bi-bearing skarn, Fletcher's Adit contains minor Cu, Au, Bi, W, Sn and Zn, and Ti Tree Creek contains small amounts of Sn and Bi. The three skarns are hosted in the basal section of the Ordovician Gordon Limestone and the upper portion of the underlying Late Cambrian to Early Ordovician Moina Sandstone. Metasomatism and mineralisation occurred during the late Devonian intrusion of the ilmenite series, Dolcoath Granite. The granite-to-prospect distance increases to the west, from Ti Tree Creek to Fletcher's Adit, to the most distal (0.5 - 1 km) Stormont deposit.

The three skarn deposits have a similar paragenesis during the metamorphic, metasomatic and early retrograde stages of skarn development. Wollastonite and salitic clinopyroxene were formed during the metamorphic stage of skarn development. Andradite (and minor Cr-rich grossular) garnet, salitic clinopyroxene and minor vesuvianite were formed during the infiltration metasomatic phase.

Epidote, actinolitic amphibole, quartz and fluorite were the major phases formed during the actinolite replacement stage of retrograde alteration, while chlorite, fluorite, muscovite, calcite and quartz were stable during the later mineralisation stage of retrograde alteration. Differences between the deposits in the late retrograde and mineralisation stages include the intensity of retrograde alteration, the abundance of minor retrograde phases, native gold, native bismuth, bismuthinite, galenobismutite, magnetite and base metal sulphides.

Opaque minerals present in the three skarns are magnetite, pyrrhotite, pyrite, marcasite, arsenopyrite, native bismuth, bismuthinite, galenobismutite, a Bi-Te sulphide, chalcopyrite, native gold, hematite and goethite. Gold is associated with bismuthinite. Generally, Au, Bi, Pb and Sn mineralisation is restricted to the calcareous host rocks, Cu, W, As, Ag and Zn mineralisation occurs in the skarn or the footwall lithologies and Mo mineralisation occurs exclusively in the footwall.

Stormont is a gold skarn, having a high pyroxene/garnet ratio, a deficiency of base metal sulphides, abundant retrograde alteration, late stage reduced mineralising fluids, statistically significant positive Au/Bi, Au/Pb and Bi/Pb metal correlation coefficients, a

statistically insignificant positive Au/Cu metal correlation coefficient, locally high Au and Bi grades, very high Au(ppm)/Cu(%) ratios, and common bismuthinite and native bismuth.

The compositions of major calc-silicate phases support Stormont's status as a gold skarn. Clinopyroxenes from Stormont belong to the diopside-hedenbergite series, ranging from $Di_{50}$ to $Di_{76}$, although they are occasionally anomalously manganiferous (up to $Jo_9$), and are not highly aluminous. Garnets from Stormont are grandites and range from $Ad_{49}$ to $Ad_{60}$.

The observed opaque mineral paragenesis and thermodynamic modelling indicate that gold was deposited (with bismuthinite) as a bisulphide complex late in the paragenesis, as a result of the mineralising fluids dropping in temperature and $fO_2$. A discrete population of high Au and Bi grades is unique to Stormont in the Moina area, indicating that the mineralising fluids that precipitated Au and Bi at Stormont were of a different character to those at Fletcher's Adit.

The gold at Stormont is hypothesized to have originated from underlying Cambrian volcanics which were leached by late stage, circulating meteoric (and magmatic?) fluids. Stormont's increased granite-to-prospect distance, fracture/fault controlled permeability and inter-granular permeability of the skarn (due to massive actinolite replacement), as well as the regionally high permeability of the footwall arenites may have assisted the development of an efficient large-scale convection cell.

# CONTENTS

# LIST OF FIGURES

# LIST OF TABLES

# LIST OF PLATES

# LIST OF APPENDICES

# ACKNOWLEDGEMENTS

I would like to extend my sincere thanks to my supervisor Dr. J.B. Gemmell, Dr. D. L. Huston and Dr. R.F. Berry, for their help with ideas, thin section problems, microprobe work, isotopes, thermodynamic calculations and assistance with phase diagram construction. The cheerful assistance of Mr. Mike Power (with oxygen isotopes), Mr. Simon Stephens and Miss Naomi Deard (with thin section preparation) was especially appreciated.

At Renison Goldfields Exp. Pty. Ltd., the help of Mr. Carlos Castro was invaluable, concerning organisation during the field season and general encouragement. Discussions with Scott Halley also proved to be extremely helpful, especially in regard to skarn petrology.

Thanks must also go to Renison Goldfields Consolidated and the Tasmanian Government for supporting my studies in the form of financial assistance.

The arduous task of proof reading was cheerfully (?) done by Mr. Rogan Brown, Dr. Bruce Gemmell and Dr. Max Banks with my kindest thanks. The mandatory last few days of complete panic were made much easier by the assistance of Rachel and Mr. Rogan Brown.

On a personal note, I express gratitude to my friends and family, especially Mr. Keith Wildman for his photographic assistance and Rachel for putting up with a lot of over-enthusiastic ranting and raving during the year.

# CHAPTER 1
# INTRODUCTION

## 1.1 GENERAL

Moina is situated 25 km NNE of Cradle Mountain in Tasmania's North West. The location of the 1:5000 scale mapping area which lies 2-4 km west of Moina is shown in Figure 1.

Access to the mapping area is via the Cradle Mountain Road initially, then along a poor gravel road to the Iris River Bridge. From there, four-wheel drive vehicular tracks lead to the Stormont Bismuth Mine and most of the way to the Ti Tree Creek Prospect. Access to Fletcher's Adit involves branching off the road to Stormont and following a foot track west to the Lea River. See Appendix H, Map 1 for prospect locations.

Vegetation in the area is predominantly mature rain forest, with areas of very thick fern growth and some dense horizontal scrub. As a result, the majority of the mapping was performed using cut grid-lines, roads and the excellent river and creek sections. The grid covering the Ti Tree Creek area (Appendix H, Maps 1, 4, and 5) is extremely overgrown.

The 1:5000 mapping area (Figure 1 and Appendix H, Map 1) contains three mineralised skarns. These deposits include the Stormont Bismuth Mine (referred to from now on as Stormont), Fletcher's Adit and the Ti Tree Creek Prospect.

Appendix H contains a 1:5000 scale geologic map of the whole field area, 1:1000 scale geologic maps for the Fletcher's Adit and Ti Tree Creek areas and relevant cross-sections for these maps (see List of Appendices).

All three skarns have been formed from the infiltration metasomatism of the basal portion (20-35 m) of the Middle Ordovician Gordon Limestone, soon after the emplacement of the Late Devonian Dolcoath Granite. These deposits are, along with numerous hydrothermal veins in the Moina area, part of the contact aureole of the Dolcoath Granite.

The Moina district has great potential for detailed studies in skarn petrogenesis for the following reasons:

1) The Dolcoath Granite plunges shallowly to the west but steeply in all other directions. This flat topped ridge extends underneath five mineralised skarns that lie along an E-W trend. The five skarns being, from east to west are:

- Shepherd and Murphy (Sn-W-F)
- Moina (Sn-W-F)
- Ti Tree Creek (Fe-Cu-Sn-W-Pb)
- Fletcher's Adit (Bi-Au-Cu-Pb-Sn-Zn)
- Stormont Bismuth Mine (Bi-Au)

Thus, this sequence represents the change in one fundamental variable - depth to the mineralising granite.

2) All five skarns are hosted in the same protolith and mineralised by the same granitoid.

3) The five deposits show distinct differences in calc-silicate compositions, ore mineral type and abundance, textures and intensity of alteration.

4) There is no post-Devonian metamorphic or structural over printing.

The deposit at Stormont has many of the characteristics of a rare class of skarn, known as gold skarns. Meinert (1989) stresses that gold skarn research is still in its infancy, and that more detailed studies need to be performed to add to the accumulating data set involving gold skarns and therefore to increase the certainty of the characteristics of this class of skarn. This request is part of the rationale for this study.

## 1.2 AIMS

The aim of this study is to fulfil the following tasks:

- To map the Fletcher's Adit and Ti Tree Creek areas on a scale of 1:1000 using nomenclature consistent with the recent 1:1000 mapping of the Stormont area performed by R.G.C. Exp. Pty. Ltd.

- To map an area encompassing the three skarn deposits on a 1:5000 scale.

- To sample the available diamond drill cores for Stormont (SD 1-6), Fletcher's Adit (FD 1-9) and Ti Tree Creek (DOM 1 and 3) for detailed petrological studies, and in particular to establish a paragenesis for these three skarns.

- To discover in what ways the three skarns are similar and/or different, and discover why these similarities and/or differences exist.

- To distinguish whether Stormont is a genuine "gold skarn", by comparing it to better known North American examples.

## 1.3 EXPLORATION HISTORY

In 1925 Richard Magee found bismuthinite in alluvial sediments along the banks of the Lea River, and traced the source of this bismuthinite back to the skarns now known as Fletcher's Adit and the Stormont Bismuth Mine (Reid, 1927). The Stormont Bismuth Mine operated from 1928 to 1934, during which time 6.3 tons of Bismuth concentrate were produced, having a grade of 51-67 % Bi, 164-1234 g/t Au and 214-360 g/t Ag (Burns, 1958).

Minor workings at Fletcher's Adit in the late 1950's concentrated on vein deposits, usually on the crests of anticlines (due to the predominance of tensional jointing). These veins reportedly contained sphalerite-galena-chalcopyrite-pyrite-wolframite with minor gold and silver (Burns, 1958).

The history of the Ti Tree Creek Prospect is obscure. It seems that minor magnetite skarn was mined for W and Sn when the larger W-Sn producing mines at Moina and Shepherd and Murphy were in operation, which was intermittently between 1893 and 1957 (Collins, 1979).

The Dolcoath Granite contact aureole has been of interest to numerous prospectors and companies for the last hundred years. Significant exploration activities during this time are outlined below:

- Geological mapping has been performed by Cordwell (1961), McKibben (1971), Flemming (1987) and White (1989).

- Geochemistry involving B-horizon soil sampling, trench sampling, chip sampling, and stream sediment sampling has been completed by Reid (1967), Foster (1969), Dandy (1970), McKibben (1971), and R.G.C. Exp. Pty. Ltd. recently. These surveys resulted in the recognition that Stormont has the greatest potential for high grade Bi-Au in the Moina area.

Soil sampling completed by C.R.A.E. in the late seventies over the Ti Tree Creek Prospect failed to identify an anomaly, and no company holes were drilled in this area.

- Geophysical exploration has involved V.H.E.M. (McKibben, 1971), resistivity, gradient array I.P., and S.P. (Dandy, 1970), scintillometry and, in the last year, regional gravity and detailed ground magnets by R.G.C. Exp. Pty. Ltd. I.P. detected NW-SE trending (?)shear zones, regional gravity defined the shape of the Dolcoath Granite on the regional scale, while ground magnetics confirmed the position of the magnetic skarn bodies and indicated that the thickness of the basalt is generally less than 50-70 m (Flemming, 1988; Castro, 1989).

- Diamond drilling by R.G.C. in 1987 at Fletcher's Adit (FD 1-9) and Stormont (SD 1-6), again confirmed that Stormont was the more encouraging of the two deposits, with SD 1 returning 13.0m @ 4.12 g/t Au and SD 3 returning 2.1m @ 12.77 g/t Au (Roberts, 1987). These grades were enough to support further drilling at Stormont in early 1990, but eventually the skarn proved to contain only patchy high grade mineralisation and does not represent a profitable mining venture.

## 1.4 PREVIOUS WORKERS

Jennings (1958 and 1979) has been the most significant contributor to the understanding of the stratigraphy, petrology and structure of the Late Cambrian to Late Ordovician rocks in the Moina area.

Kwak and Askins (1981a) published a comprehensive paper on the F-Sn-W (-Be-Zn) "wrigglite" skarn at the Moina skarn deposit, which lies only 2 km east of the Ti Tree Creek Prospect. The essential points to note from this research are:

- "Wrigglite" is a textural term, describing alternating bands of magnetite with fluorite-vesuvianite ± cassiterite and scheelite.

- The Dolcoath Granite lies only 200 m below this deposit.

- Primary F-rich skarns are enriched in F-Fe-Sn-W-Be-Li-B-Bi.

- Secondary alteration introduced Zn-Pb-Cu-S.

- When $\Sigma$FeO is approximately less than 9 wt %, "wrigglite" does not form.

- "Wrigglite" is formed by replacement at diffusion fronts, moving outwards from fractures, and is at least partially produced by a boiling, high temperature, saline solution.

Webb (1974) concentrated on the Ti Tree Creek skarn, with a very brief look at Stormont. Salient points to arise from this study include the following:

- The recognition of a second stage of metasomatic fluids which transformed the initial calc-silicate skarn into a magnetiferous skarn.

- During this second stage Fe-F-K-Rb-Y-Cu-Zn-W were enriched, while Si was depleted.

- Beneath Ti Tree Creek, the granite is at a depth greater than 324 m.

- The pyroxenes at Ti Tree Creek are slightly manganiferous salites.

- Garnets are members of the grossular-andradite series.

- Garnet zoning indicates that Fe/Al ratios fluctuated during the growth of skarns in the Moina area, without showing a particular trend.

Thus, the outstanding questions that needed to be addressed at the Stormont, Fletcher's Adit and Ti Tree Creek deposits are:

- What is the petrography of the three skarns?

- What effect does the westward increase in "prospect-to-granite" distance have on the mineralisation and petrology of these skarns?

- What is the source of the gold?

- Why is a Au-Bi bearing skarn associated with an ilmenite series granitoid?

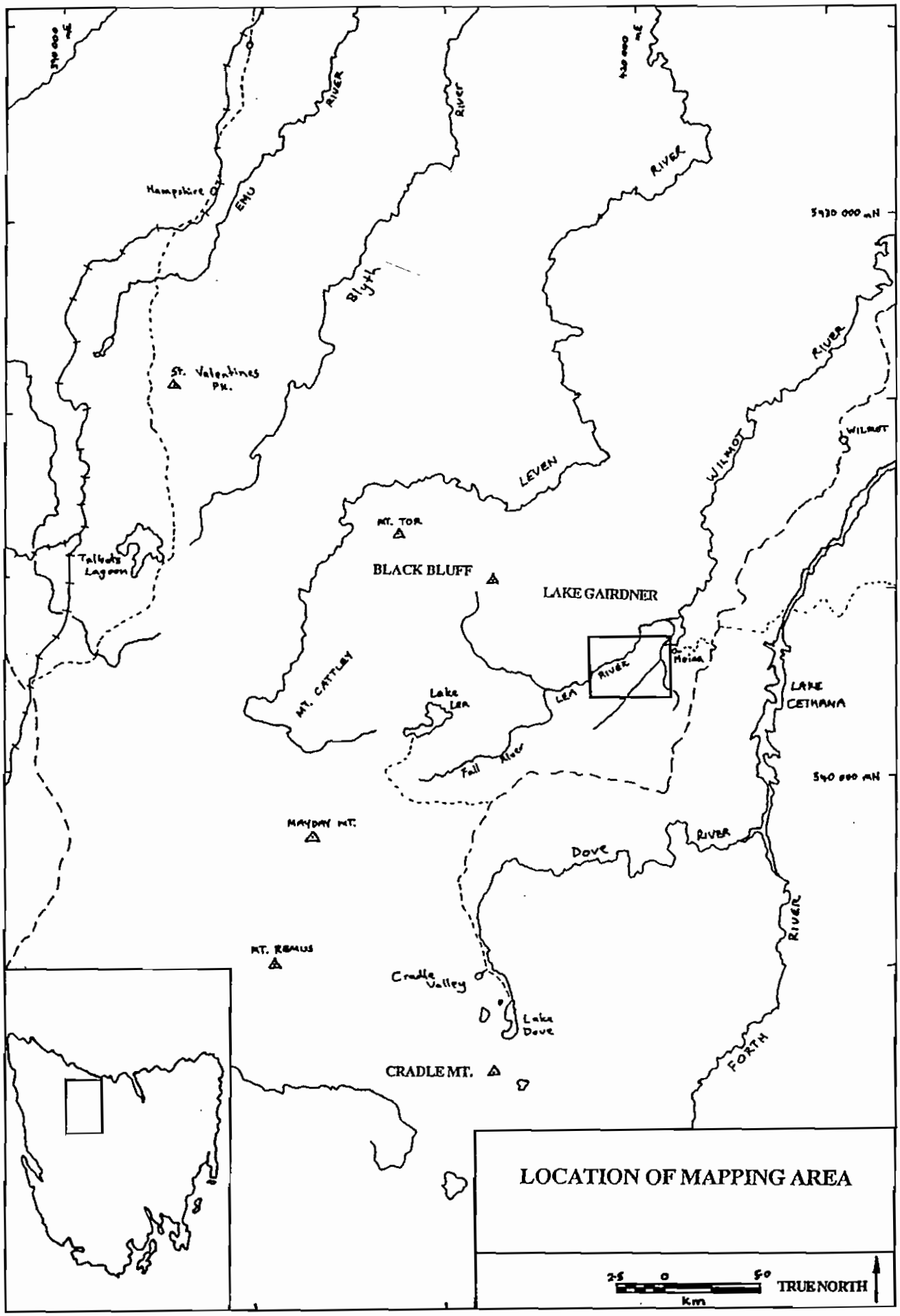


**FIGURE 1:** Location of the 1:5000 scale mapping area at Moina, NW Tasmania.

# CHAPTER 2

# REGIONAL GEOLOGY

## 2.1 STRATIGRAPHY

Twenty kilometres south of Moina, in the Cradle Mountain region, the Precambrian Tyennan Block consists of strongly deformed phyllitic and schistose pelitic rocks belonging to the Fisher Metamorphic Complex.

The Cambrian Mount Read Volcanics are represented by Tyndall and Dundas Group correlates. The volcanics closest to Moina are the Bull Creek Volcanics, which outcrop one kilometre to the south of Stormont. T have been intersected in drill core one kilometre NE of Fletcher's Adit and most probably underlie Stormont. These volcanics consist of quartz-feldspar-biotite ± hornblende porphyries, quartz phyric tuffs, quartz-feldspar-biotite phyric crystal lithic tuffs, and quartz-feldspar ± biotite phyric crystal tuffs (Pemberton and Vicary, 1989).

Lying unconformably on top of the Mount Read Volcanics are the siliciclastics of the Late Cambrian to Early Ordovician Denison Group (which is the basal member of the Wurawina Supergroup). The thickness and lithology of the earliest unit, the Roland Conglomerate (an Owen Conglomerate correlate) varies greatly in the Winterbrook-Moina area. This observation is consistent with the nature of such alluvial fan deposits which show channelling, lensing and abundant lateral variation in facies. The Roland Conglomerate consists of thickly-bedded conglomerates, sandstones, and siltstones and contains some horizons of fine grained basalt. The characteristic feature of the Roland Conglomerate is the abundance of hematite in the siliceous matrix, again consistent with an oxidising, terrestrial, alluvial fan environment of deposition. Clasts are composed of volcanic fragments at the conglomerate's base, but elsewhere are almost entirely siliceous (i.e. quartzites, cherts, reef quartz, and quartz schists) and set in a siliceous matrix which is frequently recrystallized (Jennings, 1979). The majority of clasts are derived from the Precambrian rocks of the Tyennan Block to the south (Banks and Baillie, 1989).

The upper section of the Denison Group is called the Moina Sandstone. This formation lies conformably on the Roland Conglomerate and is characterised by clean, grey, moderately

well-sorted, silicic arenites of variable bedding thickness. The Moina Sandstone is in places intensely bioturbated and, around the Moina area, it exhibits silicic and sericitic alteration associated with the intrusion of the Dolcoath Granite. The top of the Moina Sandstone locally consists of bioturbated, interbedded shales and calcareous arenites, which are correlates of the Florentine Valley Mudstone (Pemberton and Vicary, 1989). Body fossils are rare with only minor occurrences of costate brachiopods, gastropods and trilobite fragments being recognised (Banks and Baillie, 1989).

The transition from the terrestrial, unfossiliferous, alluvial fan conglomerates and sandstones of the Roland Conglomerate to the bioturbated shallow marine clastic sequence called the Moina Sandstone represents a gradual reduction in topographical gradient (from continuing erosion), and therefore a reduction in the amount of sediment supplied to the sea. It also represents a movement of the shoreline. The result is a gradual fining upwards in sediment grain size from very coarse conglomerates through sands to silts (and eventually to limestones in the Mid to Late Ordovician).

Conformably above the approximately 245 m thick Moina Sandstone, the Gordon Group is represented by the Gordon Limestone. This Mid Ordovician carbonate unit contains minor shale horizons, chert bands, stylolites and is fossiliferous in many places (Pemberton and Vicary, 1989). The basal part of the Gordon Limestone represents a tranquil environment, initially below the wave-base, which progressively shallows to become intertidal in the upper section.

The Denison Group and the Gordon Group represent a textbook example of a syn- and post-orogenic sedimentary sequence (Banks and Baillie, 1989). The base of the Gordon Limestone (and the very upper part of the Moina Sandstone) hosts five skarn deposits in the Moina area.

The Dolcoath Granite is an ilmenite series leucocratic granite of earliest Carboniferous age (340-360 ma). This granite contains quartz, perthitic microcline, plagioclase and biotite, with minor apatite, zircon fluorite, topaz, cassiterite and disseminated molybdenite and pyrite (Williams, McClenaghan and Collins, 1989; Webb, 1974). The Dolcoath Granite outcrops as

a small (1km radius) circular stock, 4 km east of Moina and has a well-defined contact aureole extending out to the west.

The only possible Silurian sediments recognised in the Sheffield/Moina area can be seen at Gunns Plains, where a small amount of white sandstone conformably overlies the Gordon Limestone (Jennings, 1979).

There is a large temporal gap in the geologic record from the Late Devonian to the Tertiary in the Moina area. The top of the Gordon Limestone often shows evidence of an extensive period of erosion, with deeply penetrating leached zones and the formation of thick paleo-soil profiles.

The first Tertiary sediments are massive to thickly bedded units of siliceous conglomerates, breccias and unconsolidated gravels ("greybilly"). On top of the "greybilly", there exist extensive flows of Tertiary basalt and hyaloclastic basaltic breccias.

The Quaternary sediments in the Moina area are varied, but generally consist of alluvium and talus/scree slope deposits.

## 2.2 STRUCTURE

The only deformation event which has any bearing on mineralization hosted in Ordovician lithologies in the Moina area, is the Mid Devonian Tabberabberan Orogeny. The intrusion of the Dolcoath Granite itself is considered to have been only a passive event with minor local folding and doming (Williams, McClenaghan and Collins, 1989).

There are two major structural trends in the Moina area, an early E-W trend and a later NNW-SSE trend.

The E-W structural trend is called the Loongana/Wilmot Trend, and is characterised by shallowly plunging, symmetrical folds that are generally open and have limb dips of approximately 20°. In the Stormont region wavelengths are in the order of 500 m. This earliest trend is thought to have resulted from the N-S convergence of the Precambrian Tyennan and northern Blocks (Jennings, 1979; Williams, McClenaghan and Collins, 1989).

Superimposed upon the early E-W folds is a NNW-SSE structural trend called the Deloraine/Railton Trend. This deformation phase is the dominant trend in the Moina area.

Axial surfaces as well as small thrust faults which are associated with this fold phase dip to the NE, which indicates a NE transport direction. Folding associated with this phase is characterised by gentle plunges (up to 20°), wavelengths of 50-200 m, slippage along bedding planes and break thrust development. Associated thrusts generally dip at 30-35° to the NE or less commonly to the SW, with displacements reaching 100's of metres in only a few places. The shallow plunge of folds produced by this fold phase represents the dips of the limbs of the earlier E-W folds (Jennings, 1979; Williams, McClenaghan and Collins, 1989).

From an economic perspective the NNW-SSE structural trend is the most significant, as the smaller wavelength folds produce locally intense jointing which, together with the associated faults, provided excellent pathways for granitic fluids to penetrate the thick, silicic Denison Group sediments which underlie the Gordon Limestone. It may be no coincidence that the position of the Dolcoath Granite and therefore the Moina mineral field coincides with the intersection of two structural domains (one dominated by an E-W trend and another by a NNW-SSE trend). This location may represent a structurally weak zone where a magma could penetrate to shallower levels most effectively.

## 2.3 GRANITE FORM

The position of mineralized prospects, the zonation of metals and the extent of alteration in the Moina area has long been thought to indicate that the Dolcoath Granite batholith has steep eastern, northern and southern margins, while the western margin is gently plunging (Gee, 1966; Collins, 1979). Leaman and Richardson (1988), in a "geophysical interpretation of granites", confirmed these original ideas through the use of a regional gravity survey. The interpretation of the Dolcoath Granite's sub-surface form is shown in Figure 2.

Salient observations from this survey and another report for R.G.C. Exp. Pty. Ltd. (Leaman, 1989) are that:

- The southern face is very steeply dipping.

- The northern face dips more shallowly towards the Housetop Granite (the two batholiths cannot yet be proved to be distinct or connected geophysically due to poor resolution).

- The western and north-western faces dip gently.

- The southern face appears to be shelved, but overall steeply dipping.

- The roof of the granite is nearly horizontal.

- Irregularities in the roof of the batholith are attributed to fractures controlling emplacement.

It has also been suggested that the areas of intersection between the flat roof and steep sides coincide with areas of mineralization. These intersections are seen as areas of tensional stress with the opening of tensile fractures allowing "roof spines" to intrude into the overlying rocks, and to channel mineralizing fluids. Leaman (1989) also does not rule out the possibility of cupolas existing on the batholith roof which dips gently to the west.

The depth to granite below Stormont is poorly constrained. The regional gravity survey indicates that the flat-topped ridge in this region is less than 1km and probably less than 500 m. Diamond drilling at the Moina Sn-W skarn intersected granite at approximately 200 m, while a Department of Mines stratigraphic drill-hole (D.O.M. 1) only 200 m WNW of the Moina skarn, failed to intersect granite at 324 m! It seems likely therefore that the roof of the Dolcoath Batholith includes cupolas.

The only other moderately deep holes west of Moina are FD 6 (drilled at Fletcher's Adit, which reached a depth of 184 m but only just intersected the Roland Conglomerate) and DDH 1 (a Comalco hole, situated 1 km NE of Fletcher's Adit, which intersected the Moina Sandstone above the Cambrian volcanics, and these continued to the end of the hole at 253 m). Thus, the granite-to-prospect depth in the Stormont and Fletcher's Adit areas could be anything from 250 to 1000 m.

## 2.4 DOLCOATH GRANITE CONTACT AUREOLE

An attempt to define a zonation of the mineralization around the Dolcoath Granite is given in Figure 3. These zones (starting from the zone closest to the granite crop on Dolcoath Hill) are:

| | |
|---|---|
| Vein style Mo-Sn-W | |
| Vein style W±Sn-Bi | Skarn style [significant W-Sn±Bi] |
| Vein style Au ± Ag | Skarn style [moderate W-Sn] |
| Vein style Pb-Zn | Skarn style [minor W-Sn-Au-Ag-Bi] |
| | Skarn style [significant Au-Bi±Ag] |

This zonation is consistent with the proposed form for the Dolcoath Granite (Leaman and Richardson, 1988). The relationship is clearest to the west of Dolcoath Hill, where the granite ridge plunges shallowly under the Moina, Shepherd and Murphy, Ti Tree Creek, Fletcher's Adit and Stormont deposits. The metal zonation is simply a function of the increasing prospect-to-granite distance, while the style of mineralization is controlled principally by the lithology of the host rock. To the south, the east and to a lesser extent the north, mineralization is extremely limited due to the steep dip of the sides of the granite batholith.

It has been reported that there is also a zonation in the attitude of vein deposits in the area. The high temperature Sn-W veins proximal to the granite occupy E-W trending veins, while the lower temperature, more distal Ag-Pb veins occupy NW-SE trending fracture

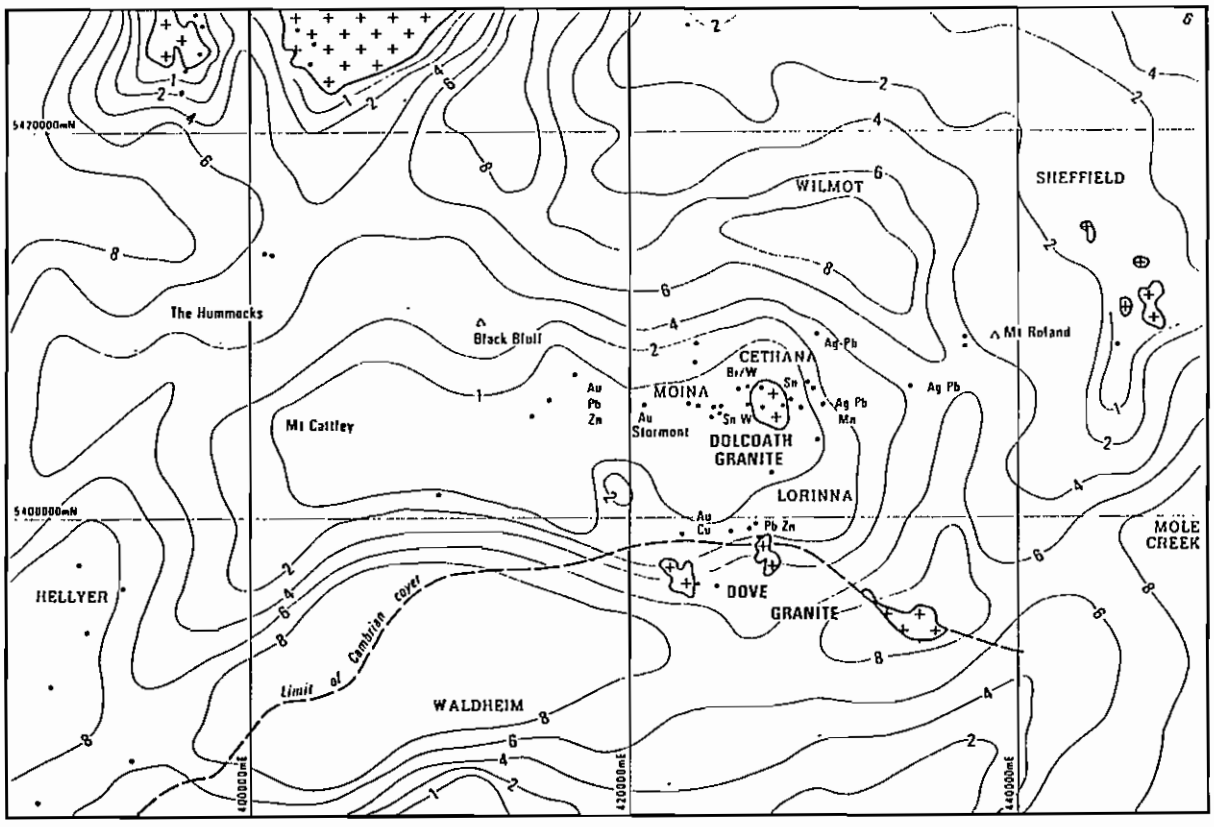


**FIGURE 2:** The Dolcoath Granite's sub-surface form. Depth contour interval is 1 km. Mineralisation sites are indicated. From Leaman and Richardson, 1988, p. 76.

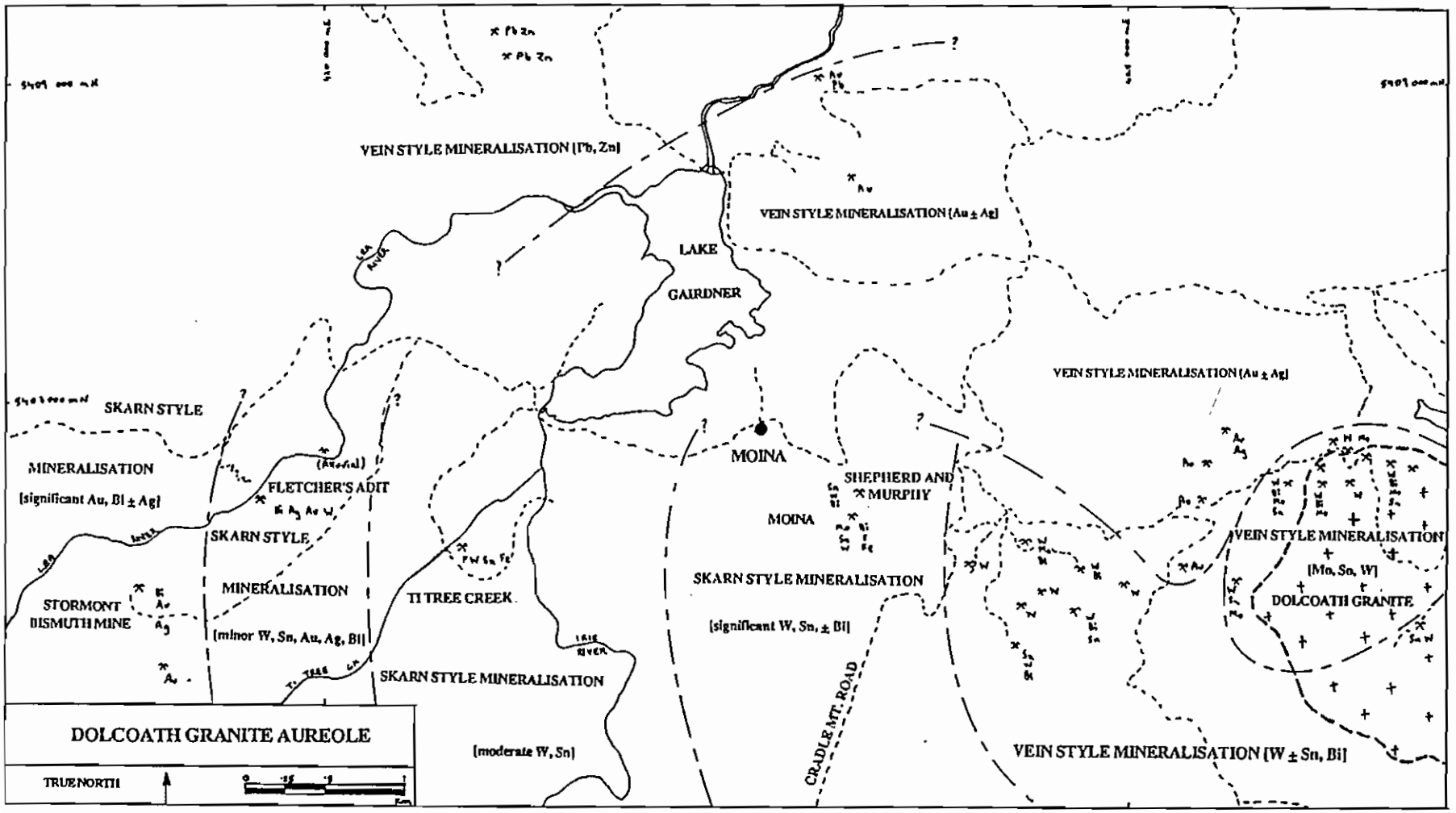


**FIGURE 3:** Mineralisation zonation associated with the Dolcoath Granite contact aureole. Prospect data from Pemberton and Vicary, 1989.

# CHAPTER 3
# LOCAL STRUCTURE

## 3.1 FOLDING

Structural measurements of poles to 253 bedding surfaces from Ordovician lithologies throughout the mapping area are plotted in Figure 21a. This stereographic projection indicates that the Roland Conglomerate, Moina Sandstone and Gordon Limestone are only gently folded in this area, with dips rarely exceeding 20-25°. The poles to bedding readings are concentrated around the horizontal orientation, but show a slight trend consistent with a fold axis at approximately 316°. This NW trend corresponds to the Deloraine/Railton Trend discussed in Chapter 2.

In the field, the rocks belonging to the Denison and Gordon Groups can be seen to have been subjected to two episodes of folding during the Devonian Tabberabberan Orogeny. The main evidence for this is the presence of a dome in the Lea River valley four hundred metres NE of Fletcher's Adit. This style of dome is typical of two interfering fold phases at approximately 90° (Hobbs et. al., 1976). This second, more obscure fold phase corresponds to the earlier E-W Loongana/Wilmot Trend. The broad spread of poles to bedding seen in Figure 21a is a result of the interference between the E-W and NW-SE fold trends.

The early E-W fold phase is difficult to recognise due to its longer wavelength (approximately 500 m according to Jennings, 1978) and the dominance of the later phase. Only the vergence folds associated with this phase are obvious when interfering with the later NW trending folds. Dips on the later NW trending folds may be directly attributed to this phase.

The later NW-SE fold phase plays an important role in the structural control on mineralization. Folds associated with this phase are parallel (or class 1B from Ramsay's 1967 classification), short wavelength (10-100 m), shallowly dipping (0-10°), upright and are open style. Common features associated with these folds throughout the mapping area are slippage along the bedding planes (indicated by striations and quartz rods), locally intense jointing, break thrusts and normal and reverse faults. Folding during this latter phase involved

substantial amounts of brittle deformation, implying a low ambient temperature (i.e. shallow depths) and/or rapid NE-SW compression.

## 3.2 FAULTING

Poles to 18 fault planes are plotted in Figure 21b. This sample space is small but does indicate a NW (≈320°) trend consistent with the NW (≈320°) fold trend. The steep reverse faults are found on the steepest limbs of the NW trending folds, while the thrust faults are found on the more open folds. Normal reverse and thrust faults are present throughout the field area and their occurrence is explained in Figure 22. This diagram indicates that for an antiform, thrusting and high angle reverse faulting can occur in the core while, in the outer regions of the fold, normal faulting and jointing are favoured.

The NW trending faults play a major role in providing fluids with access to carbonate horizons. Stormont has a large normal fault bounding the skarn to the NE, and Fletcher's Adit has a small thrust and two small near-vertical reverse faults at the NE skarn/hornfelsic shale boundary. No major faults were recognised in the vicinity of the Ti Tree Creek skarn.

## 3.3 JOINTING

Figure 21c is a plot of poles to 302 joint surfaces from Ordovician sediments in the mapping area. The contoured stereographic projection depicts the existence of two major orientations. The dominant joint orientation in the field area strikes at ≈335° and dips 80-90° NE, while the secondary orientation strikes at ≈73° and dips ≈85° N. The dominant joint orientation corresponds to radial joints from the dominant NW-SE trending fold phase. The second population of joints corresponds to the first E-W trending phase of folding, or are "a-c" joints (Hobbs et. al., 1976) associated with the later NW-SE trending fold phase. This latter suggestion is preferable as the data for this joint population represent a restricted range of orientations which indicates that this population has not been deformed by a later fold phase. If, however, the minor joint population does represent radial joints from the first fold generation, later folding along a fold axis at ≈90° to the first fold axis theoretically would not change the orientations of these joints.

It is most likely that the majority of the joints in the area are associated with the second phase of folding due to the second phase folds being tighter and having a shorter wavelength. If we assume therefore that all the data in Figure 21c are associated with the NW-SE fold phase then the major joint population corresponds to radial joints, the secondary population corresponds to either "a-c" (transverse) joints or oblique joints. Figure 23 describes the types of joints typically present in intensely jointed rocks such as those at Moina.

Plate 6 indicates the intensity of jointing that can occur in the hinge regions of anticlines and synclines in the footwall arenites. Such jointing, if penetrative, would provide excellent hydrothermal fluid pathways to the overlying skarn. Veining is common in joints and to a lesser extent faults in these areas. Poles to 28 vein orientations are plotted in Figure 21d. These orientations coincide with both the fault and the radial joint orientations which are associated with the NW-SE trending fold phase.

# CHAPTER 4

# LOCAL GEOLOGY AND PETROLOGY

## 4.1 INTRODUCTION

The local stratigraphy is schematically presented in Figure 4, however it must be noted that this is an idealized section, incorporating all rock units seen in the mapping area in their correct stratigraphic position.

Here, rock units are described and discussed according to their relative age (starting from the oldest), except for the metasomatic lithologies which are described separately in Chapter 5.

Silicic, sericitic, and pyritic alteration associated with the intrusion of the Dolcoath Granite show erratic spatial variations, and are generally weak (except for immediately below the skarn/quartzite transition, where silicic ± pyritic and sericitic alteration is locally intense).

Whenever a sample is referred to in any form in the text, a corresponding field number and grid reference (of the location where the sample was collected) are available for reference in Appendix G.

## 4.2 IGNEOUS PETROLOGY

### 4.2.1 BASALTIC HYALOCLASTIC BRECCIA

This Tertiary breccia is extremely uniform in character throughout the mapping area. It consists of angular fragments of olivine basalt, generally surrounded by a rim of glassy material. Fragments usually range from 0.5 to 20 mm in diameter, but can reach 1m. In the field this unit has an intimate association with the voluminous Tertiary basalts.

The breccias commonly occur at the base of the Lea River valley and are unusual in that they are sub-horizontal in outcrop, except for the occasional 50-100 cm, near-spherical, basalt bomb or fragment which protrudes from this surface. The other most striking feature of this unit is the large quantity of zeolite acting as a cement to this breccia (Plate 1).

Under the microscope this rock contains glasses ranging from black through to a light amber in colour, with alteration fronts defining these colour variations. The pinky brown

glasses are the freshest varieties of glass. The olivine basalt rock fragments commonly display "splinter" forms. The olivine basalt is indistinguishable from the massive Tertiary basalts nearby.

There are two pore-filling minerals present in this very porous and permeable rock type. The earliest of these accounts for 20% of the rock, while the later one comprises 10%. These minerals have been precipitated from meteoric waters, which leached Na, K, Si, Al and Ca from the adjacent basaltic rocks.

The earliest cementing mineral is a zeolite, which is clear, is prone to abundant spherulite development (the spherulites nucleate on the corners of angular rock fragments), has a granular fabric, is anisotropic, has a relief <1.54, a birefringence < 0.004, has a moderate 2V (approximately 50°) and has a negative biaxial figure. It appears optically to be chabazite (Deer et. al., 1980) and the composition for this mineral given in Appendix A (i.e. $Ca[Al_2Si_4O_{12}].6H_2O$) is consistent with this identification.

The later pore-filling mineral is white, is prone to form spherulites with "snow flake" forms, develops a brown alteration rim, is isotropic and has a relief <1.54. It looks optically like the zeolite faujasite (Deer et. al., 1980), but the electron microprobe analysis for this mineral given in Appendix A (i.e. $Ca_6AlSi_8.XH_2O$) indicates that the Al:Si ratio is 0.125. Zeolites have Al:Si ratios greater than 2 (Deer et. al., 1978) which indicates that either this mineral is not a zeolite, or the grain analysed was contaminated by impurities.

The hyaloclastic basalt breccias are most likely to have been formed by Tertiary basalt flowing into the large Lea River valley. The subsequent contact with water (in the Lea River valley) would cause violent brecciation, analogous to phreatic eruptions.

### 4.2.2 OLIVINE BASALT

Large amounts of Tertiary basalt exist in the Moina area and partially cover all three skarn deposits in the 1:5000 scale mapping area. The basalt is commonly vesicular and amygdaloidal, with chabazite filling vesicles. Outcrop is only consistently obtained in the river sections, where flows can be seen to exhibit columnar jointing and are fed by dykes usually of 1-2 m width (Plate 2).

# STRATIGRAPHIC COLUMN

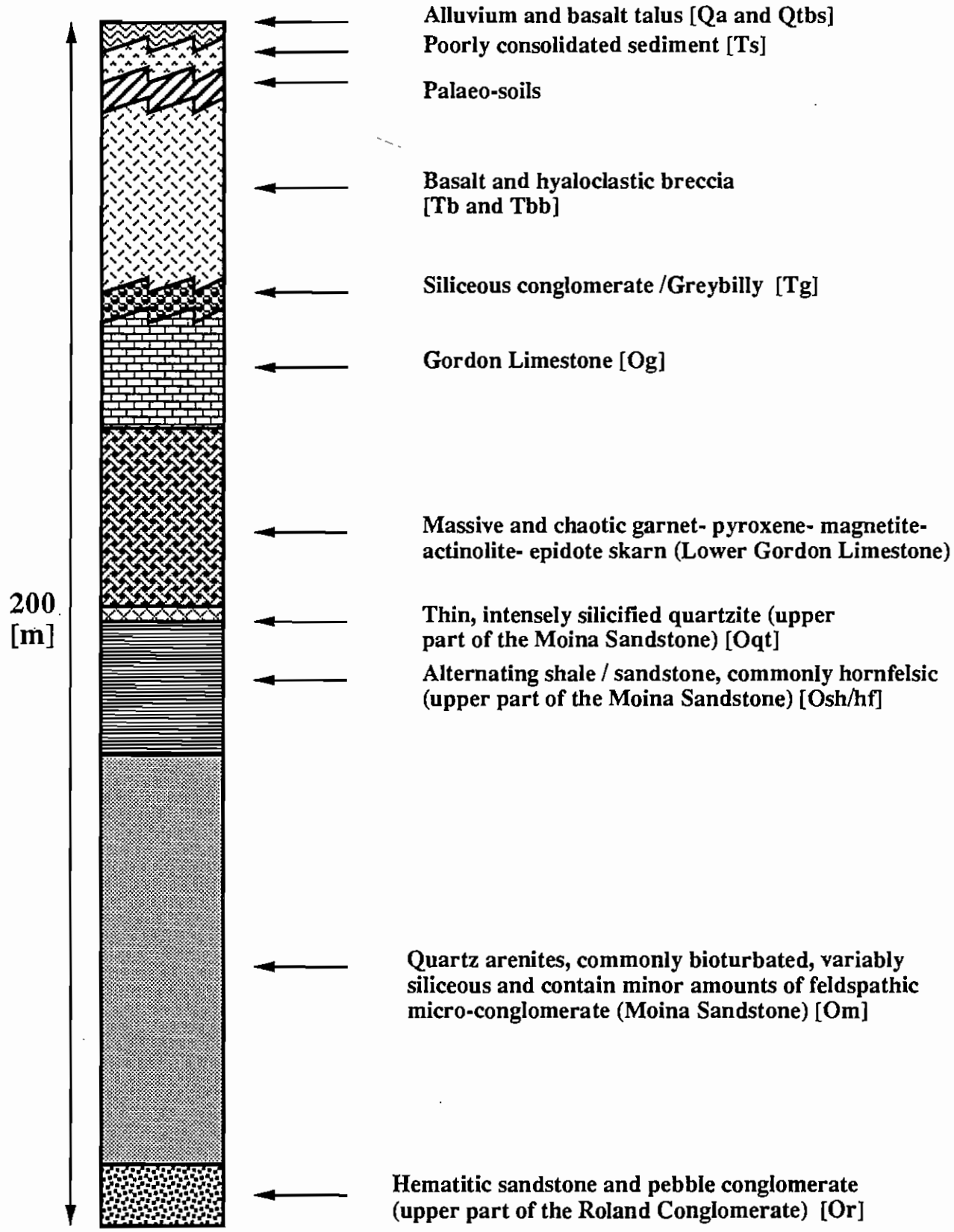


**FIGURE 4:** Schematic stratigraphic column for the Moina area. The Rowland Conglomerate continues below the base of this section.

Sample N$^{o}$ 73919 [168] was taken from a dyke which cuts through the hyaloclastic breccias and contains visible olivine phenocrysts. Under the microscope, this rock can be seen to be an olivine basalt, with olivine phenocrysts up to 3 mm long.

Modal abundances:

- Olivine phenocrysts ≈ 30%
- Titan augite ≈ 20-25%
- Plagioclase laths ≈ 40-50%
- Opaques ≈ 5%

The clinopyroxene occurs as small, elongated, mottled crystals with opaques. The plagioclase laths average 0.3 mm in size and are labradorites to bytownites (Deer et. al., 1980).

The most striking of features in this rock type is the olivine phenocryst forms. The majority of these phenocrysts are classic skeletal olivines which may have formed via rapid growth. The olivine phenocryst was able to lose heat at the corners of the crystal more effectively, which leads to promoted growth in these areas, finally giving rise to a skeletal phenocryst such as the one portrayed in Plate 3.

## 4.3 SEDIMENTARY PETROLOGY

### 4.3.1 ROLAND CONGLOMERATE

This Late Cambrian to Early Ordovician rock unit is seen in a small number of outcrops in the south of the 1:5000 scale mapping area (Appendix H, Map 1) and in the last few metres of FD 6 and SD 1. The Roland Conglomerate intersected in FD 6 consists of a quartzite pebble conglomerate, with a silica-hematite matrix which gives this unit the typical pink-purple colour. In the outcrops seen in the southern portion of the mapping area the clasts contained in the top of this unit are of sand size.

This unit can be seen to fine-up considerably towards the upper boundary. The section exposed along the Ti Tree Creek exhibits a gradation in grainsize from a coarse to a fine arenite, as well as bedding thickness which decreases up the sequence (from 0.4 m to 2 mm). The fine hematitic arenite represents the waning of the very high energy, terrestrial, oxidizing, alluvial fan environment of deposition, as a response to the topographical gradient being gradually reduced via processes of erosion.

The characteristic features that are constant throughout this laterally discontinuous alluvial fan sequence are the abundant hematite disseminated in the matrix, and the domination of silicic clasts.

The only contact visible between the Roland Conglomerate and the Moina Sandstone can be seen in FD 6, where there is an abrupt and irregular contact between a basal hematitic conglomerate and an upper white conglomeritic sandstone. It seems that this contact at Fletcher's Adit represents a disconformity, but in the south the gradation of grainsize suggests a conformable transition.

### 4.3.2 MOINA SANDSTONE

The Moina Sandstone is a thick sequence (approximately 140 m in the Fletcher's Adit area) of arenitic and argillaceous shallow marine clastic sediments. The basal sediments consist of coarse sandstones which grade into the major rock type, which is a grey siliceous arenite that is commonly bioturbated. The upper section of the Moina Sandstone (approximately the top 20 m) consists of interbedded shale and sandstone, which is again commonly bioturbated (Plate 4). The proportion of shale to sandstone varies vertically and laterally, with the shale/sandstone ratio increasing up the sequence consistent with the overall trend of the grainsize fining upwards.

In drill core, the basal coarser sandstones and gravels contain only quartz and quartzite rock fragments, but at a number of locations over the field area a distinctive arkosic micro-conglomerate occurs (only as float) near the basal contact. Bioturbation is rare in these coarser sediments.

The thickly bedded (50-300 cm) arenites which occur in the middle section of the Moina Sandstone are often strongly bioturbated, with worm burrows being 0.6-0.8 mm in diameter and up to 0.3 m long (Plate 5). The arenites are extremely consistent in clast composition, but become increasingly silicified up the stratigraphic section resulting in intense silicification just below the skarn horizon.

Due to the high permeability of these moderately to well-sorted, wave-washed and often intensely jointed sediments (Plate 6), there is invariably some evidence of hydrothermal

fluid activity originating from the underlying granite. Silica, pyrite, sericite and calc-silicates are the most common alteration mineralogies. No large-scale zonation of alteration assemblages was recognised in this area. Veining is abundant throughout the Moina Sandstone and common assemblages include quartz-muscovite-pyrite or quartz-muscovite-fluorite.

Typically the grainsize of the arenites (e.g Sample Nº 73922 [254]) varies from 0.05 to 3.0 mm, and averages 0.3 mm in diameter. Commonly clasts consist of:

- Monocrystalline, weakly undulose, large, plutonic quartz (≈75%).
- Monocrystalline, strongly undulose, small, metamorphic quartz (≈10%)
- Highly strained cherts and quartzite rock fragments (≈7-8%)
- Monocrystalline, pseudo-hexagonal volcanic quartz (≈5%).
- Detrital zircon, tourmaline and sphene(≈2-3%)

The provenance of the arenites is therefore most likely to be the Cambrian Dove Granite, with a lesser component from Cambrian volcanics and Precambrian metamorphics to the south.

Typically the matrix consisting of <0.05 mm diameter quartz grains and contains 2-3% sericite. The sericite may be a product of hydrothermal fluid activity or simply part of the matrix composition. The sericite is concentrated along grain boundaries and in areas where the average grainsize is low. Minor silica cementation often occurs (≈1-2%) and seems to have originated from the annealing of the fine grained quartz clasts. This annealing and redistribution of silica is concentrated in areas where the average grainsize is small, as these areas have a higher grain boundary energy component. This process may be due to contact metamorphism.

Some arenites have a spotted appearance (sample Nº 73922 [254]) due to 0.5 mm patches of magnetite-pyrite-hematite. The paragenesis is magnetite + pyrite initially being later replaced by hematite in equilibrium with more oxidised fluids. The isolated "clots" of mineralization tend to coincide with areas of greater inter-granular porosity. Hematite also coats the rims of larger grains giving the impression that mineralizing fluids permeated quite easily through the arenites via pore spaces. This may help to explain why there are a number of small patches of skarn in the Ti Tree Creek area, and very little in the way of faults.

Occasionally an isolated, brown, isotropic, mottled substance acts as a cement to the arenites (Sample Nº 73907 [215]). In areas where this cementing agent is present, the

- Very well-sorted and moderately well-rounded quartz grains (≈90%)
- Hydrothermally introduced biotite and sericite (≈4%)
- Chlorite replacing biotite (≈4%)
- Blebs of pyrite>chalcopyrite>pyrrhotite>magnetite with hematite rims (≈2%)
- Detrital tourmaline (trace)

Additionally, quartz grains (which average 0.1mm in diameter) are often annealed locally, as indicated by triple point junctions. These burrows seem to be acting as miniature aquifers, allowing mineralizing fluids to penetrate the impermeable hornfelsic shales (Plate 35). There is also considerable lateral fluid movement in the porous sandy layers, as indicated by laterally extensive presence of disseminated mineralization and actinolite, chlorite, biotite and muscovite (Plate 41).

This rock type is commonly cut by 1mm wide quartz-fluorite-muscovite-bismuthinite-chalcopyrite-pyrrhotite-pyrite veins (Plate 7).

The environment of deposition for this rock type is most likely to have been an intertidal mud flat. Current conditions alternated from quiet (when the muddy units were deposited) to a higher energy environment (when sands could be transported and sorted).

### 4.3.3 GORDON LIMESTONE

Un-metasomatised limestone is only seen along the Iris River and Ti Tree Creek sections (Appendix H, Maps 1 and 5 ) due to its susceptibility to weathering. The limestone is commonly interbedded with 1-3 cm thick chert bands, 5-10 cm apart (Plate 8). The chert bands are often more resistant to surface weathering, and thus give this rock type a "ribbed" appearance in the field.

The Gordon Limestone in this area has been described by Webb (1974) as unfossiliferous and non dolomitic, but thin section examination reveals that this unit can be highly fossiliferous and is locally a dolomite. The limestone often appears totally unaltered and not recrystallized only tens of metres away from small "pods" of metasomatic minerals, which may suggest that the movement of granitic fluids was often very focused.

Limestone from a position just above the skarn/limestone contact (or in the "marble front") at Fletcher's Adit, has been partially recrystallised, but some original textures are still

visible. Here the limestone comprises areas of 0.05-0.1 mm diameter calcite rhombs, which grade out into a sparite (Sample Nº 73893 [1]). These rhombs represent dolomite crystals which have been calcified or de-dolomitized by meteoric waters. In areas where these rhombic pseudomorphs are abundant, there is also an abundance of carbonaceous material. These wispy carbonaceous layers may represent algal laminae. The initial presence of dolomite in the lower portion of the limestone in this area suggests that the environment of deposition was supratidal, analogous to the sabkhas of the Persian Gulf.

A very rare texture which was only seen at one location along Ti Tree Creek (Sample Nº 73929 [302]), is where the limestone has been partially replaced by fine grained silica and pyrrhotite in an extremely irregular fashion (Plate 9). Original sedimentary features are well-preserved in the unreplaced limestone. The rock depicted in Plate 9 is an echinoderm-bearing sparite (the average calcite crystal size being approximately 0.25 mm), with 5-8% of the rock consisting of 0.4-1.2 mm arm and stem plates of stalked echinoderms (Plate 10). These plates are variable in shape (due to the presence of a number of different species and types of plate) and each consists of a single calcite crystal which can be porous in the central region. As a result of this porosity, anhedral grains of pyrrhotite are concentrated in these regions.

The environment of deposition for this limestone horizon was probably subtidal, above the wave-base, and exposed to the open sea. Justification for this hypothesis is that stalked echinoderms are dominantly subtidal organisms and are attached to the substrate, making areas that are turbulent accessible for habitation, whereas non-attached organisms are not favoured in this environment.

### 4.3.4 SILICEOUS CONGLOMERATE

Typically this Tertiary sediment is a coarse, white, variably silicified, lithic conglomerate or breccia (Plate 11). Clasts are rounded to angular, 2-200 mm in diameter, and very poorly sorted. The clasts are mainly quartzites and sandstones. Bedding was only observed at two locations over the whole field area, and where it does occur it is characterised by variations in the pebble/sand ratios. In the rare sandy beds, grading can be seen to be fining upwards.

**PLATE 1:** Tertiary hyaloclastic basalt breccia (Sample Nº 73897 [13]). The matrix consists of two varieties of zeolite, one clear and one white. Scale indicated by a 1¢ coin (17mm in diameter).

**PLATE 2:** Tertiary basalt dyke intruding hyaloclastic breccias in the base of the Lea River valley. This dyke strikes at 120º and dips 82º to the north. Note the irregular boundaries, created as it intruded a pile of porous, unconsolidated breccias. Scale indicated by the geology pick in the centre of the plate.

**PLATE 3:** A photomicrograph of a skeletal olivine phenocryst hosted in an olivine basalt dyke (Sample Nº 73919 [168]), similar to the one depicted in Plate 2. Transmitted polarized light, long axis of the plate = 2mm, mag. 50x.

**PLATE 4:** A bioturbated and metasomatised, interbedded hornfelsic shale and calc arenite (Sample Nº 73916 [148]). This unit lies immediately below the limestone. The green layers are arenites that contain actinolite and pyrrhotite. Note the white rim that often borders the green and purple/brown units. Scale indicated by a 1¢ coin.

**PLATE 5:** A branching, 12 cm long worm burrow cast from the middle portion of the Moina Sandstone (Sample Nº 73918 [158]). This burrow is positioned perpendicular to bedding. Scale as shown.

**PLATE 6:** Intense jointing in the footwall arenites at Fletcher's Adit, in the Lea River valley. Jointing is invariably concentrated in the hinge areas of the tightest anticlines and synclines. Scale is indicated by the 10 cm wide compass in the centre of the plate.

**PLATE 7:** A photomicrograph of an interbedded hornfelsic shale/calc arenite hosting a muscovite-quartz-fluorite vein (Sample Nº 73900 [23]). Note the development of a weak cleavage at approximately 60º to the fine scale bedding. Transmitted polarized light, long axis of the plate = 4mm, mag. 25x.

**PLATE 8:** Chert bands (with a minor clastic component) in unaltered Gordon Group limestone along the banks of the Iris River. These siliceous bands may have contributed to the growth of wollastonite and clinopyroxene in the limestone during the metamorphic stage of skarn development. Scale indicated by the 15 cm long magnet.


1


2


3


4


5


6

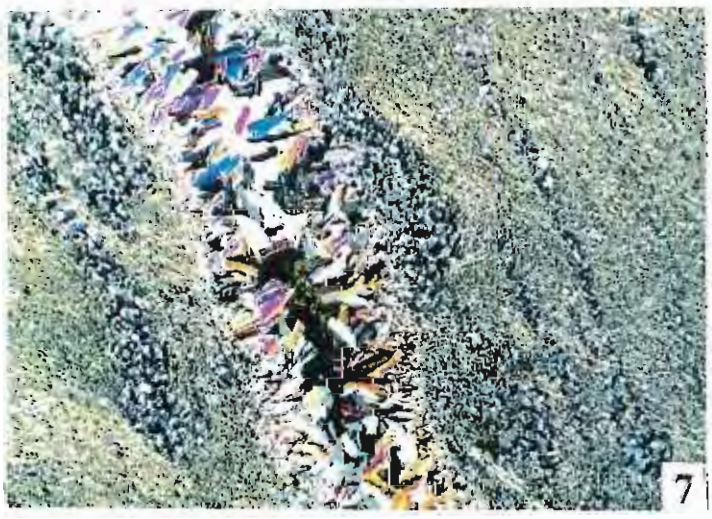
7

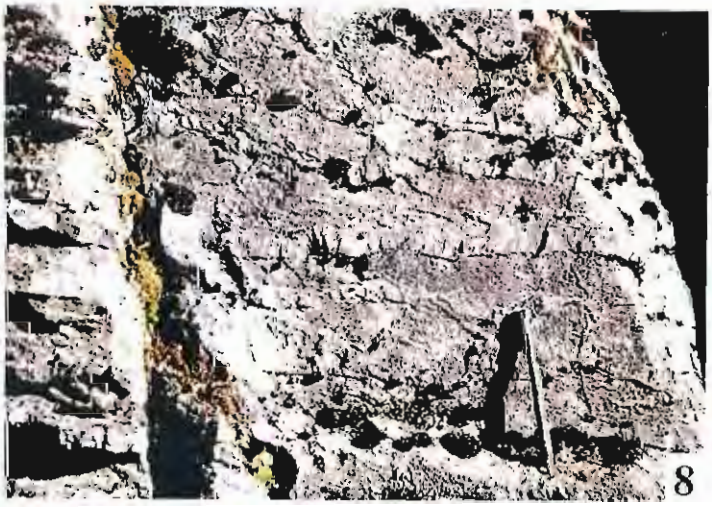
8

Across the field area the siliceous conglomerate occurs as small patches which may reflect restricted deposition or, more likely, the patches represent areas that have been well-silicified (presumably by the overlying Tertiary basalt) and are therefore resistant to processes of denudation.

This poorly sorted conglomerate typically contains clasts ranging from 1-10 mm, which consist of:

- Reworked silicified Moina Sandstone rock fragments (≈80%).
- Monocrystalline undulose quartz (≈10%).
- Chert rock fragments (≈5%).
- Vein quartz (≈ 3%).
- Sphene and tourmaline (≈2%).

All of these clasts could be derived from local sources, namely the Moina Sandstone (although in a few places the conglomerate can be seen to contain large quantities of magnetite indicating that the skarns have been reworked also). The matrix is a poorly sorted mixture of monocrystalline quartz, rock fragments and vein quartz, and is generally less than 0.1 mm in diameter (Sample Nº 73911 [65]). The clasts on average have a roundness of 0.3 and sphericity of 0.5, using the classification of Powers (1953).

The environment of deposition for these sediments is most likely to have been a steep gradient fluvial system or an alluvial fan. Only these environments could account for the enormous range in clast size, the very poor sorting, the poor sphericity and rounding, the massive bedding, the local provenance, and the restricted occurrence in the field area.

### 4.3.5 UNCONSOLIDATED FERRUGINOUS SEDIMENT

This rarely outcropping sediment is a massive limonitic and hematitic clay with variable clastic content. Weathered clasts of basalt (often altered to kaolinite) are the major constituent, with minor amounts of fragmented carbonaceous material with a woody (or cellular) texture. Clasts of altered basalt are poorly sorted, and range in size from 1 to 20 mm. The unit may represent a Tertiary soil profile or a lacustrine sediment.

### 4.3.6 BASALT TALUS

Basalt talus is a "group name" used in field mapping to describe the basalt and basaltic breccia float which covers almost 40% of the field area. The age of this mapping unit ranges from Tertiary to Quaternary. Generally the basaltic breccia blocks are much larger (up to 3 m in diameter) than the basalt blocks(10 mm to 1 m) and usually well-rounded. This difference is likely to be a function of the intensity of jointing in the two rocks from which the talus is derived, with the basalt being strongly jointed (from post-eruptive cooling) and the basaltic hyaloclastic breccias being well-cemented by zeolites and relatively un-jointed.

### 4.3.7 ALLUVIUM

Along the large Lea and Iris Rivers, Quaternary alluvium is commonly concentrated on the insides of major bends and often takes the form of a flat topped bench or flood plain. The sediments are poorly sorted and often crudely stratified gravels and sands (Plate 12). Placer gold hosted in these sediments has been worked on a very small scale operation at the Lea River Alluvial Prospect 500 m NE of Fletcher's Adit (Appendix H, Map 1).

Clasts are well-rounded, have a high sphericity, locally derived, imbricated in places, range in size from 5 mm to 0.5 m, and are matrix supported. The matrix comprises sandy and silty material, derived principally from the Moina Sandstone.

# CHAPTER 5

# SKARN PETROLOGY

## 5.1 INTRODUCTION

When mapping it was essential to break down the metasomatised limestone (or skarn) into units that were readily identifiable in the field. One of the aims of the project was to complete maps of the area (of varying scale) using internally consistent nomenclature, and thus the following mapping units were used as they had recently been defined in a 1:1000 scale mapping project around the Stormont Mine area recently completed by R.G.C. Exp. Pty. Ltd.:

- **Magnetite skarn:** commonly exhibiting a "wrigglitic" texture, and containing minor fluorite, pyrite and actinolite (Plate 13).

- **Garnet actinolite skarn:** usually red or brown euhedral garnets with voluminous fibrous actinolite, with minor quartz and carbonate (Plates 14 and 20).

- **Transitional skarn:** highly silicious light green hornfelsic skarn containing a variety of calc-silicates and sulphides.

There are two schools of thought in skarn literature, one which emphasises the spatial zonations in metasomatites, and the other which stresses the importance of temporal zonations or sequences (Einaudi et. al., 1981). The three skarns discussed here exhibit poor spatial zonations "down-hole" and laterally. The reason for this poor spatial zonation is that the limestone has been metasomatised along numerous fractures, resulting in the formation of complex vein networks often in "stockwork" patterns, "wrigglite" textures (Plate 13), pods and patches of an equilibrium mineral assemblage surrounded by a totally different assemblage (Plate 15) and generally a chaotic appearance.

At Fletcher's Adit, in the drill core from FD 1, FD 6 and FD 9 especially, a very broad vertical zonation can be recognised but cannot be consistently traced laterally to other nearby drill-holes. This broad spatial zonation is as follows:

| |
|---|
| **TOP** Light brown-yellow skarn with Gt>Act>Pyx, with common Mag + Cal veins. |
| Green (Act>Pyx) and brown-red (andraditic Gt >>Cal+Qtz) uniformly banded, and rarely veined skarn. |
| Magnetite skarn, displaying very distorted banding (similar to "wrigglitic" banding), vuggy calcite development and grades from massive to finely banded towards the top of the unit. |
| Massive Gt>Act>Cal skarn, with minor veining and iron-rich garnets. |
| Magnetite, garnet and actinolite in equal proportions, quartz-muscovite-pyrite greisen veining, and some large pink carbonate veins (possibly due to a Mn impurity, or intergrown K-feldspar). |
| **BOTTOM** Silicious, dark green to black skarn containing abundant quartz-muscovite-pyrite-chalcopyrite veins and disseminated sulphides increasing in abundance towards the base. |

Temporal zonations are much easier to identify and correlate extremely well between the three skarns being studied. As a result this chapter will describe the skarn rock types in a temporal sequence, starting from isochemical metamorphism then infiltration metasomatism and finishing with retrograde alteration. The skarn mineralogy paragenesis for Ti Tree Creek, Fletcher's Adit and Stormont is shown in Tables 1, 2 and 3 respectively. Associated mineralization will be discussed in Chapters 6 and 8.

## 5.2 PETROLOGY

### 5.2.1 CONTACT METAMORPHISM

Evidence for contact metamorphism within the skarn itself is difficult to prove due to extensive overprinting by later infiltration metasomatism. Wollastonite ($CaSiO_3$) is almost certainly a product of contact metamorphism as patches of wollastonite from the "marble front" in Sample Nº 72893 [1] (from Fletcher's Adit) are not associated with any introduced silica in the form of veins. The host limestone has enough silica in the form of chert bands and disseminated clastic content (abundant in the basal portions) to enable wollastonite to form without introduction of additional elements.

# TI TREE CREEK

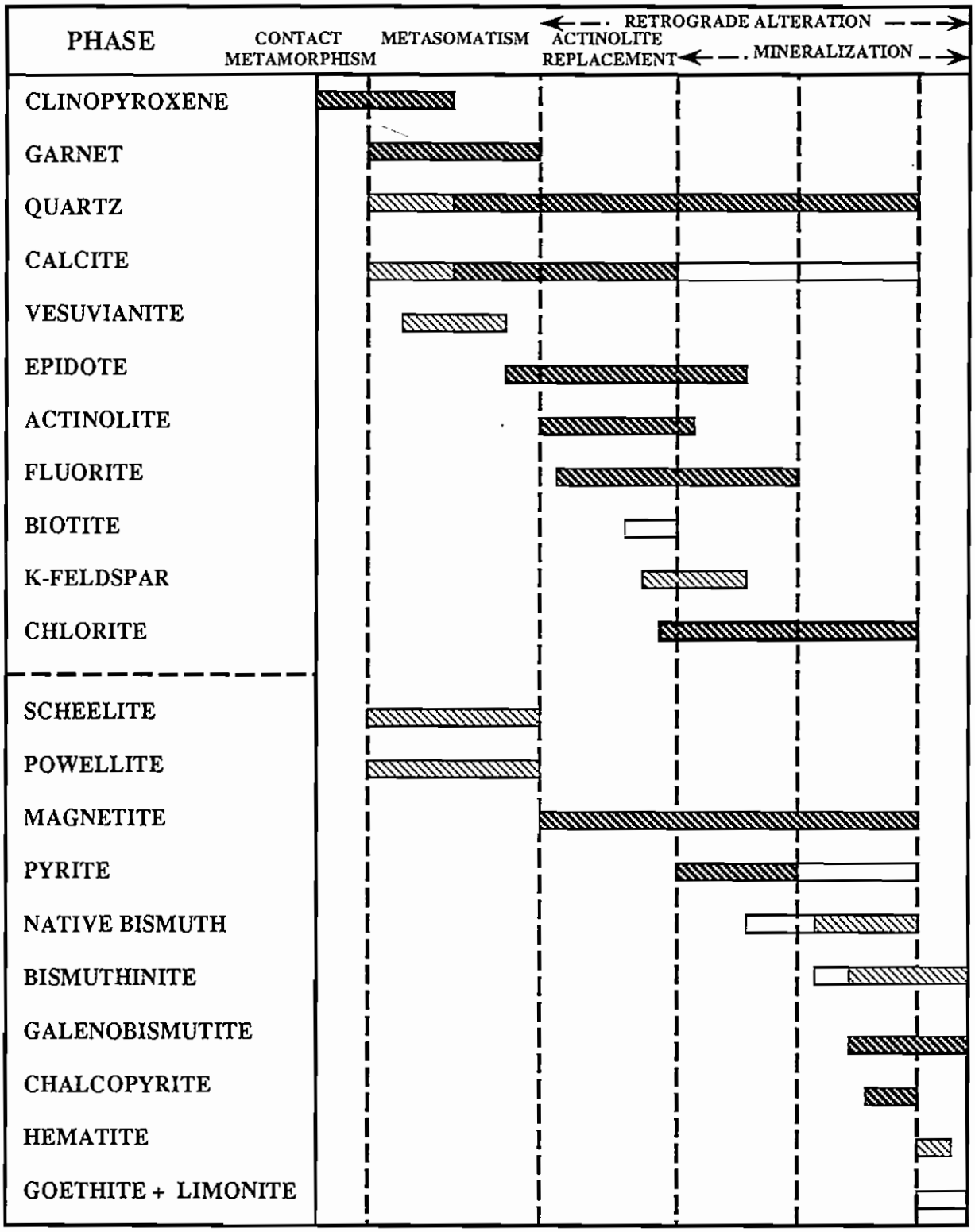


**TABLE 1:** Summary of the paragenesis of minerals identified in skarn lithologies at Ti Tree Creek. Dark hatching indicates common minerals with a clear paragenetic position. Intermediate hatching indicates minor phases. No hatching indicates an uncertain paragenetic position, and/or very low abundances.

# FLETCHER'S ADIT

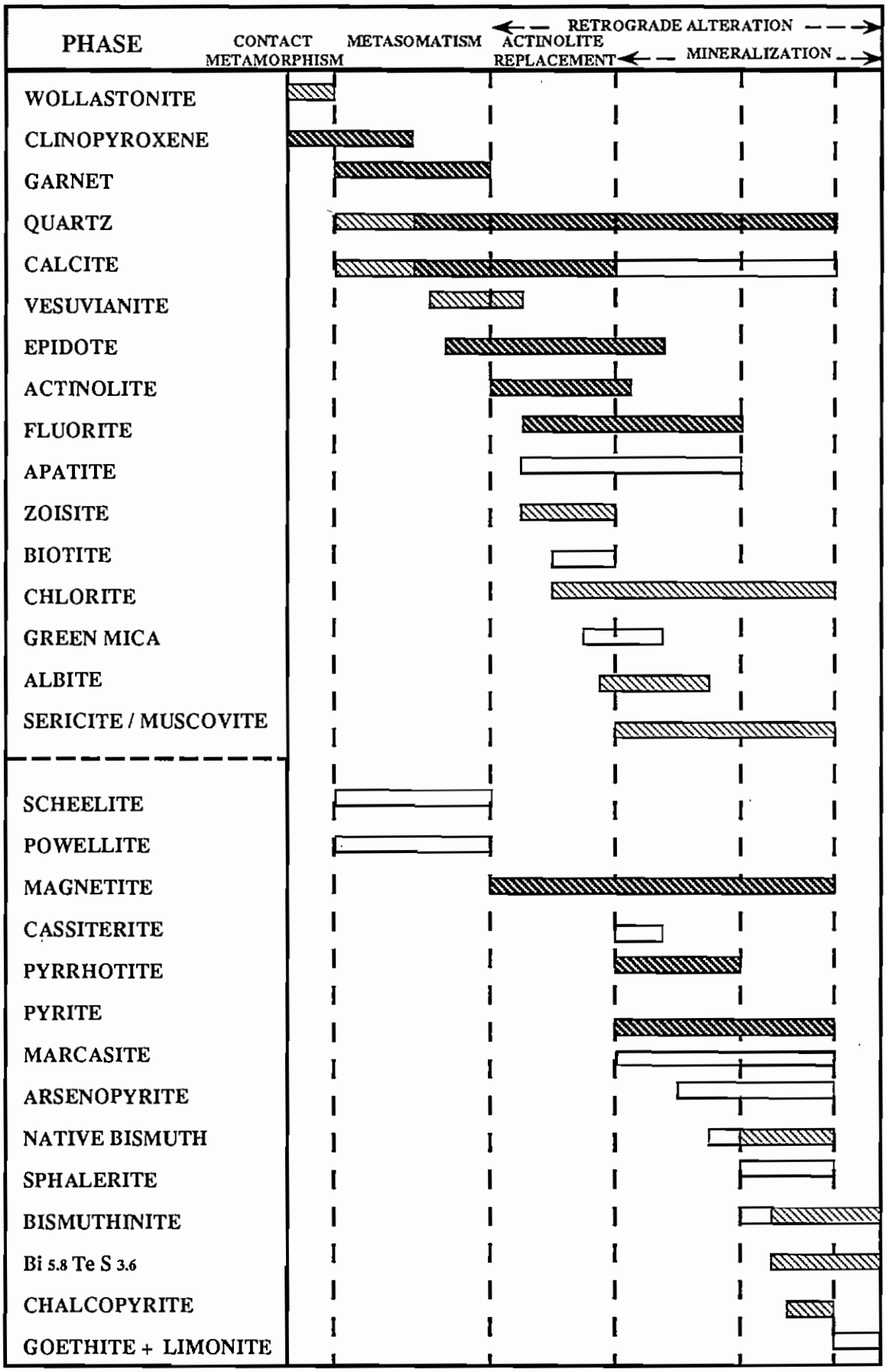


**TABLE 2:** Summary of the paragenesis of minerals identified in skarn lithologies at Fletcher's Adit. Dark hatching indicates common minerals with a clear paragenetic position. Intermediate hatching indicates minor phases. No hatching indicates an uncertain paragenetic position, and/or very low abundances.

# STORMONT

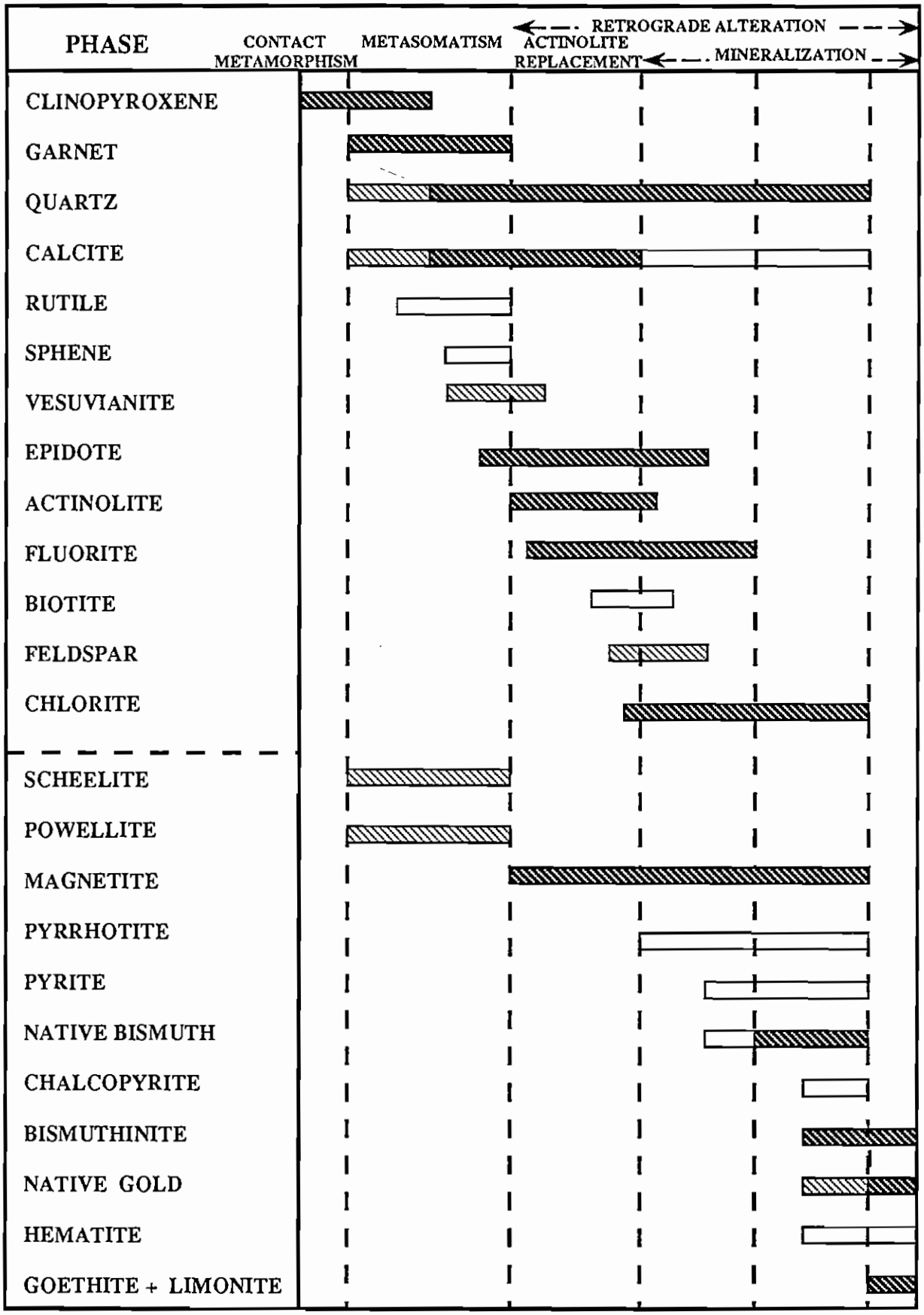


**TABLE 3:** Summary of the paragenesis of minerals identified in skarn lithologies at Stormont. Dark hatching indicates common minerals with a clear paragenetic position. Intermediate hatching indicates minor phases. No hatching indicates an uncertain paragenetic position, and/or very low abundances.

The reaction is: $CaCO_3 + SiO_2 = CaSiO_3 + CO_2$

[Deer et. al., 1980]

Clinopyroxene is abundant at Ti Tree Creek (with rocks containing up to 50% clinopyroxene), less so at Fletcher's Adit and rare at Stormont (with a maximum modal abundance <10%). This does not mean that when the skarns formed the abundances were any different, but the amount of retrograde alteration increases markedly towards the west, and thus Stormont's clinopyroxene is almost completely broken down to form amphibole.

The clinopyroxene's chemistry allows that it may at least have been partially formed in an isochemical system. Electron microprobe results for clinopyroxenes (from each deposit) are shown in Appendix A but, in general clinopyroxenes from Ti Tree Creek are Mg-rich and Mn-poor in comparison to the other two deposits, while those at Stormont have occasionally anomalously high amounts of Mn. The clinopyroxenes show much less variation in composition in comparison to the garnets which are strongly zoned and differ greatly between deposits.

The salitic clinopyroxenes are generally low in $Fe^{2+}$ and $Mn^{2+}$ but high in $Mg^{2+}$. This can be explained by the isochemical growth of clinopyroxene in a limestone which has sufficient Fe (Webb, 1974) and once contained zones of coarse grained dolomite, as indicated by the presence of calc-silicate and calcite pseudomorphs of dolomite crystals. In Sample N$^{o}$ 73899 [21] (from Fletcher's Adit) large rhombs of dolomite have been pseudomorphed by quartz and clinopyroxene (Plate 16). Therefore it appears that the clinopyroxene "scavenged" Mg from the dolomitic portions of the protolith through the reaction:

$$\underset{\text{(Dolomite)}}{CaMg(CO_3)_2} + 2SiO_2 = \underset{\text{(Diopside)}}{MgCaSi_2O_6} + 2CO_2$$

Additional evidence for the clinopyroxene being at least partially formed by contact metamorphism is that the clinopyroxenes are not zoned, in contrast to the garnets which are nearly always zoned in colour and composition. The zonation in the garnet can be attributed to metasomatic fluids fluctuating in Fe, Ca, $\pm$ Ti, Mg, Al, Cr and Mn concentration (Figure 6), but if the clinopyroxenes are also metasomatically derived why do they lack similar zonations? In a metasomatic fluid which is co-crystallising garnets and clinopyroxenes, Fe can be

partitioned into the garnet, which can explain the co-existing Fe-rich garnets and Mg-rich clinopyroxenes but not the lack of chemical zonation.

In Sample Nº 73924 [283] (from the Iris River area), clinopyroxene occupies areas that once contained a calcareous (and probably dolomitic) matrix to a calcarenite (or dolo-arenite). Its texture and location throughout this sample is totally unrelated to fractures, unlike the later zoned and obviously metasomatic chrome-rich grossular garnet, which also is hosted in this rock type.

### 5.2.2 INFILTRATION METASOMATISM

Tables 1, 2 and 3 summarise the paragenesis of the three skarns, but it must be noted that the many textural interpretations needed to construct such tables are often open to debate and thus these types of tables should always be viewed with some caution. For this reason paragenetic relationships that are obvious are shown in different shades from those that are more obscure.

Despite differences in mineral abundance, major calc-silicate compositions and the occurrence of some minor phases, the paragenetic sequence of mineral growth in the three skarns is nearly identical. The major difference between the three skarns is the degree of retrograde alteration and type of mineralization.

#### 5.2.2.1 Ti Tree Creek

Characteristic metasomatic textures seen at Ti Tree Creek include massive and wrigglitic magnetite, granular garnet-pyroxene skarn, complexly veined pyroxene dominated skarn, pervasive epidote retrograde alteration, and massive and fibrous actinolite-chlorite retrograde alteration.

Ti Tree Creek contains more magnetite (both the massive and "wrigglitic" varieties) than the other two deposits. An example of classic "wrigglite skarn" from the Shepherd and Murphy deposit in the Moina district is shown in Plate 13. "Wrigglite" is a metasomatic textural term which describes a distinctive rock type consisting of fine and usually contorted bands of alternating fluorite (± other fluorine-bearing mineralogies) and iron-bearing mineralogies (usually magnetite) or rarely berillium-rich minerals (Kwak and Askins, 1981a).

**PLATE 9:** A partially metasomatised and mineralised, echinoderm-bearing limestone (Sample Nº 73929 [302]). The light areas represent extremely fine-grained quartz, pyrrhotite, and relict calcite grains. The dark area is the unreplaced limestone. Scale indicated by a 1¢ coin.

**PLATE 10:** A photomicrograph of a stalked echinoderm's monocrystalline arm plate, hosted in the unmetasomatised limestone from plate 9 (Sample Nº 73929 [302]). The dark patches in the centre of the arm plate are grains of pyrrhotite infilling biogenic cavities. Transmitted plane light, stained section, long axis of the plate = 1mm, mag. 100x.

**PLATE 11:** An example of the silicified breccias and gravels known as "greybilly", from the Stormont area. Note the variation in clast size and general high angularity. Clasts are derived principally from the Moina Sandstone. Scale is indicated by the 15 cm long pencil.

**PLATE 12:** Quaternary alluvium and lacustrine sediments along the Iris River. The height of the river bank is approximately 3m.

**PLATE 13:** A typical example of "wrigglite" skarn from the Shepherd and Murphy prospect (Sample Nº 73917 [150]). The light layers consist principally of fluorite-actinolite, with many rarer F-bearing phases. The dark layers are comprised primarily of magnetite. Scale is indicated by a 1¢ coin.

**PLATE 14:** Garnet-actinolite-calcite ± quartz skarn from Stormont (Sample Nº 73925 [291]). Note the patchy nature of this lithology. Native bismuth and bismuthinite occur in the permeable, actinolite-rich (green) areas. Coarse calcite occurs interstitially to the red andradite garnets. Scale is indicated by a 1¢ coin.

**PLATE 15:** "Chaotic" garnet-actinolite-salite-calcite-quartz-magnetite skarn from Fletcher's Adit (FD 6 @ 24.8-24.95m). Note the variability of garnet colour from red to cream, and the complexity of metasomatic textures. Scale as shown.

**PLATE 16:** A photomicrograph of a dolomite rhomb which has been pseudomorphed by clinopyroxene and quartz, in fine-grained skarn which has not been affected by retrograde alteration (Sample Nº 73893 [21]). Transmitted plane light, long axis of the plate = 0.25mm, mag. 400x.

9


10


11


12


13


14


15


16

Kwak and Askins (1981a) suggest that granitic fluids must contain greater than 9 wt % fluorine, and emanate from high level crustal intrusions of ilmenite series granitoids to facilitate wrigglite formation.

Wrigglite forms from the movement of Fe, F, Si, Sn, Be and W-rich fluids through areas of greatest permeability (mainly along fractures in the skarns at Moina), where components in this fluid replace and diffuse into the calcareous host in response to activity and diffusion gradients (Kwak and Askins, 1981a; 1981b). In the calcareous environment fluorine is the first element to become supersaturated so that fluorite (and other F-bearing minerals such as fluoro-vesuvianite, cuspidine, fluoro-margarite, fluoro-biotite and fluoro-tourmaline) precipitates to form the first layer. The nucleation of F-rich minerals to form the so-called "light layer" drastically changes the chemistry of the remaining fluid. This residual fluid continues to diffuse through the host until supersaturation (typically in iron) promotes the nucleation of Fe-rich minerals (such as magnetite, pyrrhotite and pyrite) to form a "dark layer" (Kwak and Askins, 1981a; 1981b). This process continues for many cycles until a rock such as the one depicted in Plates 13 and 17 results.

It is significant that the quantity of wrigglitic magnetite decreases to the west, as Kwak and Askins (1981b) conclude that the formation of wrigglite skarn is promoted by high temperature, boiling and saline solutions. Obviously the more distal the deposit, the more likely that temperature and salinity will decrease. The decrease in quantity of magnetite (and overall iron content) to the west is likely also to be a function of granite-to-prospect distance, as the further the granitic fluids have to travel the lower their ability to transport iron complexes.

The proportion of fine grained pyroxene dominant skarn is the highest at Ti Tree Creek compared to the other two skarns. This is more likely to be a function of the lesser amounts of retrograde alteration (which increases to the west) than original pyroxene formation.

In the Ti Tree Creek area, the calcarenites immediately below the skarn can be seen to contain up to 4 modal percent apple-green coloured, zoned and occasionally sector-twinned Cr-rich grossular garnets (Sample Nº 73924 [283]). The garnet can be seen to be intimately

associated with fractures and is later than the laths of clinopyroxene which make up approximately 35-45 modal % of this metasomatised calcarenite.

These ugrandites (uvarovite-grossular-andradite series) contain approximately 20-30 mole % uvarovite, 40-60 mole % grossular, 10-20 mole % andradite and 2-4 mole % pyralspite (pyrope-almandine-spessartine series) (Appendix A). The core and rim compositions have been plotted on a ternary graph in Figure 5. From core to rim the grossular mole % decreases substantially, while the uvarovite/andradite ratio only decreases slightly. Additionally, the mole % pyralspite decreases by a factor of ≈2.3 from core to rim (Appendix A).

In the coarse grained garnet-pyroxene-magnetite skarn at Ti Tree Creek (Sample Nº 73935 [317]) the garnets show a very interesting zonation in colour and isotropy. There are two distinctly different types of garnet present, which are:

1) A canary yellow, isotropic variety which comprises the cores of the large euhedral garnets, as well as thin bands situated approximately halfway between the rim and the core (Plate 18).

2) A creamy brown, anisotropic and sector-twinned variety, which comprises the majority of the rims of the large garnets.

An electron microprobe analytical traverse was performed across a garnet showing the same zonation as the one in Plate 18, and the results are plotted in Figure 6c. The canary yellow, isotropic garnet is approximately 98 mole % andradite, while the creamy brown, anisotropic garnet is 40-50 mole % grossular. The mole percent of pyralspite fluctuates between 2 and 3.5 mole %, with the near-pure andradite having a smaller pyralspite component. The conclusion that can be gained from Figure 6c is that the iron content is fluctuating enormously during the growth of these garnets and surprisingly the first garnets to form are Fe-rich.

Why the andradites are isotropic while the grossulars are anisotropic is problematical, largely because variations in isotropy are at present poorly understood. A possible explanation may be that the anisotropic garnets represent garnets that have grown at a faster rate than the isotropic ones, and thus have been able to incorporate elements into their lattice that are the

wrong size and/or charge (such as Ti, Al and Mn which are enriched in the grossular-rich, anisotropic garnets).

The coarse grained garnet-pyroxene-magnetite skarn at Ti Tree Creek also has a very high pyroxene/garnet ratio (approximately 60:40), in comparison with Fletcher's Adit (approximately 80:20), which indicates one of three possibilities:

1) that the protolith at Ti Tree Creek had a higher Mg content (i.e. there was more Mg available to crystallise metamorphic salites)

2) that Ti Tree Creek is either more distal to the granite than Fletcher's Adit (as garnetiferous skarn is usually positioned proximal to the granitoid while pyroxene dominated skarn forms at a more distal position) or, more likely comma the fluids at Ti Tree Creek were at a lower temperature

3) that the metasomatising fluids at Ti Tree Creek were simply Mg-enriched in comparison to those forming the skarn at Fletcher's Adit (i.e. there was more Mg available to crystallise metasomatic salites).

The composition of garnets from Ti Tree Creek (Sample Nº 73935 [317]) have been plotted on a pyralspite-andradite-grossular ternary diagram (Figure 7). The compositions of garnets from Ti Tree Creek are extremely varied in comparison with examples from the other three skarn deposits, ranging from nearly pure andradite to equal amounts of grossular and andradite. The iron-rich garnets do not plot in the fields defined by Meinert (1989) for gold skarns or copper skarns. However these garnet compositions are consistent with those from British Columbian iron skarns such as Iron Hill (Meinert, 1984).

Clinopyroxene compositions from Ti Tree Creek (Sample Nº 73935 [317]) have been plotted on a diopside-hedenbergite-johannsenite ternary diagram (Figure 8). The Ti Tree Creek salites are very consistent in composition, being approximately 80 mole % diopside, 18 mole % hedenbergite and 2 mole % johannsenite. These compositions plot within the gold and copper skarn fields (Figure 8) and also the iron skarn field (Meinert, 1984). Thus, the only class of skarn that has similar garnet and clinopyroxene compositions to those at Ti Tree Creek is an iron skarn.

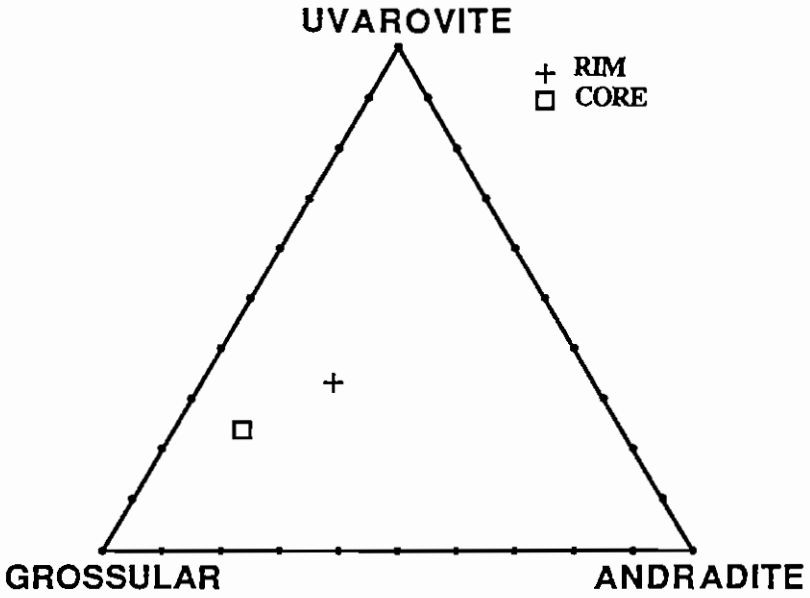


Cr RICH GROSSULAR

**FIGURE 5:** Electron microprobe analysis (mole %) of the core and rim of a zoned, green, Cr-rich, grossular garnet from the Iris River area.

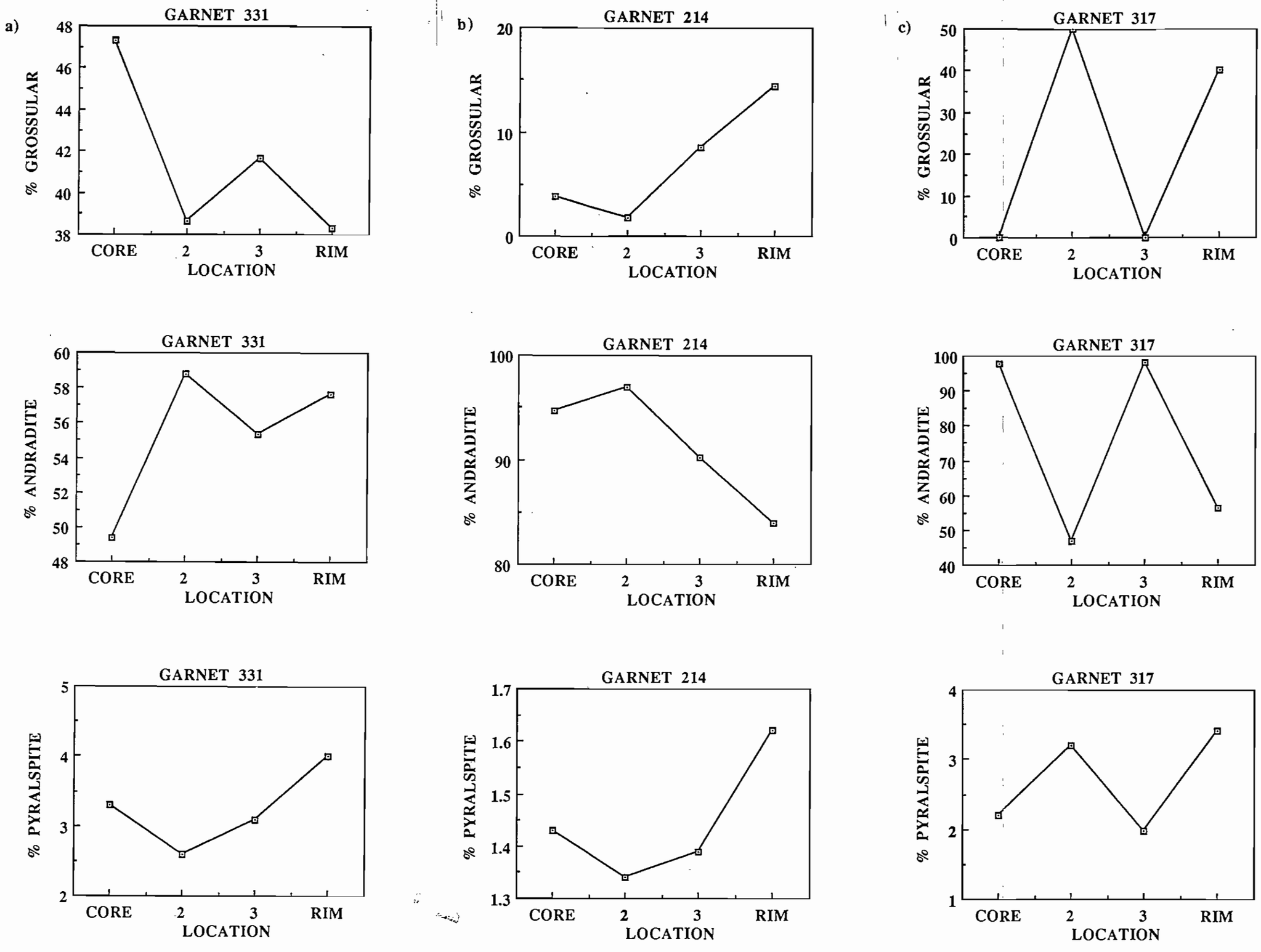


**FIGURE 6:** Electron microprobe core to rim analysis (mole %) of garnets from a)Stormont, b)Fletcher's Adit and c)Ti Tree Creek.

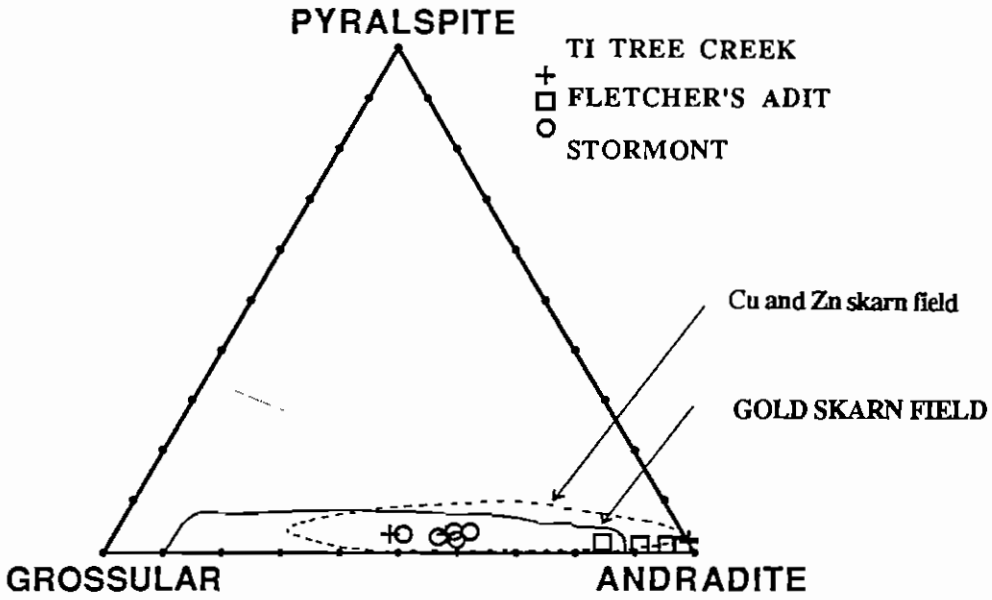


GARNETS FROM THE MOINA AREA

**FIGURE 7:** Electron microprobe analysis (mole %) of garnets from Stormont, Fletcher's Adit and Ti Tree Creek. Fields for gold, copper and zinc skarns are included (from Meinert, 1989, p. 544). Grossular = $Ca_3Al_2Si_3O_{12}$, andradite = $Ca_3Fe_2Si_3O_{12}$, and pyralspite = $(Mg,Mn,Fe)_3Al_2Si_3O_{12}$.

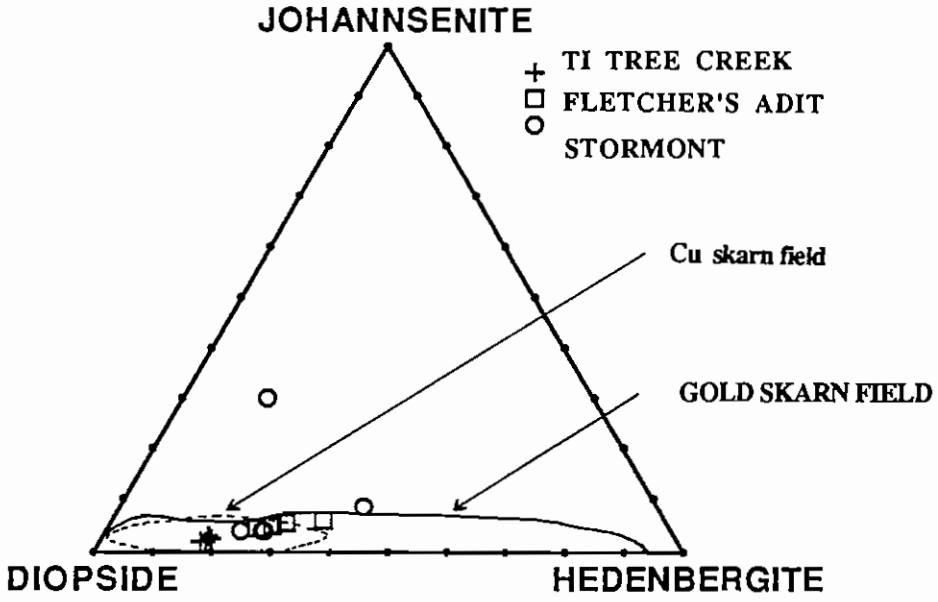


CLINOPYROXENES FROM THE MOINA AREA

**FIGURE 8:** Electron microprobe analysis (mole %) of clinopyroxenes from Stormont, Fletcher's Adit and Ti Tree Creek. Fields for gold and copper skarns are included (from Meinert, 1989, p. 544). Diopside = $CaMgSi_2O_6$, hedenbergite = $CaFeSi_2O_6$, and johannsenite = $CaMnSi_2O_6$.

### 5.2.2.2 Fletcher's Adit

Fletcher's Adit has an enormous number of complex textures and mineral assemblages. The skarn's appearance is "chaotic", as it consists of ovoid patches, lenses, laminae, swirls and concentric bands of a variety of mineral assemblages. The dominant minerals at Fletcher's Adit are garnet (which ranges in colour from light cream to dark brown and deep red), actinolite, magnetite (massive and wrigglitic), epidote, pyroxene and massive to finely laminated sulphides. Table 2 summarises the paragenesis of all the minerals identified at Fletcher's Adit.

In the coarse grained garnet-pyroxene-quartz-calcite-actinolite-magnetite skarn at Fletcher's Adit, garnets are up to 12 mm in diameter (Sample Nº 73920 [214]) and are euhedral when crystalising against calcite or quartz and subhedral when crystallising against other garnets. Retrograde alteration is restricted to the salites, and is more pronounced here than at Ti Tree Creek.

The garnets from Fletcher's Adit show the same trends as those at Ti Tree Creek, in that they have isotropic cores and anisotropic rims. In addition to the zonation of anisotropy, there is a zonation in the amount of salite inclusions in the garnet. The isotropic cores have only minor clinopyroxene inclusions and zoning is not obvious. The anisotropic garnets which comprise the rims have an abundance of clinopyroxene inclusions as well as obvious, narrowly spaced bands of alternating colour and chemical composition. These observations are consistent with the hypothesis that the anisotropic garnet represents a rapid growth period.

A core-to-rim compositional traverse of a garnet that shows the type of zonation described above is shown in Figure 6b. The garnet overall is andraditic in composition, varying from approximately 94 to 97 mole % andradite. The isotropic core corresponds to an extremely Fe-rich andradite, while the rim represents a grossular enriched andradite. Thus, in a similar fashion to the Ti Tree Creek garnets, it is the grossular enriched andradite that is responsible for the anisotropism.

The mole percentage of pyralspite is less than half the value seen at Ti Tree Creek and Stormont (Figure 6). The mole percentage of pyralspite in garnets from Fletcher's Adit shows

a sympathetic relationship with the grossular mole percentage and an antipathic relationship to the andradite mole percentage.

The analysis by electronprobe of the compositions of garnets from Fletcher's Adit that were analysed by electron microprobe are plotted in Figure 7. These compositions can be seen to be consistently and extremely iron-rich and are lower in Mn, $Fe^{2+}$ and Mg in comparison to garnets from the other two deposits. The garnet compositions for Fletcher's Adit plot mostly outside the fields defined by Meinert (1989) for gold, zinc and copper skarns, and do not resemble compositions found in Canadian iron skarns (Meinert, 1984).

Clinopyroxenes from Fletcher's Adit are salitic in composition and are distinct from those at Ti Tree Creek and Stormont, in that they are very low in aluminium (Appendix A). The compositions of four clinopyroxenes from this sample are plotted in Figure 8. From this ternary diagram, the salites from Fletcher's Adit can be seen to be lower in Mg, higher in Mn and higher in $Fe^{2+}$ than those at Ti Tree Creek. The only significant difference between the pyroxene compositions at Fletcher's Adit and those at Stormont is the occasionally anomalously high johannsenite mole percentage in pyroxenes from Stormont.

From the salite compositions plotted in Figure 8, it seems unlikely that Fletcher's Adit is a copper skarn. Although these compositions do plot within the gold skarn field the clinopyroxenes contain virtually no $Al_2O_3$, which is totally uncharacteristic of gold skarns. The clinopyroxene compositions at Fletcher's Adit do not resemble those found in iron skarns either (Meinert, 1984) which raises the question: What class of skarn is Fletcher's Adit?. This question is made harder to answer by the fact that Fletcher's Adit is a very low grade, polymetallic deposit, making classification by metal content inconclusive. The most probable answer is that Fletcher's Adit is a very low grade copper or iron skarn that has had its fluids modified by wall-rock reactions, so that fluid compositions differed from those which mineralized/metasomatised high grade Cu and Fe skarns. This could account for the slightly atypical calc-silicate compositions and low metal grades, and the unusual combination of metals at Fletcher's Adit compared with the classic examples.

#### 5.2.2.3 Stormont

The early metasomatic stage of Stormont's paragenesis is difficult to characterise because of extensive retrograde alteration and late stage leaching. Clinopyroxenes are relatively rare, with fresh, large and euhedral clinopyroxenes being virtually non-existent. The skarn at Stormont displays many "chaotic" textures that are similar to Fletcher's Adit, such as: ovoid pods, irregular laminae and bands of cream, brown and red garnet, massive actinolite and epidote alteration, and oxidised leached zones. The main differences between the two deposits are that Stormont has less garnet, more actinolite, more chlorite and epidote alteration, more numerous and extensive leached zones, and very little base metal sulphides, but has an elevated abundance of visible bismuth minerals and has minor sphene and rutile.

Plate 14 is an example of the ore-bearing skarn at Stormont, consisting of dark brown to red garnets, fibrous to coarsely crystalline actinolite, coarse grained calcite and some quartz that is inter-granular to the garnet, and often native bismuth and bismuthinite grains are present. Stormont does contain most of the features that characterise the skarns to the east, i.e. wrigglitic magnetite, garnet dominated zones, base metal sulphides and "stockwork" vein networks, but in lesser proportions.

The least altered skarn at Stormont consists of garnet, clinopyroxene, clear vesuvianite and the retrograde assemblage actinolite-quartz-calcite-opaques (Sample Nº 73942 [331]). The garnets here are yellow to light brown, zoned, euhedral to subhedral and relatively small (being on average 0.6 mm in diameter). Clinopyroxenes are included in the cores of garnets and occasionally in the rims, but rarely in between. Clinopyroxenes in the cores seem more susceptible to retrograde alteration, possibly implying a different composition to the later clinopyroxenes. These two generations represent an early metamorphic and a later metasomatic population.

Clear vesuvianite is included in the rims of the larger garnets implying a relatively early paragenetic position. In areas interstitial to garnet masses, clinopyroxene can be seen to be breaking down to actinolite-calcite-quartz and opaques. Maximum salite/actinolite ratios are in the order of 30:70.

The textures and mineral relationships of the early formed minerals at Stormont are almost identical to those at Ti Tree Creek and Fletcher's Adit, but are overprinted in most cases by extensive and pervasive retrograde alteration. For example, in areas interstitial to garnet clusters at Ti Tree Creek, the skarn would usually consist of granular clinopyroxenes with minor quartz and calcite, but at Stormont these areas are usually represented by just fibrous or crystalline actinolite (Plate 20), or occasionally by actinolite with clinopyroxene relicts. Stormont also commonly contains garnets that have corroded margins and atoll textures, which are textures not present at Ti Tree Creek or Fletcher's Adit.

Electron microprobe analyses of garnets from Stormont are given in Appendix A. The compositions obtained from a core-rim traverse across a zoned garnet from Stormont are plotted in Figure 6c. This single traverse shows a very different garnet composition trend in comparison with Ti Tree Creek and Fletcher's Adit. The garnet at Stormont is of andradite composition, but is much less iron-rich (being ≈49-60 mole % andradite) in comparison with the other two deposits that have andradite mole percentages in the high nineties. From core to rim the grossular mole percentage drops overall instead of rising, although it does fluctuate nearer the rim.

Similarities between Stormont and the other two deposits include an antipathic relationship between the andradite and grossular mole percentage, as well as the high similarity of the pyralspite mole percentage trend to that seen at Fletcher's Adit despite the differences in Al and $Fe^{3+}$ zonation (Figures 6a and 6b). The pyralspite mole % is much higher than the garnets from Fletcher's Adit and on average higher than those at Ti Tree Creek. The sympathetic relationship between the grossular and pyralspite mole percentages is less pronounced at Stormont than at the other two deposits.

Six garnet compositions have been plotted on a grossular-andradite-pyralspite ternary diagram (Figure 7). As with garnets from the other two deposits the Stormont examples belong to the grandite series, having only minimal pyralspite content. Six garnet compositions from Stormont plot in the centre of the gold skarn field and are more grossular-rich than most of the garnet compositions from the other deposits except for one microprobe analysis from a garnet from Ti Tree Creek (Figure 7).

The clinopyroxene compositions (Appendix A) indicate that Stormont's pyroxenes are salites, but vary greatly in Mn content. The $Al_2O_3$ content of pyroxenes at Stormont is generally much higher than at Fletcher's Adit, but lower than at Ti Tree Creek. The ternary diagram for clinopyroxene compositions in Figure 8 indicates that salites at Stormont contain $Mg:Fe^{2+}$ ratios that are similar to those at Fletcher's Adit and lower than those at Ti Tree Creek.

The unusual feature of clinopyroxene compositions at Stormont is the Mn content, or johannsenite mole percentage (Figure 8). Three out of five analyses have a Mn content that is similar to those reported for gold skarns; one is fractionally high and the remaining one contains more than three times the accepted levels of Mn concentration. Manganese concentration in pyroxenes is an indicator of a distal position in a skarn forming system, and therefore the clinopyroxene compositions shown in Figure 8 are consistent with the hypothesis that Stormont is the most distal of the skarns in the Moina area. As well as the Mn content of pyroxenes rising as the granite-to-prospect distance increases, the $Fe^{2+}/Mg$ ratio is known to increase also (Meinert, 1987). Stormont clinopyroxenes do show a $Fe^{2+}/Mg$ enrichment with distance from the granite in comparison to those at Ti Tree Creek. However, Stormont clinopyroxene cannot be distinguished from that at Fletcher's Adit.

At Stormont some of the epidote displays inclusion relationships that indicate that at some time garnet and epidote were co-precipitating (Sample Nº 73940 [329]). Typically garnet breaks down to epidote and other minor retrograde phases such as calcite, quartz and magnetite (Plate 21), but occasionally euhedral laths of epidote are included in the rims of sub to euhedral garnets (Plate 22).

Appendix B contains descriptions of thin sections representing the major types and styles of metasomatic rocks in the Moina area.

### 5.2.3 RETROGRADE ALTERATION

Minerals associated with retrograde alteration include actinolite, epidote, fluorite, biotite, K-feldspar, zoisite, apatite, green mica (possibly fucsite), sericite/muscovite, magnetite, quartz, calcite and chlorite. Opaque mineralogies will be discussed in Chapter 5.

Retrograde alteration increases in intensity towards the west, which may be a function of granite-to-prospect distance, fluid access, skarn permeability, the creation of a convecting meteoric water cell or the abundance of easily altered minerals (such as clinopyroxene). The major retrograde minerals and textures are consistent over the three skarns involved in this study and will be discussed in paragenetic order.

The earliest retrograde reactions form epidote and actinolite. Actinolite is produced from the breakdown of clinopyroxene and epidote from garnet. Euhedral epidotes are pre-, syn- and (very rarely) post-actinolite (using inclusion and textural relationships as evidence) but are generally less abundant than actinolite, due to the pyroxenes breaking down much more readily than the garnets during the retrograde alteration phase.

Actinolite first develops as small fibres rimming tabular salite crystals (Plate 23), then as pseudomorphs of salite crystals (Plate 22) and finally as the pyroxene-dominated zones become increasingly altered the actinolite becomes coarsely fibrous (Plate 14) or crystalline (Plate 20). During the last stages of this sequence, the actinolite replacement may become so intense that no pre-retrograde textures are preserved. The equation governing the breakdown of salite to actinolite is:

$$5Ca(Mg,Fe^{2+})Si_2O_6 + 3CO_2 + H_2O = Ca_2(Mg,Fe^{2+})_5Si_8O_{22}(OH)_2 + 3CaCO_3 + 2SiO_2$$

[Salite] [Actinolite] [Calcite] [Quartz]

(Modified from Deer et. al., 1980).

Actinolites from all three deposits have been analysed using the electron microprobe (Appendix A). All amphiboles analysed, except one from Stormont, are within the compositional range of actinolites, having values for [100Mg/(Mg+$Fe^{+2}$+$Fe^{+3}$+Mn)] between 20 and 42. The amphibole from Stormont had a [100Mg/(Mg+$Fe^{+2}$+$Fe^{+3}$+Mn)] value of 18 and is therefore classed as a ferro-actinolite (Deer et. al., 1980).

Amphibole compositions have been plotted on Mg-Fe-Mn and Mg-Fe-Al ternary diagrams in Figures 9 and 10, respectively. Actinolites from all three deposits are similar in Al and Mn content, with a single sample from Stormont being slightly enriched in Al. The most obvious trend is an increase in $Fe^{2+}$:Mg ratios from Fletcher's Adit to Ti Tree Creek to

Stormont. The reason for this compositional variation is not obvious as the $Fe^{2+}$:Mg ratios of salites from the three deposits increase from Ti Tree Creek to Stormont then to Fletcher's Adit.

There is a distinct lack of amphibole compositional data from skarn deposits, which makes comparisons between different classes difficult. Nevertheless the actinolites from Moina show no compositional resemblance to actinolites from Au-rich copper skarns (Figure 10), and are not as aluminous as amphiboles from high grade gold skarns (Meinert, 1989).

Epidote is more common at Stormont, due to a greater intensity of retrograde alteration being required to start to break down the garnets (in comparison to only small amounts of lower temperature fluid activity being required to alter clinopyroxene to actinolite). Given the paragenetic position of epidote at Stormont, the most likely reactions for the breakdown of grandite to epidote is:

$$3Ca_3(Fe^{+3},Al)_2Si_3O_{12} + 7CO_2 + H_2O =$$

[Grandite garnet]

$$2CaFe^{+3}Al_2O.OH(Si_2O_7)(SiO_4) + 7CaCO_3 + 3SiO_2 + O_2$$

[Epidote]

[From equations synthesised from Berman et. al.'s (1988) "Geo-calc" program].

The above retrograde reaction occurs as epidote rimming and replacing grandite garnets (Plate 21), and areas of large (up to 12 mm in length) epidotes containing small embayed relicts of garnet.

Large euhedral epidotes are commonly zoned and are pre-actinolite development (Plate 24). An electron microprobe traverse (Appendix A) of one of the zoned epidotes from Stormont (Plate 24) is shown in Figure 11. The amount of Al and $Fe^{+3}$ substitution in epidotes is measured by the percentage of pistacite ($Ps = 100Fe^{+3}/[Fe^{+3} + Al]$). Pistacite is a theoretical Fe-rich end member ($Ca_2Al_2FeSi_3O_{12}[OH]$) of the epidote family. Although some confusion exists in the nomenclature of epidote, it is generally accepted that epidote contains 15-33 mole % pistacite (Deer et. al, 1978). Mole % pistacite increases from 23.7 at the core to 27.1 at the rim for epidote from Stormont (Figure 11). Thus, this epidote is becoming progressively more iron-rich as it continues to crystallise. This trend indicates that the fluid composition is progressively becoming more Fe-rich with time.

PLATE 17: A photomicrograph of "wrigglite" skarn from Fletcher's Adit (Sample Nº 73898 [20]). Light layers are chlorite-actinolite-fluorite, while the dark layers consist of magnetite-pyrrhotite-pyrite. Transmitted plane light, long axis of the plate = 4mm, mag. 25x.

PLATE 18: A photomicrograph of a zoned andradite garnet from Ti Tree Creek (Sample Nº 73935 [317]). The yellow core of this garnet (and one band towards the top of the plate) is isotopic and andradite-rich. The cream portions of this garnet are anisotropic and are grossular enriched. Transmitted plane light, long axis of the plate = 2mm, mag. 50x.

PLATE 19: A photomicrograph of two green uvarovite garnets hosted in footwall calc arenites at Fletcher's Adit (Sample Nº 73904 [28]). Note the inclusions of small salite crystals in the core of the garnet on the left hand side of the plate. Transmitted plane light, long axis of the plate = 2mm, mag. 50x.

PLATE 20: Crystalline and fibrous actinolite amongst euhedral andradite garnets and calcite, from Stormont (Sample Nº 73925 [291]). Scale is indicated by a 1¢ coin.

PLATE 21: A photomicrograph of an anisotropic, zoned, andradite garnet being replaced by epidote, as a result of the intense retrograde alteration phase of skarn development present at Stormont (Sample Nº 73939 [326]). Transmitted polarized light, long axis of the plate = 1mm, mag. 100x.

PLATE 22: A photomicrograph of an embayed andradite garnet with an included, large, euhedral epidote (Sample Nº 73940 [329]). Note also the two included, tabular, clinopyroxene pseudomorphs (now actinolite, quartz and calcite), and the rim of retrograde quartz around the garnet in the lower right hand corner of the plate. Transmitted plane light, long axis of the plate = 1mm, mag. 100x.

PLATE 23: A photomicrograph of a salitic clinopyroxene being broken down to form actinolite, quartz and calcite (Sample Nº 73920 [214]). Note the presence of disseminated magnetite in association with actinolite. Transmitted plane light, long axis of the plate = 2mm, mag. 50x.

PLATE 24: A photomicrograph of zoned euhedral epidote crystals from Stormont (Sample Nº 73938 [325]). These large epidotes pre-date the fibrous actinolite. Transmitted polarized light, long axis of the plate = 4mm, mag. 25x.


17

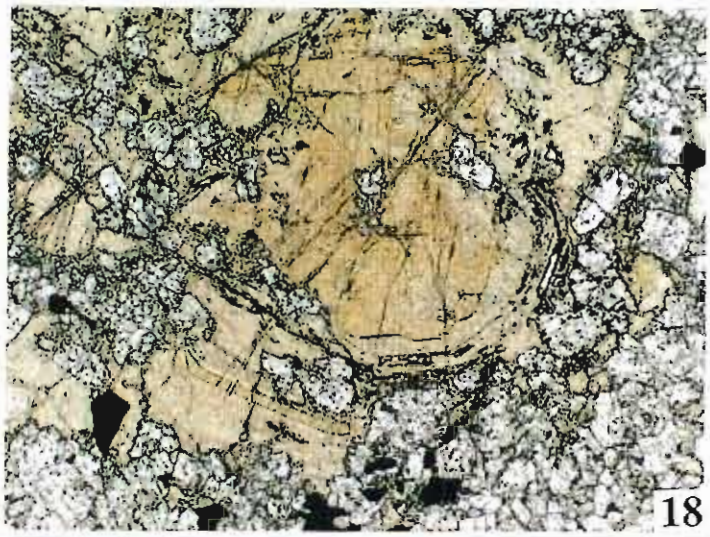
18


19


20


21


22


23


24

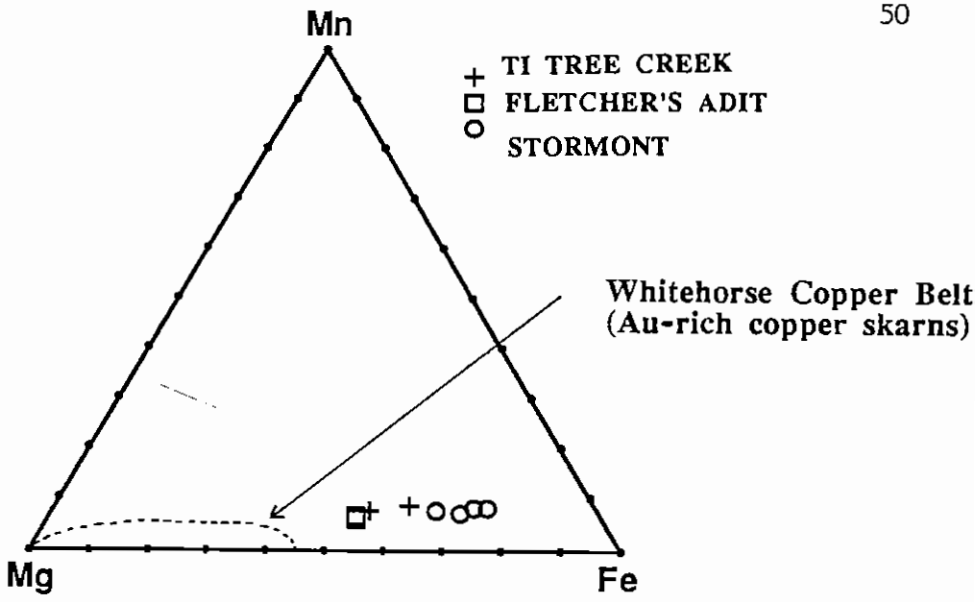


**FIGURE 9:** Electron microprobe analysis (Mg vs Fe vs Mn) of amphiboles from Stormont, Fletcher's Adit and Ti Tree Creek. The Whitehorse Copper Belt's field has been constructed from data in Meinert, 1986.

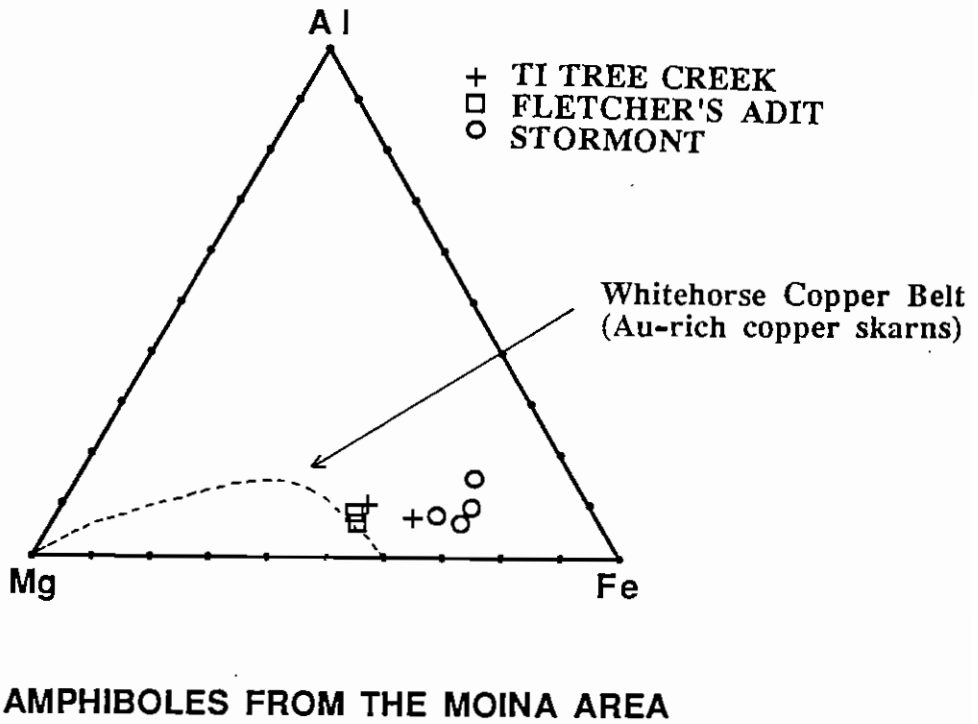


**FIGURE 10:** Electron microprobe analysis (Mg vs Fe vs Al) of amphiboles from Stormont, Fletcher's Adit and Ti Tree Creek. The Whitehorse copper belt's field has been constructed from data in Meinert, 1986.

Shortly following the growth of epidote, a phase involving abundant magnetite is formed. Magnetite is stable over much of the retrograde alteration stage (Tables 1, 2 and 3). Magnetite occurs as disseminations and is commonly intimately associated with actinolite. After epidote and actinolite have incorporated as much of the iron released from the breakdown of the salites and grandites as possible, magnetite appears to be the retrograde mineral that incorporates the excess Fe ($Fe^{2+}$ and $Fe^{3+}$). Magnetite also exists as wrigglite skarn with fluorite, actinolite and chlorite (Plate 17). Wrigglitic magnetite occurs after the disseminated magnetite and usually just before (or occasionally with) the start of the Fe-sulphide mineralization phase.

Fluorite is common in all three skarns. Fluorite occurs as the dominant constituent of veins containing sulphides (Plate 29), as granular fluorite-epidote-actinolite-magnetite retrograde skarn, as the light bands in wrigglite skarn, and as coarse green crystals in quartz-muscovite-fluorite greisen veins (Plate 25).

Chlorite occurs as chlorite-calcite veins and as an alteration product of actinolite and epidote. The chorite that occurs in late stage veins is commonly Mg-rich. The transition of epidote and actinolite to chlorite coincides with the change from the epidote-amphibolite facies to greenschist facies. The equation is as follows:

$$3(Mg,Fe)_5Al_2Si_3O_{10}(OH)_8 + 10CaCO_3 + 21SiO_2 =$$

[Chlorite]

$$2Ca_2Al_3Si_3O_{12}(OH) + 3Ca_2(Mg,Fe)_5Si_8O_{22} + 10CO_2 + 8H_2O$$

[Clinozoisite] [Actinolite]

(Deer et. al., 1980).

Minor retrograde phases include:

- boitite (which is commonly chloritised)
- a green mica (which is possibly fucsite and which forms tabular crystals and is associated with fluorite and actinolite)
- apatite (which occurs as small laths associated with quartz and fluorite)
- zoisite (which is intimately associated with actinolite and epidote)
- K-feldspar (which occurs as late stage veins and usually is pink in colour possibly due to disseminations of hematite).

#### 5.2.3.1 Veining

Veining is common in all three deposits, especially towards the base of the skarn. The majority of veins are orientated horizontally implying significant lateral movement of fluids. Lateral movement of late hydrothermal fluids was likely to have been promoted by the presence of relatively impermeable garnet and pyroxene skarn. The fractures that the veins infill may be either joints and small fractures that have retained their fracture permeability throughout the skarn forming process, or more likely are fractures produced by volume changes during the early stages of metasomatism.

Veining occurs throughout the entire paragenesis but is concentrated (or simply best preserved) during the retrograde alteration stage. Early garnet-quartz-calcite veins and late chlorite-calcite veins are rare, unlike the fluorite-feldspar-quartz-opaques, fluorite-muscovite-quartz-magnetite or epidote-fluorite-quartz-actinolite veins which represent the "actinolite replacement" stage of the paragenesis (Tables 1, 2 and 3). Quartz-muscovite-fluorite-opaques greisen veins are very abundant beneath the skarns (Plate 25) and often are surrounded by a halo of disseminated magnetite.

Very late stage leaching and oxidation of the skarn is normally restricted to intensely jointed and faulted areas (Plates 26 and 27). In these areas limonite (especially goethite) is widespread. The leaching of actinolite firstly results in the formation of a brown amorphous mixture of calcite, magnetite and silica. As oxidation continues this magnetite converts to hematite and finally to goethite, to give the skarn an orange colouration (Plate 26).

Appendix B contains descriptions of thin sections representing the major types and styles of retrograde alteration and vein zonations.

## 5.3 DISCUSSION

Metamorphic, metasomatic and retrograde rock types from all three skarns indicate the major calc-silicate phases are similar petrographically and occur in similar paragenetic sequences. Compositional differences occur in the metasomatic and retrograde phases, where the garnet, clinopyroxene and amphiboles from the three deposits can be seen to differ in

chemistry. The degree of retrograde alteration, mole % grossular in garnet and mole % johannsenite in clinopyroxene increases westwards.

The difference in clinopyroxene, amphibole and garnet compositions from the three deposits is highly significant in the classification of skarn deposits. Differences in the intensity of retrograde alteration are important for the style, type and grades of mineralization, due to the increase in permeability as retrograde alteration continues.

From reactions identified in each skarn's paragenesis (such as salite to actinolite and calcite to wollastonite), temperature estimates can be made by using internally consistent experimental data (such as Powell and Holland, 1988) or by comparison with skarn studies which utilise fluid inclusions and stable isotope geothermometry (such as Kwak and Askins, 1981a; 1981b).

To obtain a temperature estimate via the above methods, firstly an approximate pressure must be obtained. The skarns from the Moina area are hosted in Middle Ordovician sediments and were formed in the Late Devonian; therefore the only sediments that could have been stratigraphically above the Gordon Limestone during metasomatism are Eldon Group correlates. There are no Siluro-Devonian sediments in the Moina area now but thicknesses of a couple of kilometres most probably were present, as the Dolcoath Granite could not have intruded to extremely shallow levels without exploding (R.F.Berry, pers. comm., 1990). Kwak and Askins (1981a) tentatively suggest intrusion depths for the Dolcoath Granite of <3 km. Thus, confining pressures of 0.5 to 1 kb would seem reasonable.

The activity of $CO_2$ also strongly affects the construction of phase diagrams involving metasomatic phases associated with skarns. Workers in the field of skarn research assume very low values for $XCO_2$, usually 0.1 (Einaudi et. al., 1981).

Figure 12 displays the fields for contact metamorphism. The existence of wollastonite at Fletcher's Adit supports a hornblende-hornfels contact metamorphic facies. The formation of wollastonite from calcite and quartz is:

$$CaCO_3 + SiO_2 = CaSiO_3 + CO_2$$

This reaction occurs at ≈610 °C at 0.5 kb (Turner, 1981) which is in the high temperature region of the hornblende-hornfels facies stability field. This field can be seen to have an upper temperature limit of ≈630 °C at 0.5 kb (Figure 12).

The metamorphic crystallisation of Mg-rich clinopyroxene from dolomite and quartz at 0.5 kb occurs at ≈490 °C (Turner, 1981). The equation for this reaction is:

$$\underset{\text{(Dolomite)}}{CaMg(CO_3)_2} + 2SiO_2 = \underset{\text{(Diopside)}}{CaMgSi_2O_6} + 2CO_2$$

The andradite-salite assemblage that characterises the early metasomatic stage of all three skarns is typical of the hornblende-hornfels facies temperatures and pressures (350-600°C at 0.5 kb) (Webb, 1974). Kwak and Tan (1981), Shoj (1971) and Zharikov (1968) give optimal temperatures for the stability of andradite and diopside in skarns as approximately 550°C. Vesuvianite has been reported by Shoji (1971) and Sobelov (1972) to be stable at approximately 500°C.

Epidote can exist from 200-600°C but its optimal temperature of formation in epidote skarns is 300-500°C (Sobelov, 1972). Since some of the epidote can be seen to co-precipitate with the grandite and by far the majority of the epidote is pre-actinolite, temperatures are most likely to have been approximately 500°C.

The retrograde alteration of salite to actinolite occurs when water starts to enter the system and temperatures are less than 550°C (Turner, 1981; Kwak and Tan, 1981; Taylor and O'Neill, 1977). Actinolite can still be produced at temperatures down to 400°C, which accounts for the abundance of actinolite in a later paragenetic position than epidote. The formation of muscovite (or sericite) in the late greisen veins most likely occurred at temperatures in the range of 300-400°C, based on associated iron sulphide/oxide stabilities and optimal temperature as ranges defined by Sobelov (1972).

An $fO_2$-temperature phase diagram, at 0.5 kb of fluid pressure and $XCO_2 = 0.1$, for the system Ca-Fe-Si-C-O-H is given in Figure 13. The paragenesis of the earliest minerals formed in the Moina district (i.e. wollastonite, grandite, salite, quartz, calcite and magnetite) is represented by the bold arrow. The stable temperatures indicated in this diagram for each assemblage conform with those given above.

From Figure 13 it can be seen that $fO_2$ decreases with temperature (at least during the early stages of metasomatism) from approximately $10^{-23}$ to $10^{-26}$ over the first 100°C drop in temperature. An attempt was made to improve on Figure 13, by constructing a T-$fO_2$ diagram for P = 0.5 kb, $XCO_2$ = 0.1 but using the system Mg-Fe-Ca-Si-C-O-H, and considering the additional phases actinolite, epidote and grossular. The phase diagram was constructed using the Powell and Holland (1988) data base and the Berman et. al. (1988) "Geo-calc" program. Unfortunately the program appears to have difficulty in computing these compositions at such low oxygen activities. Nevertheless Figure 14 supports the notion that as temperature declined, the oxygen fugacity also declined. There are eleven possible metasomatic reactions that follow this trend defining a field where the fluid was most likely to be evolving (see Figure 14 for this field's position in T-$fO_2$ space).

The rationale for constraining the skarn forming fluid's chemical evolution with time is that the retrograde stage includes the mineralization stage. By understanding how the metasomatic, retrograde and mineralizing fluids (Chapter 6) change in chemistry with time, hypothesises can be synthesised concerning why Stormont is a gold-bearing skarn in a tin-tungsten skarn forming granite system (Chapter 12).

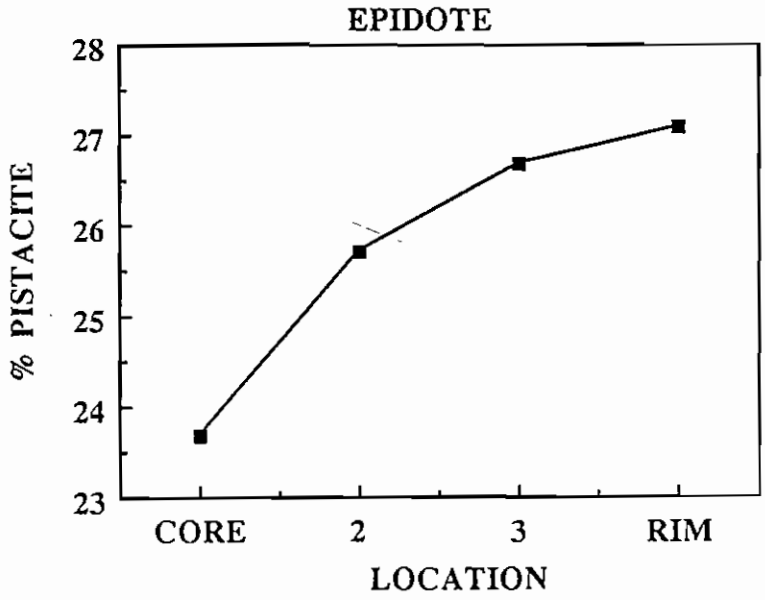


**FIGURE 11:** Electron microprobe core to rim analysis (mole % pistacite) of a zoned epidote from Stormont. % pistacite = $100Fe^{3+}/[Fe^{3+}+Al]$ (Deer et. al., 1978, p. 3).

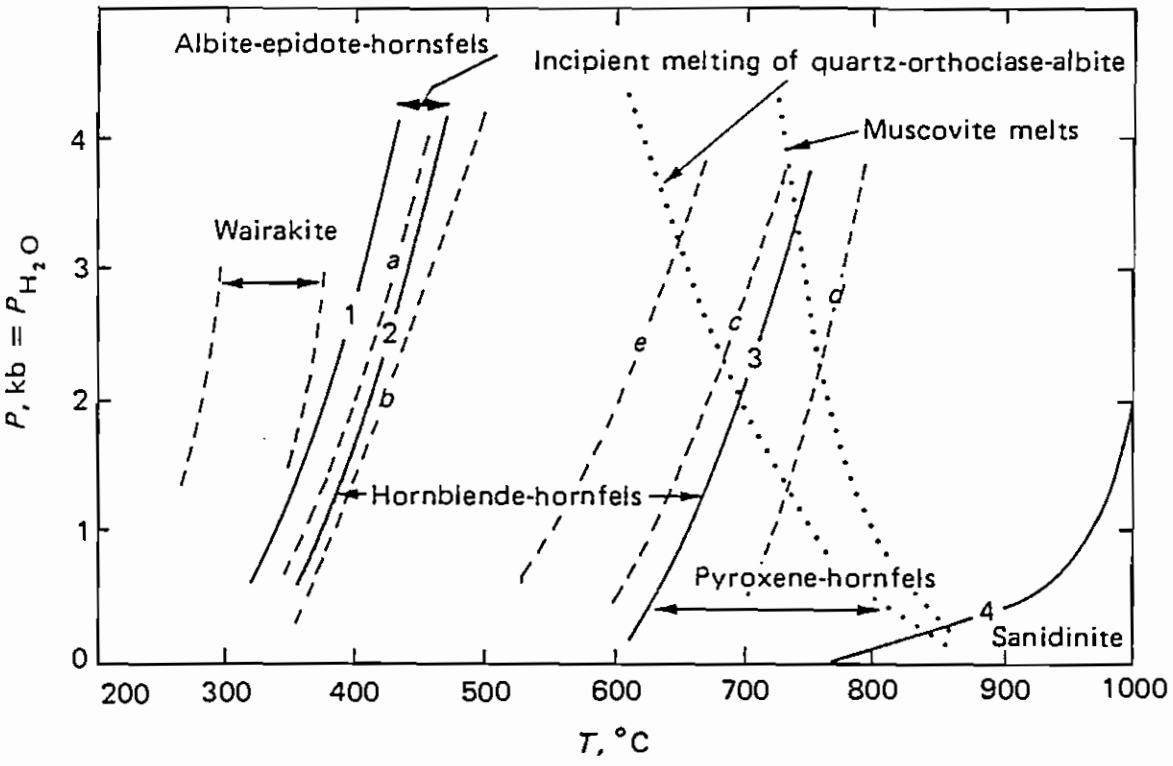


**FIGURE 12:** Temperature-pressure fields of facies of contact metamorphism. From Turner, 1981, p. 296.

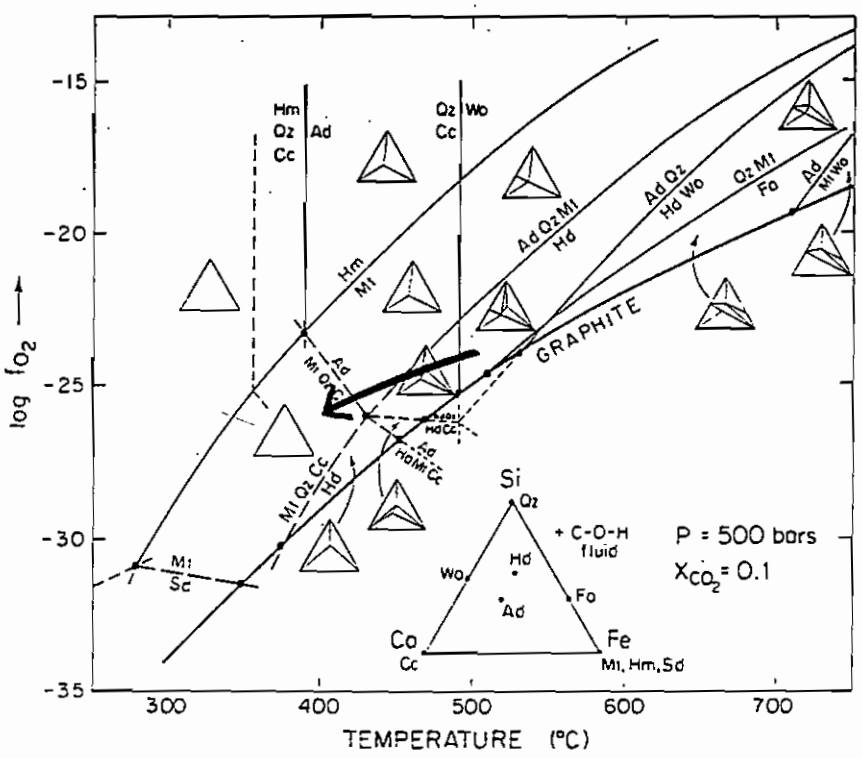


**FIGURE 13:** Log $FO_2$-temperature phase diagram at 500 bars fluid pressure, $X_{CO2} = 0.1$, for the system Ca-Fe-Si-C-O-H. Standard abbreviations used. From Einaudi et. al., 1981, p. 373.

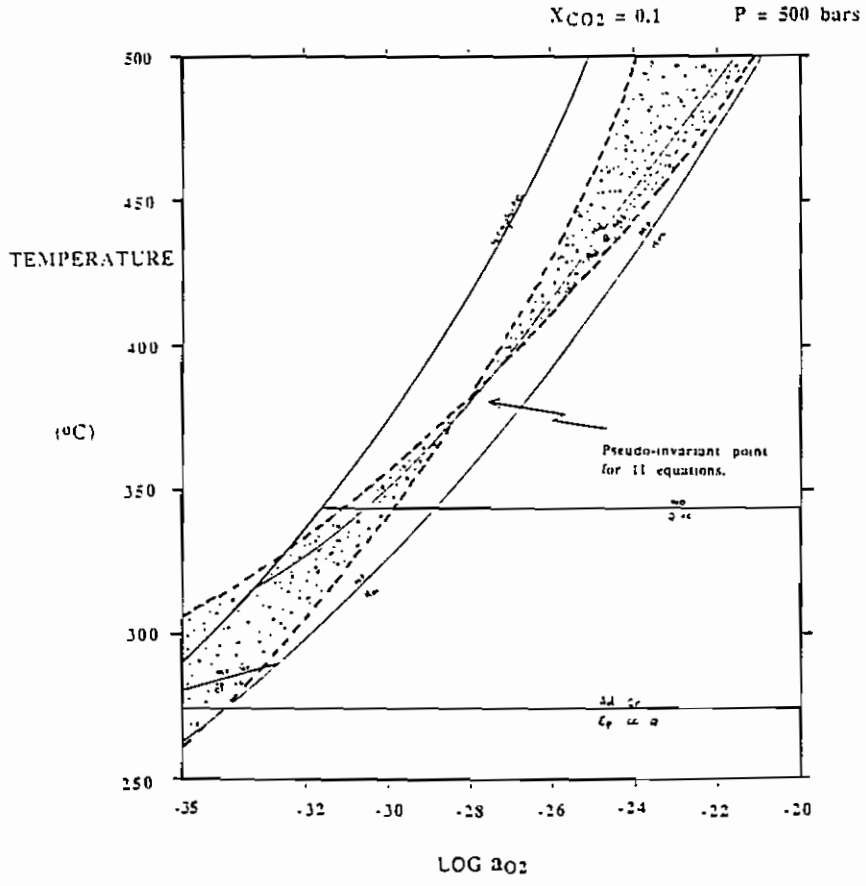


**FIGURE 14:** Log $a_{O2}$-temperature phase diagram at 500 bars fluid pressure, $X_{CO2} = 0.1$, for the system Ca-Fe-Mg-Si-C-O-H. Reactions that are plotted involve phases present at Stormont. Stippled area is a zone which contains 11 reactions relevant to skarn formation at Stormont. Reactions in this zone occur at all stages of the paragenesis, and therefore the stippled area is a good indication of the metasomatising fluid's evolutionary path (i.e. as T decreases, $FO_2$ decreases). Graph calculated via Berman et. al.'s (1988) "Geo-calc" program, using the Powell and Holland (1988) data base.

# CHAPTER 6

# MINERALIZATION

## 6.1 INTRODUCTION

Tables 1, 2 and 3 summarise the paragenesis of the opaque minerals in each deposit. In a similar fashion to the silicates, the major opaque minerals can be seen to have a paragenetic sequence that is consistent across the three deposits.

Apart from very small amounts of disseminated scheelite and powellite, the opaque mineralogies were introduced during the retrograde phase of the three skarns' evolution. The mineralization field in the paragenesis tables (Tables 1, 2 and 3) has been divided into three sectors. The earliest of these divisions corresponds to the first appearance of an Fe sulphide phase, either pyrrhotite or pyrite. The intermediate division starts when native bismuth becomes abundant. The latest division corresponds to the end of native bismuth, chalcopyrite, sphalerite, pyrite, pyrrhotite and magnetite precipitation, and the start of hematite, goethite and supergene native gold formation. Obviously these divisions vary slightly in timing between the deposits, but they seem to fall into distinct stages and make paragenetic comparisons more comprehensible.

## 6.2 OPAQUE MINERALS

### 6.2.1 SCHEELITE AND POWELLITE

Scheelite ($CaWO_4$) and powellite ($CaMoO_4$) were identified with the use of an ultraviolet lamp. This technique must be used with caution due to the abundance of fluorite in these deposits. Generally scheelite fluoresces to a bright white, powellite to a bright yellow and fluorite to a purple-white. Minor amounts of scheelite and trace amounts of powellite were found in all three skarns as disseminated specks interstitial to garnets and in calcite veins. Scheelite is finer grained than the powellite. Powellite forms isolated crystals up to 1 $mm^3$.

### 6.2.2 MAGNETITE

Magnetite first appears very early in the paragenesis as small disseminations associated with the breakdown of Fe-rich calc-silicate phases (Plate 28). Precipitation of massive and wrigglitic magnetite followed the formation of the disseminated variety. Wrigglitic magnetite

(Plates 13 and 17) originates from fractures and often is overprinted by massive magnetite, possibly due to later remobilisation. The magnetiferous rocks often have large (up to 2 mm in diameter) hexagonal crystals of magnetite at the contact between the massive magnetite and the calc-silicate skarn.

At Fletcher's Adit (Sample Nº 73898 [20]) the opaque bands of wrigglite skarn consist of alternating assemblages of magnetite>pyrrhotite, pyrite, pyrrhotite>magnetite, pyrrhotite and pyrite+magnetite. The bands that contain pyrrhotite often have small amounts of late chalcopyrite replacement. Magnetite displays textural stability over most of the retrograde alteration stage defined in Tables 1, 2 and 3, but by far the majority of the magnetite is formed in the late "actinolite replacement stage" and early "mineralization stage". The abundance of magnetite decreases westwards, as does the proportion of wrigglite giving way to massive and disseminated magnetite.

Large euhedral crystals of magnetite commonly nucleate on andraditic garnets at Fletcher's Adit (Sample Nº 73894 [4]). This phenomenon can be explained by a lack of $Fe^{3+}$ and/or oxygen in the hydrothermal fluid. The $Fe^{3+}$ and/or oxygen is scavenged from the Fe-rich garnets (up to ≈98 mole % andradite at Fletcher's Adit) to form magnetite ($Fe^{2+}Fe^{3+}{}_2O_4$).

### 6.2.3 PYRRHOTITE

Pyrrhotite is not present at Ti Tree Creek, is a major sulphide phase at Fletcher's Adit and is rare at Stormont. Pyrrhotite is commonly the earliest of the iron sulphides. Pyrrhotite occurs with magnetite in the wrigglite skarn and as massive sulphide replacement (Plate 32). Pyrrhotite is present in the footwall hornfelsic shales/arenites and as disseminations and pods of sulphide in permeable horizons. Pyrrhotite grains are often concentrically surrounded by actinolite, then (?)wollastonite and then biotite in altered argillaceous arenites (Plate 33). More massive pyrrhotite can be seen to have been replaced by marcasite (Plate 34) and pyrite.

### 6.2.4 PYRITE

Pyrite occurs as disseminations in the footwall, skarn and marble front, as grains in greisen veins especially towards the base of the skarn and in the footwall (Plate 29), and occasionally as a massive sulphide replacement of limestone. Pyrite is the most common sulphide phase at Ti Tree Creek occurring as disseminations in the magnetite skarn, as

euhedral to subhedral crystals in fluorite-quartz-epidote-calcite veins and more rarely in actinolite-quartz-calcite veins. Pyrite crystals are typically situated in the centre of zoned veins, being intimately associated with fluorite and quartz.

At the old workings at Fletcher's Adit, large veins of actinolite-quartz-fluorite-sericitised K-feldspar-muscovite introduce pyrite with magnetite, pyrrhotite, marcasite, bismuthinite and native bismuth (Plate 32). Pyrite here is either syn- or post- pyrrhotite. Occasionally pyrite occurs as delicate laminations in a wrigglitic texture (Plate 31).

### 6.2.5 MARCASITE

Marcasite is a rare mineral in the Moina area being found only in one sample from Fletcher's Adit. Here marcasite replaces pyrrhotite (Plate 34). The large marcasite grains contain lunate or crescentic fractures which are orientated in different directions throughout the slide. This texture is typical of marcasite (or pyrite) replacing pyrrhotite which results in a change of the unit cell's volume and therefore facilitates fracturing (R.R. Large, pers. comm., 1990).

### 6.2.6 ARSENOPYRITE

Small amounts of arsenopyrite occur at Fletcher's Adit as small bladed crystals associated with native bismuth and a Bi-Te-sulphide.

### 6.2.7 NATIVE BISMUTH

Thirteen bismuth-bearing minerals from all three deposits were analysed by electron microprobe (Appendix A). Table 6 is a summary of these compositions. In general the Bi-bearing minerals occur where inter-crystalline and/or fracture permeability is high (either in fractures or in areas of massive actinolite replacement). They usually occur as discrete disc-shaped grains or as replacements of earlier Fe-sulphides. A consistent replacement texture is bismuthinite replacing native bismuth.

Native bismuth is rare at Ti Tree Creek, occurring as isolated anhedral masses, and is commonly positioned interstitially to magnetite euhedra (or less commonly garnet). Associated minerals include bismuthinite and galenobismutite.

PLATE 25: An example of the muscovite-quartz-fluorite veins hosted in the footwall arenites and argillites (Sample Nº 73896 [10]). These veins commonly infill joints that are abundant in the hinge regions of folds (see Plate 6). Scale is indicated by a 1¢ coin.

PLATE 26: The leached, high grade Au-Bi ore from Stormont (Sample Nº 73937 [322]). This oxidised sample assays approximately 12 ppm of Au, over a 1m interval. Scale as shown.

PLATE 27: An alteration front associated with the late stage oxidation and leaching at Fletcher's Adit (Sample Nº 73905 [32]). The light green skarn is comprised of actinolite and pyroxene. Fluids are able to easily penetrate the actinolite-rich areas. Scale is indicated by a 1¢ coin.

PLATE 28: A photomicrograph of an example of the early stages of actinolite replacement (Sample Nº 73920 [214]). Granular clinopyroxenes are surrounded by actinolite and disseminated magnetite, while the small euhedral garnets are unaltered. Note the large areas of calcite and quartz, with fibrous actinolite. Transmitted plane light, long axis of the plate = 4mm, mag. 25x.

PLATE 29: An example of the near-horizontal fluorite veins at the base of the skarn at Fletcher's Adit (Sample Nº 72903 [27]). These veins cut skarn which is predominantly garnetiferous, but contains some massive magnetite and disseminated pyrite. Scale is indicated by a 1¢ coin.

PLATE 30: A photomicrograph of a single opaque band from "wrigglite" skarn (Sample Nº 73894 [4]). Fluids moved in the direction from the top of the plate to the bottom, precipitating fluorite and then magnetite ± pyrrhotite. Note the late stage brown-coloured oxidation of the actinolite ± chlorite. Transmitted plane light, long axis of the plate = 1mm, mag. 100x.

PLATE 31: Fine laminae (could be classified as wrigglite) of pyrite in chlorite-actinolite-clinopyroxene skarn from Fletcher's Adit (Sample Nº 73898 [20]). Note the abundance of micro-veins and complex textures. Scale is indicated by a 1¢ coin.

PLATE 32: The most mineralised sample collected from the Moina area (Sample Nº 73929 [292]). Pyrrhotite, magnetite, bismuthinite, marcasite, pyrite and chalcopyrite are associated with several generations of veins containing fluorite, K-feldspar, quartz and muscovite. Scale is indicated by a 1¢ coin.


25

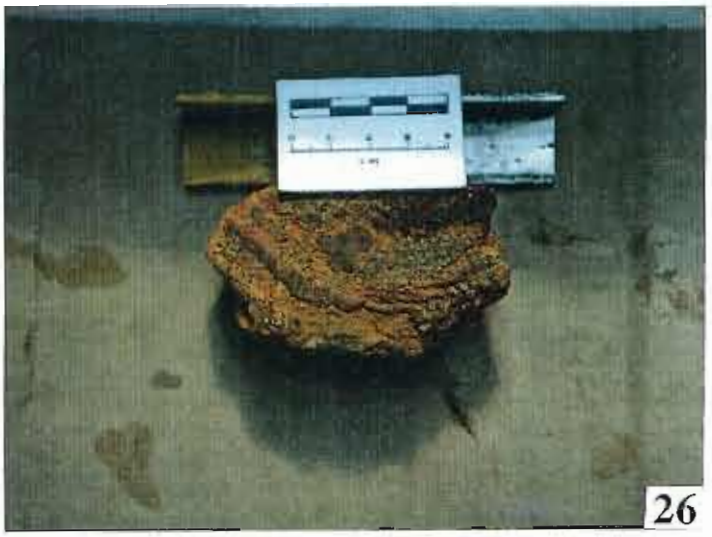
26


27

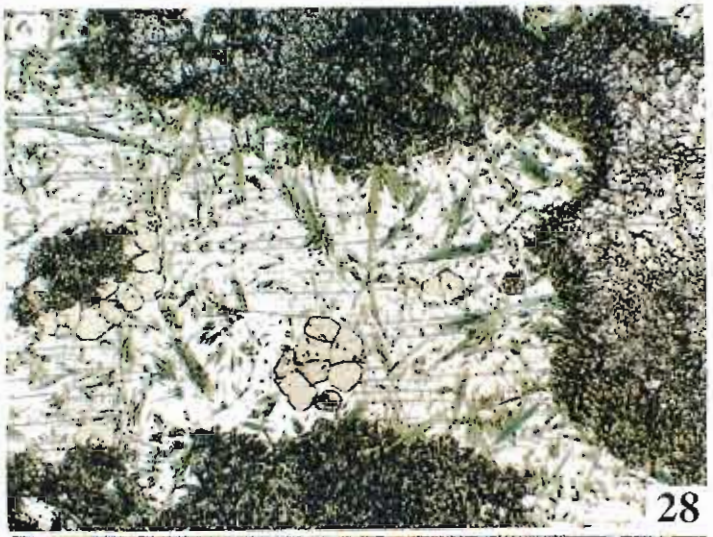
28


29

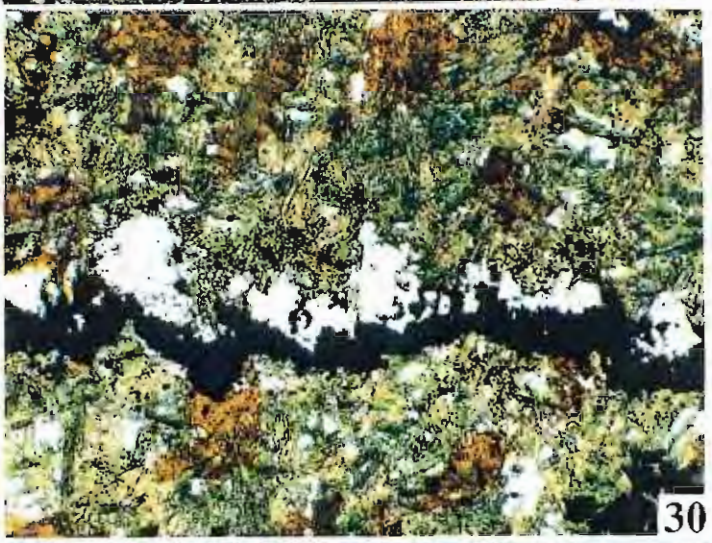
30


31


32

At Fletcher's Adit native bismuth occurs with bismuthinite and rarely with a Bi-Te-sulphide. Native bismuth is found in portions of the skarn that have a high fracture or inter-crystalline permeability. At Fletcher's Adit bismuthinite is more abundant than native bismuth.

Stormont has an abundance of native bismuth. Plate 35 depicts a 2 mm wide, white/cream, cleaved grain of native bismuth. Commonly native bismuth is replaced by bismuthinite (Plate 35). The large grains of native bismuth and bismuthinite are found in areas of intense actinolitic replacement (Plates 14 and 20) but are interpreted to be later than the actinolite replacement process. This association with actinolite is due to increased permeability in these rock types.

### 6.2.8 BISMUTHINITE

Bismuthinite at Ti Tree Creek exists in close association with galenobismutite and to a lesser extent native bismuth. Bismuthinite also occurs interstitially to magnetite grains. At Fletcher's Adit the bismuthinite occurs as grains associated with other sulphides. Commonly small amounts of bismuthinite replace the edges of pyrrhotite.

Stormont has an abundance of large bismuthinite grains (up to 5 mm in diameter) which are either syn- or post-native bismuth (Plate 35). At Stormont bismuthinite occurs in the same rock types as native bismuth. Bismuthinite from Stormont and Fletcher's Adit on average contains small amounts of Cu and Pb (Table 6). This substitution (Cu and Pb with Bi) probably accounts for a significant proportion of Stormont's Cu and (to a lesser extent) Pb contents.

### 6.2.9 GALENOBISMUTITE

Galenobismutite ($PbBi_2S_4$) is a very common bismuth mineral in metasomatites from Ti Tree Creek, but has not been identified in samples from the other two deposits. Metal correlation matrices for Stormont and Fletcher's Adit suggest that this mineral (or another type of Pb-Bi sulphide) is present in these deposits. Galenobismutite has not been identified west of Ti Tree Creek primarily because this mineral is very similar in appearance to bismuthinite, and only thirteen bismuth minerals were analysed during this study.

Galenobismutite occurs in voids between magnetite octahedra and in fractures passing through areas of massive magnetite. Table 6 indicates that on average the galenobismutite is very pure with only trace amounts of gold.

### 6.2.10 $Bi_{5.8}TeS_{3.6}$

Only one grain of this mineral was analysed (Table 6) which may mean that this analysis does not represent a discrete phase, but an intergrowth of two minerals that cannot be distinguished optically. If this analysis does represent a discrete phase then it is either a new or very rare mineral, as its molecular formula does not correspond with any of the bismuth minerals known to a specialist in bismuth minerals, Dr. G. Mummy at the C.S.I.R.O in Melbourne (pers. comm., 1990).

The one occurrence of this mineral from Fletcher's Adit is shown in Plate 37. It occurs paragenetically after native bismuth and is either syn- or (more likely) pre-chalcopyrite.

### 6.2.11 SPHALERITE

Only minor sphalerite was identified at Fletcher's Adit (Sample Nº 73920 [214]), where it exists as small anhedral grains and is associated with pyrrhotite.

### 6.2.12 CHALCOPYRITE

Chalcopyrite is present in all three deposits and decreases in abundance to the west. At Ti Tree Creek, chalcopyrite is the latest of the base metal sulphides commonly replacing pyrrhotite, magnetite and rarely galenobismutite, or occurring in veins with pyrite, magnetite and galenobismutite. At Fletcher's Adit, chalcopyrite commonly replaces pyrrhotite (Plate 36), magnetite, co-precipitates with and replaces bismuthinite, replaces the "$Bi_{5.8}TeS_{3.6}$ mineral", but rarely replaces pyrite.

At Stormont chalcopyrite is not common as indicated by the average grade of Cu in skarn rock types of 38 ppm (Table 4). Chalcopyrite occurs as small anhedral grains and replaced rims of larger grains of pyrrhotite.

### 6.2.13 NATIVE GOLD

Native gold has only been identified in this study in the very oxidised and leached zones associated with faults and major joints. Plate 26 depicts a sample of highly oxidised and

Au-rich skarn (averaging 12 ppm over a metre) associated with areas of intense and focused leaching.

Sample Nº 73937 [322] is an example of the high grade leached Au-Bi ore at Stormont. This sample consists of sub to euhedral epidote (≈30 modal %), poikiolitic quartz (≈40%), goethite and limonite (≈28%), and small grains of bismuthinite and native gold (≈1-2%). The native gold is not intergrown with bismuthinite, but occurs as rounded, discrete anhedral grains which are up to 0.1 mm in size. The gold is associated with bismuthinite (rather than native bismuth) and with the larger areas of quartz in this rock type (Plates 38 and 40).

Electron microprobe analysis of five gold grains (from Stormont) are given in Appendix A and summarised in Table 6. The five analyses indicate that these grains have a very consistent fineness, with the average fineness (defined as 1000Au/(Au+Ag)) being 822.1 (Figure 15). All grains are therefore native gold by definition containing less than 20 wt% Ag.

### 6.2.14 HEMATITE

Hematite at Ti Tree Creek can be found in the weathered portions of the magnetite-pyrite skarn. A sample from the Ti Tree Creek area (Sample Nº 73923 [256]) is an excellent example of hematite rimming pyrite cubes and filling fractures which anastomose through areas of massive pyrite and magnetite.

At Stormont minor hematite occurs in the Au-rich leached zones as "boxwork" pseudomorphs, presumably after magnetite or possibly pyrite. This association is consistent with the hypothesis of late, low temperature (and/or oxidised) Au-rich fluids passing through these areas of high, fracture-controlled permeability.

### 6.2.15 GOETHITE AND LIMONITE

Within the leached Au-Bi ore, acicular actinolite crystals have been replaced by limonite. The dominant constituent of the limonite is goethite. Goethite pseudomorphs the actinolite fibres and replaces most of the hematite "boxwork" textures.

**PLATE 33:** A mineralised worm burrow in the footwall calc arenites (Sample Nº 73930 [305]). These burrows are consistently mineralised in the same concentric sequence from centre to margin, i.e. from pyrrhotite to actinolite to (?)wollastonite to biotite. Scale is indicated by a 1¢ coin.

**PLATE 34:** A photomicrograph of marcasite replacing pyrrhotite at Fletcher's Adit (Sample Nº 73929 [292]). Note the crescentic fractures which are a common texture resulting from this type of replacement. Reflected plane light, long axis of the plate = 1mm, mag. 100x.

**PLATE 35:** A photomicrograph of bismuthinite (blue) and native bismuth (white) at Stormont (Sample Nº 73936 [320]). Small quantities of native bismuth is preserved in the centre of the later bismuthinite grain. Reflected plane light, long axis of the plate = 2mm, mag. 50x.

**PLATE 36:** A photomicrograph of pyrrhotite, magnetite, native bismuth and chalcopyrite at Fletcher's Adit (Sample Nº 73903 [27]). Reflected plane light, long axis of the plate = 0.5mm, mag. 200x.

**PLATE 37:** A photomicrograph of a Bi-Te-sulphide (blue) intergrown with native bismuth (white), from Fletcher's Adit (Sample Nº 73906 [35]). Chalcopyrite is either syn- or post-native bismuth. Pyrite and magnetite are early phases. Reflected plane light, long axis of the plate = 0.25mm, mag. 400x.

**PLATE 38:** A photomicrograph of the oxidised Au-Bi ore sample from Stormont shown in Plate 26 (Sample Nº 73937 [322]). The small yellow/white specks are native gold. Note the "boxwork" textures on the left hand side of the plate, formed by progressive oxidation of pyrite to form hematite, and finally goethite. The bulk of the Au mineralisation is interpreted to be associated with the pyrite to hematite stage. Reflected plane light, long axis of the plate = 1mm, mag. 100x.

**PLATE 39:** Metasomatised, interbedded hornfelsic shale and calc arenite from the Iris River area (Sample Nº 73916 [140]). The green units consist of actinolite, pyrrhotite and quartz. The white reaction rim is (?)wollastonite. The pink units are metamorphosed shale containing some biotite. Units like this provide strong evidence for lateral fluid migration. Scale is indicated by a 1¢ coin.

**PLATE 40:** A photomicrograph of native gold associated with goethite and quartz from Stormont (Sample Nº 73937 [322]). Note the partially fibrous nature of the goethite. Reflected plane light, long axis of the plate = 0.25mm, mag. 400x.


33

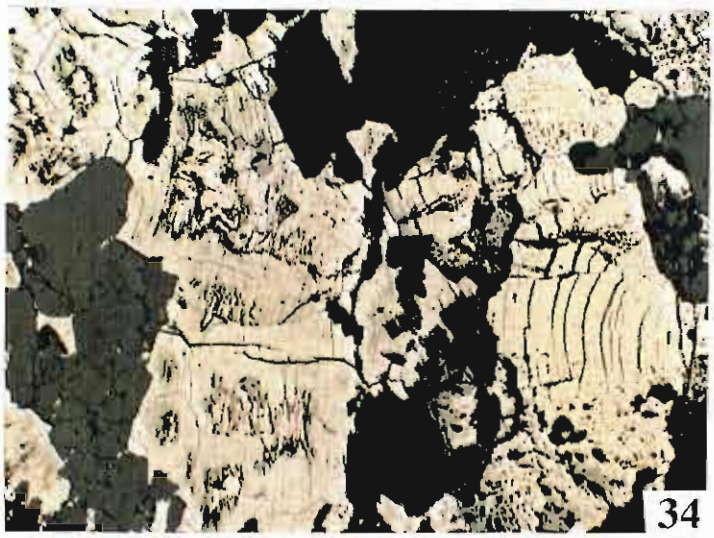
34

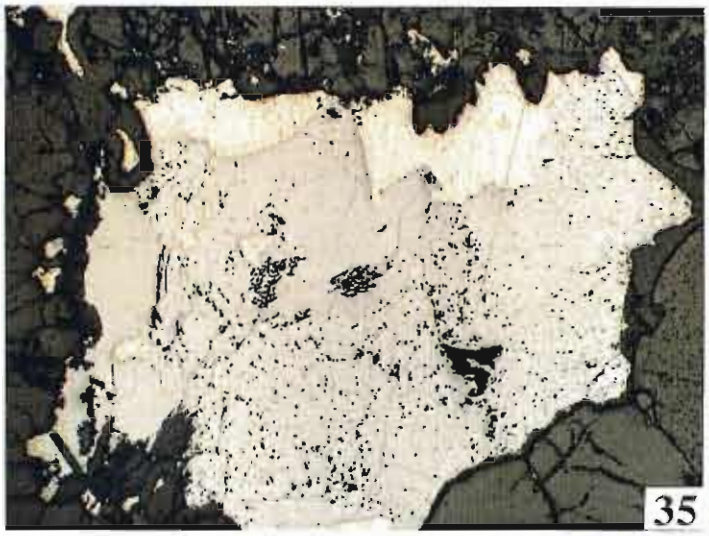
35

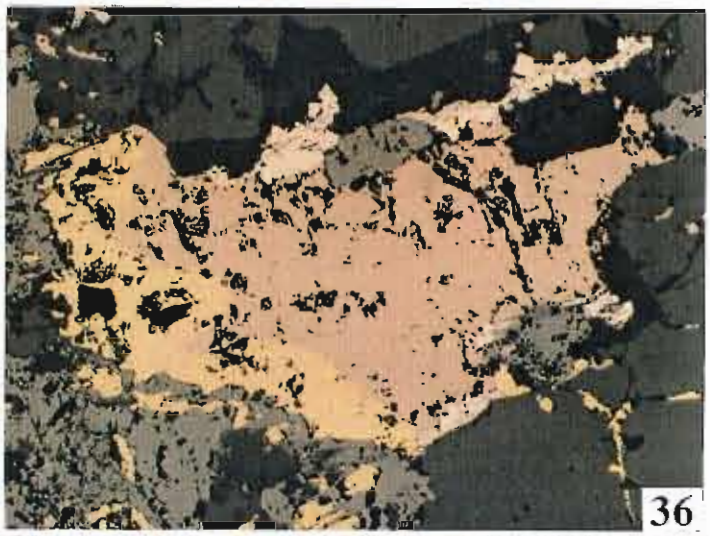
36


37

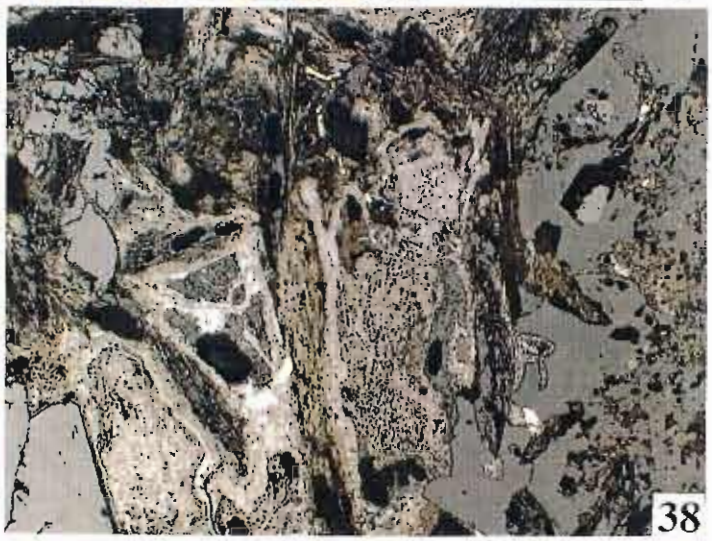
38


39


40

## 6.3 STYLE AND GRADE

Tables 4 and 5 contain the statistics for metal grades from Stormont and Fletcher's Adit, respectively. These statistics were obtained by taking all the assays from skarn rock types intersected in drill holes SD 1-SD 6 and FD 1-FD 9. Analyses that were below the detection limit for each element were recorded as zero values. For Stormont 75 samples were assayed, while at Fletcher's Adit 165 were analysed.

Very small amounts of scheelite and powellite were found as isolated disseminated grains in the garnetiferous portions of all three skarns, and abundances decrease westward.

No wolframite was identified in either of the deposits, indicating that the tungsten present in the metasomatic rock types originates from scheelite. Similarly no molybdenite was identified, so the Mo content (albeit extremely low) of each skarn most likely reflects the quantity of powellite present.

Some of the $W^{4+}$ could substitute for $Fe^{3+}$ or $Ti^{4+}$ into the lattice of the andradite garnets, perhaps explaining why Fletcher's Adit (with its high modal percent of garnet and mole percentage of andradite in these garnets) has higher W grades than Stormont.

Table 5 indicates that the W content of Fletcher's Adit is substantial in comparison to other metals present in this skarn. Stormont however contains very little W. The Mo content of both skarns is virtually negligible, although Mo grades tend to peak in the footwall vein systems (Chapter 8).

Tin occurs rarely as cassiterite, with only a few grains of cassiterite found in wrigglite skarn from Fletcher's Adit. Tables 4 and 5 indicate that Sn grades can be as high as 0.3% at Fletcher's Adit, but average approximately 540 ppm. Stormont has less Sn, averaging approximately 12 ppm. Kwak and Askins (1981a) reported that garnets from the Moina skarn to the east contained up to 0.7 wt% Sn in solid solution. It is likely therefore that the majority of the Sn at Stormont and Fletcher's Adit is incorporated in the andradite garnet (especially at Fletcher's Adit where the andradite mole % of the garnets reaches ≈98). It is unlikely that Sn occurs in sphene, as Stormont has the highest proportions of this mineral and also the lowest Sn grades. No malayaite was identified.

Pyrrhotite and pyrite are the first of the base metal sulphides. They occur as small anhedral grains associated with wrigglitic magnetite and occasionally as massive sulphide pods. The more massive variety occurs at Fletcher's Adit, where the sulphide mineralization stage is more voluminous, commonly consisting of massive pyrrhotite, pyrite, marcasite, chalcopyrite and arsenopyrite as well as magnetite (Plate 32). The massive sulphide patches are confined to areas that are intensely jointed or faulted, such as the small workings at Fletcher's Adit where there is an obvious fault, and base metal sulphides (with magnetite) comprise up to 90% of the skarn.

Tables 4 and 5 show arsenic to be in low abundance in both deposits, reflecting the low quantities of arsenopyrite. The lack of As at Stormont is significant in that most large grade, North American gold skarns have anomalous amounts of this element (Meinert, 1989).

Zinc content is quite high in both deposits considering only a small number of grains of sphalerite were identified. Webb (1974) postulates that Zn (and Cu) may substitute into the clinopyroxene lattice (for $Fe^{2+}$), but this suggestion seems unjustified as electron microprobe analysis reveals no such substitution and the paragenetic positions of salite and the late sulphide stage are distinctly separated (Tables 1, 2 and 3). It is a strong possibility however that Zn (and Cu) are substituting for $Fe^{2+}$ in actinolite.

Average Pb grades are less than half the average Zn grades at both deposits. Galena was not observed in any of the three skarns. The Pb present in these skarns is found in galenobismutite and in solid solution in bismuthinite (Table 6).

Cu occurs principally as small inclusions of chalcopyrite and replacement relationships indicate that chalcopyrite occurs late in the paragenesis. Cu grades are over three times as large at Fletcher's Adit when compared to Stormont, which is consistent with the modal abundance of chalcopyrite from these two deposits. Minor amounts of Cu also substitute into the lattices of native bismuth, bismuthinite and probably actinolite (a common feature of actinolites from the gold-rich skarns from theWhitehorse copper belt [Meinert, 1986]).

Bismuth occurs as native bismuth, galenobismutite, bismuthinite and rarely as Bi and Te sulphide(s). The majority of the bismuth minerals occur late in the paragenesis and are most abundant at Stormont. Bismuth grades at Stormont reach 1.15% and average 0.101%, while

at Fletcher's Adit the grades are much lower, averaging only 0.026%. The Bi-bearing minerals occur as replacements of early iron sulphides, as discrete phases, as intergrowths with other Bi ± Te-bearing minerals and commonly replace other late stage Bi-bearing minerals. Bismuthinite and native bismuth at Stormont are found as large "flakes" in actinolite-garnet skarn or in heavily oxidised and limonised leached zones (Plate 26). This later association produces the highest Bi and Au grades and most probably represents at least partial supergene enrichment.

Silver abundance is generally low in these skarns, averaging only 0.6 ppm in both Stormont and Fletcher's Adit. Silver contents reach 18 and 8 ppm for these two skarns respectively. Apart from native gold at Stormont (which contains on average 17.8% Ag), no significant Ag-bearing mineral was identified.

Native gold occurs principally as isolated grains in the leached zones at Stormont. In small zones Au values are as high as 21.2 ppm over a one-metre assay interval, but over the whole skarn the gold grade averages only 1.08 ppm. Fletcher's Adit has negligible amounts of Au, averaging only 0.07 ppm, but elevated grades (up to 2.61 ppm) occur in isolated leached zones. Metal correlation coefficients suggest that Au is associated with bismuthinite and/or native bismuth and/or Bi-Pb sulphides (Tables 7 and 8). Later low temperature hydrothermal fluids and/or supergene processes concentrated the Au and Bi into isolated fracture zones forming the oxidised, goethite-rich, high grade ore as seen in Plate 26.

Although no native gold was identified in (or with) the large grains of bismuthinite present in other skarn rock types at Stormont, the metal correlation coefficient matrix for Stormont strongly indicates that Au and Bi are associated on the deposit scale. This association may represent either discrete but associated Au and Bi phases, intergrowths and solid solution series involving these phases, or the existence of Au-Bi (± Te, Pb) minerals such as maldonite ($Au_2Bi$) or aurobismuthinite ($(Bi,Au,Ag)_5S_6$).

| | MEAN | STD. DEV. | VARIANCE | MINIMUM | MAXIMUM |
|---|---|---|---|---|---|
| Au | 1.08 | 3.14 | 9.84 | 0.00 | 21.2 |
| Cu | 38.1 | 107 | 11400 | 5.00 | 910 |
| Pb | 127 | 364 | 133000 | 90.0 | 2200 |
| Zn | 283 | 163 | 26400 | 0.00 | 1250 |
| Ag | 0.610 | 1.58 | 2.51 | 0.00 | 8.00 |
| Bi | 1030 | 2350 | 5540000 | 0.00 | 11500 |
| Mo | 1.07 | 4.52 | 20.5 | 0.00 | 20.0 |
| As | 14.2 | 36.5 | 1330 | 0.00 | 266 |
| Sn | 12.0 | 97.1 | 9420 | 0.00 | 456 |
| W | 17.1 | 31.2 | 970 | 0.00 | 176 |

**TABLE 4:** Statistics involving the metal assays from all skarn lithologies analysed at Stormont. N= 75, each sample was analysed for 10 metals, and assays represent averages over a 1m interval. All assays are in ppm. Values below the detection limit for each metal have been recorded as a zero value. Assay data from R.G.C. Exp. Pty. Ltd..

| | MEAN | STD. DEV. | VARIANCE | MINIMUM | MAXIMUM |
|---|---|---|---|---|---|
| Au | 0.07 | 0.23 | 0.05 | 0.0 | 2.61 |
| Cu | 130 | 210 | 4500 | 0.0 | 1300 |
| Pb | 92 | 130 | 17000 | 10 | 1300 |
| Zn | 190 | 1500 | 23000 | 50 | 1750 |
| Ag | 0.60 | 2.50 | 6.0 | 0.0 | 18.0 |
| Bi | 260 | 420 | 180000 | 0.0 | 3000 |
| Mo | 34 | 35 | 1200 | 0.0 | 330 |
| As | 10 | 16 | 240 | 0.0 | 150 |
| Sn | 540 | 490 | 240000 | 25 | 3100 |
| W | 150 | 280 | 80000 | 0.0 | 2630 |

**TABLE 5:** Statistics involving the metal assays from all skarn lithologies analysed at Fletcher's Adit. N= 165, each sample was analysed for 10 metals, and assays represent averages over a 1m interval. All assays are in ppm. Values below the detection limit, for each metal have been recorded as a zero value. Assay data from R.G.C. Exp. Pty. Ltd..

NATIVE BISMUTH (Bi)

| ELEMENT | AV ATOMIC CONC | |
|---|---|---|
| Bi | 99.69 | |
| Cu | 0.16 | |
| S | 0.05 | |
| Au | 0.05 | |
| Ag | 0.04 | |
| TOTAL | 99.99 | [N = 3] |

$Bi_{5.8}$ Te $S_{3.6}$

| ELEMENT | ATOMIC CONC | |
|---|---|---|
| Bi | 55.27 | |
| S | 34.70 | |
| Au | 0.02 | |
| Pb | 0.44 | |
| Te | 9.57 | |
| TOTAL | 99.93 | [N = 1] |

BISMUTHINITE ($Bi_2S_3$)

| ELEMENT | AV ATOMIC CONC | |
|---|---|---|
| Bi | 36.37 | |
| Cu | 0.89 | |
| S | 60.00 | |
| Au | 0.03 | |
| Ag | 0.01 | |
| Pb | 0.59 | |
| Te | 0.02 | |
| TOTAL | 97.94 | [N = 6] |

NATIVE GOLD (Au)

| ELEMENT | AV ATOMIC CONC | |
|---|---|---|
| Au | 82.28 | |
| Ag | 17.81 | |
| TOTAL | 100.09 | [N = 5] |

FINENESS OF GOLD:

"Fineness" = 1000Au/(Au + Ag)

Average = 822.10 [N = 5]

GALENOBISMUTITE ($PbBi_2S_4$)

| ELEMENT | AV ATOMIC CONC | |
|---|---|---|
| Bi | 27.70 | |
| Cu | 0.02 | |
| S | 57.70 | |
| Au | 0.15 | |
| Pb | 14.56 | |
| Te | 0.01 | |
| TOTAL | 100.14 | [N = 2] |

**TABLE 6:** Average compositions of ore minerals from Stormont, Fletcher's Adit and Ti Tree Creek. Averaged from data contained in Appendix A. Analyses attained via a Cameca electron microprobe.

## 6.4 DISCUSSION

The basic paragenesis of the opaque minerals in all three deposits is magnetite to pyrrhotite to pyrite and, at the end of this sequence, the bismuth minerals are introduced. Bismuthinite and native bismuth are never pre-pyrrhotite, and are usually post- to syn-pyrite. The gold is deposited with bismuthinite which often replaces native bismuth. Hematite follows gold deposition in the very leached areas. Therefore the basic sequence is:

Magnetite ----> pyrrhotite ----> pyrite
native bismuth ----> bismuthinite/native gold ----> [hematite]

Major differences between these deposits include the abundance of sulphides in general, wrigglitic magnetite, pyrrhotite, galenobismutite and the gold and bismuth grades. Additionally, the abundance of limonite (especially goethite) and the presence of some rarer Bi-Te-Pb-S phases differs between the three skarns.

Wrigglitic and massive magnetite occurs at a later paragenetic position than the disseminated magnetite associated with the first stages of actinolite replacement. After this early disseminated magnetite stage, hot saline Fe-bearing (and possibly boiling) fluids permeated the system (aided by the increased permeability caused by the increased retrograde alteration) and resulted in the precipitation of the massive and wrigglitic magnetite. Magnetite in general and wrigglitic magnetite decreases in abundance to the west. The skarn forming fluids at Stormont being the more distal may have been cooler, less saline and possibly more reduced (Chapter 7), resulting in less magnetite deposition especially of the wrigglitic variety.

At Fletcher's Adit bismuthinite is more abundant than native bismuth and iron sulphides are common, while at Stormont bismuthinite and native bismuth are in equal proportions and iron sulphides are not abundant. This may indicate a higher sulphur fugacity of the mineralizing fluids at Fletcher's Adit in comparison with those at Stormont.

Table 6 indicates that the $Bi_{5.8}TeS_{3.6}$ phase contains only minor amounts of Pb. If this is an intergrowth of two minerals, and not a very rare or previously unidentified mineral, the obvious question is: of which two minerals? No other Te-bearing minerals have been identified in any previous work in the Dolcoath Granite contact aureole. Additionally, there is too much Te present to suggest Te substitution into a common bismuth sulphide (D.L.

Husten, pers. comm., 1990). Another puzzling aspect is that if the Bi and S contents originate from bismuthinite (intergrown with a Te mineral), then why is there no Cu impurity as in all the bismuthinite grains from the three skarns?

The oxidised Au-Bi ore at Stormont (Plate 26) is often referred to as a fault gouge or pug. Under the microscope however, this rock type is just intensely oxidised with no evidence of strain, indicating that the associated fracturing was a brittle event with no ductile deformation. These oxidised zones are intensely jointed and faulted areas which have been the conduits for late low temperature Au-Bi rich fluids which precipitated gold in a very late paragenetic position.

The anomalously high Au and Bi grades in these spatially restricted regions may be partially the result of supergene enrichment, as similar oxidation occurs at the upper weathered and leached contact of the skarn. However, the weathered top of the skarn unit at Stormont does not have the consistently high Au and Bi grades that characterised these oxidised fracture zones, and therefore supergene enrichment is not considered to be the primary reason for the anomalously high grades. The very late high grade gold was most likely deposited from a low temperature hydrothermal fluid as a bisulphide complex with bismuthinite on the "gold solubility cliff" (Chapter 7). The hydrothermal fluid continued to drop in temperature precipitating pyrite then hematite. Later ground waters precipitated goethite as pseudomorphs replacing pyrite and hematite.

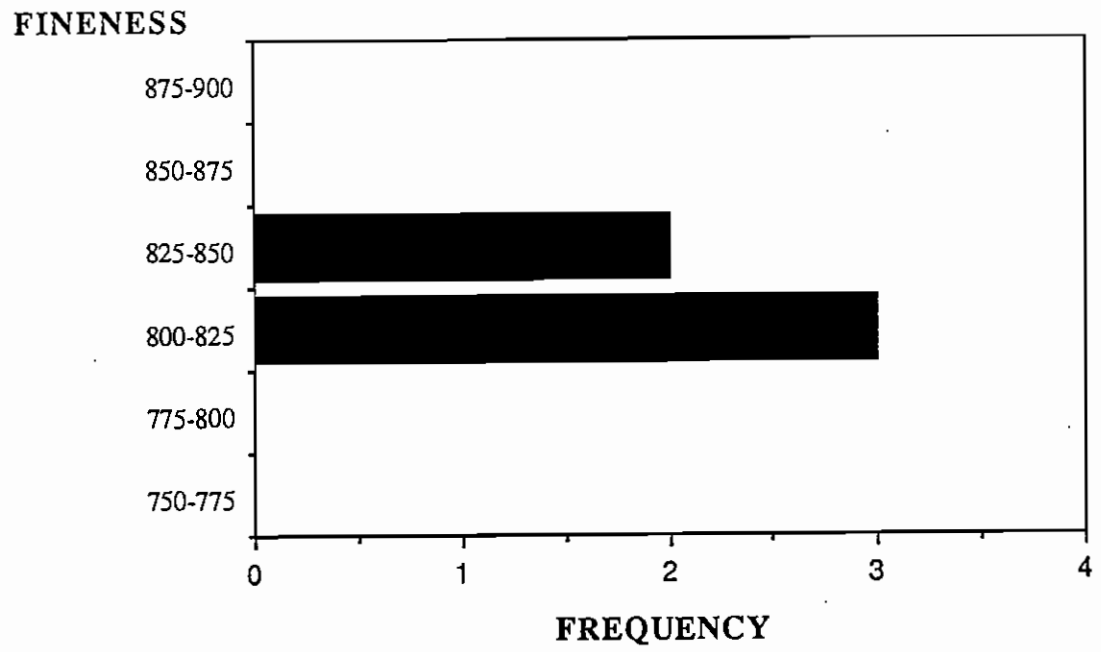


**FIGURE 15:** The fineness of native gold from Stormont. Electron microprobe data shown in Appendix A.

# CHAPTER 7

## FLUID GEOCHEMISTRY & THERMODYNAMIC MODELLING

From the paragenetic relationships in Tables 1, 2 and 3 it is possible to see how the mineralizing hydrothermal fluids varied over time with respect to temperature, oxygen fugacity, sulphur fugacity and pH. Once the fluid's nature is characterised, it is then possible to suggest reasonable hypotheses for the processes that promoted significant Bi-Au mineralization at Stormont.

The first difficulty in achieving the above goal is that this type of thermodynamic modelling is rarely done for skarn conditions, and therefore some of the phase diagrams had to be calculated from the basic thermodynamic data. Assumptions also had to be made involving the salinity and pH of ore forming solutions, as no fluid inclusion studies have been performed involving any of the three deposits. Appendix C contains the rationale and calculations for pH and salinity estimates.

Briefly, a pH estimate can be attained via the pH limitations of the stability of muscovite and K-feldspar (which are common mineralogies in greisen veins associated with mineralization). Salinity estimation is achieved via analogy with the Shepherd and Murphy deposit to the east, which has undergone extensive fluid inclusion analysis by Kwak and Askins (1981a). For Stormont, the estimated salinity is approximately 4, while at the other two deposits this estimate is slightly higher being ≈5-6 (Appendix C). Salinities for the three deposits are likely to be in the order of 4 M NaCl (Appendix C).

The basic paragenesis of the opaque minerals in all three deposits is:

Magnetite ----> pyrrhotite ----> pyrite
native bismuth ----> bismuthinite/native gold ----> [hematite]

Appendix C contains the essential thermodynamic calculations needed to create or modify $fO_2$-T, $fO_2$-$fS_2$ and $fO_2$-pH phase diagrams which are applicable to the ore forming fluids at Stormont. The $fO_2$-T phase diagram (Figure 18) was calculated from the basic thermodynamic data, due to the strong influence of salinity making existing phase diagrams (for V.M.S deposits) unrealistic for fluid compositions at Stormont.

Calculated in Appendix C are:

1) The relevant equations to locate the position of the bismuthinite/native bismuth transition on the three phase diagrams mentioned above for the estimated fluid conditions at Stormont.

2) The relevant equations to construct aqueous sulphur predominance diagrams in $fO_2$-T and $fO_2$-pH space for the estimated fluid conditions at Stormont.

3) The relevant equations to construct an Fe-S-O phase diagram in $fO_2$-T space for the estimated fluid conditions at Stormont.

4) The position of the the $Au(HS)_2^-$ <-----> $AuCl_2^-$ switch-over line in $fO_2$-T space.

5) The positions of gold solubility contours for both Au species in $fO_2$-T space.

The data calculated in Appendix B are plotted in Figures 16 ($fO_2$-$fS_2$), 17 ($fO_2$-pH) and 18 ($fO_2$-T).

Figure 16 has been modified from Brown and Nesbitt (1987), with the native bismuth/bismuthinite transition being constrained further. The proposed fluid evolution path for Stormont is superimposed on this diagram. Although this diagram indicates that it is possible to precipitate bismuth minerals at any time during this fluid's history, the bulk of the bismuthinite and native bismuth are precipitated in the pyrite/hematite transition region. Gold deposition occurs very late in the fluid's history with bismuthinite, and is shortly followed by hematite in the very leached areas. Thus, as the hydrothermal fluid evolves, the oxygen and sulphur fugacities both increase, resulting in the paragenesis seen in these skarns and especially at Stormont.

Obviously there are factors other than $fO_2$ and $fS_2$ changing in the fluid contemporaneously, such as the temperature and pH of the fluid, but a rising $fS_2$ is a very effective way of explaining both the native bismuth to bismuthinite transition and this reaction's position in the overall paragenesis of opaque minerals.

Figure 17 has been modified from Large (1977), with the native bismuth to bismuthinite transition being added to a fO2-pH phase diagram including the Py-Po-Mag-Hem stability fields. A proposed fluid path for Stormont has been superimposed on this diagram. The fluid path shown is again consistent with the paragenesis seen in these skarn

deposits. The small field of bismuthinite stability indicates that gold deposition (being syn-bismuthinite) is most likely to have occurred near the Py-Hem boundary at pH's of 3-5 and $fO_2$'s of $10^{-32}$ to $10^{-35}$ (at T = 250°C and $\Sigma S = 10^{-2}$). The fluid path drawn on this phase diagram corresponds to a mineralizing fluid that is evolving to become more acidic and oxidising.

Figure 18 is the most informative phase diagram, and given that the previous two diagrams are consistent with the paragenetic sequence, the assumed constants for pH and $\Sigma S$ seem realistic. Appendix C contains all the calculations for the construction of this $fO_2$-T phase diagram. A hypothetical fluid path for Stormont is again superimposed on the stability fields for Py-Po-Mag-Hem. This fluid path is also consistent with the observed paragenesis, and indicates that with time the fluid is becoming more reduced and is cooling.

Figure 18 also contains gold solubility contours which indicate how much Au can be carried in the mineralizing solution (as either the $Au(HS)_2^-$ or $AuCl_2^-$ species). For example, if the fluid path moves from the 10 ppb contour to the 1 ppb contour, then gold is precipitated. From this diagram, it is clear that large amounts of gold can be precipitated from the chloride complex at temperatures greater than ≈300°C, but this is inconsistent with the paragenetic position of the native gold (i.e. the early formed magnetite zones assay very poorly for gold). Thus it seems that the chloride complex is not the major contributor. On the other hand, native gold occurs with bismuthinite and generally with (or after pyrite) and before hematite, which suggests that the majority of the gold is being deposited on the "gold solubility cliff" from the $Au(HS)_2^-$ complex. The occurrence of large quantities of native gold in discrete, oxidised zones (Plate 26) supports the hypothesis of a relatively rapid precipitation event on the "gold solubility cliff" at low temperatures (although some supergene enrichment in these zones is likely to have been partially responsible for the elevated Au grades).

Why the gold chloride complex did not seem to play a role in the deposition of the gold during the high temperature stage of the ore fluid is puzzling. The fluid may have had low salinities. The answer may lie in the source of the gold. Cambrian volcanics are very likely to be present between the Roland Conglomerate and the Dolcoath Granite beneath Stormont (S. Halley, pers. comm., 1990; Pemberton and Vicary, 1989). If this is the case, the volcanics

could be a source for the gold. The gold could be extracted most effectively from the volcanics by the establishment of a convecting/circulating meteoric water cell. It is well-documented that fluid compositions in skarns change from metamorphic to magmatic to meteoric in nature with time (Einaudi et. al., 1981 and Meinert, 1983). The establishment of an effective convecting meteoric water cell at the distal Stormont deposit therefore would have been a later, lower temperature development (oxygen isotopes indicate at least after the magnetite formation, as discussed in Chapter 10), perhaps explaining why the high temperature $AuCl_2^-$ complex was not a significant transportation agent for gold.

Towards the end of the hydrothermal system's lifetime the fluids were cooler, the $Au(HS)_2^-$ species was the most effective gold transportation complex, a convecting meteoric water cell had been effectively established and gold was being leached from the Cambrian volcanics. The greater prospect-to-granite distance at Stormont (compared to the other deposits in the area) may have promoted the development of a larger and more effective convection cell. The auriferous fluids then ascended and deposited native gold with bismuthinite on the "gold solubility cliff" (Figure 18) in areas with a high fracture controlled permeability.

Figure 18 is also extremely instructive in characterising the differences in mineralizing fluids from the three deposits. Ti Tree Creek has an abundance of magnetite, some pyrite and no pyrrhotite indicating that the fluids were more oxidised and higher temperature than at Stormont. Fletcher's Adit on the other hand has a similar fluid path to Stormont, but contains a greater quantity of pyrrhotite and lacks the quantity of bismuth minerals and associated native gold. Fletcher's Adit's mineralizing fluid path may not have crossed the "gold solubility cliff", or may simply not have contained as much gold, possibly being a function of the sub-surface thickness of the Cambrian volcanics and/or the granite-prospect distance.

The opaque mineral paragenesis at Stormont clearly indicates that the retrograde stage and the mineralization stage have continued for the longest time at this deposit. This is important as the mineralizing fluid is becoming more reduced with time. Gold skarns are characterised by very reduced mineralizing fluids (Meinert, 1988; Meinert, 1989) and therefore the longer the mineralizing fluids evolved at Stormont, the more like "gold skarn forming fluids" they became.

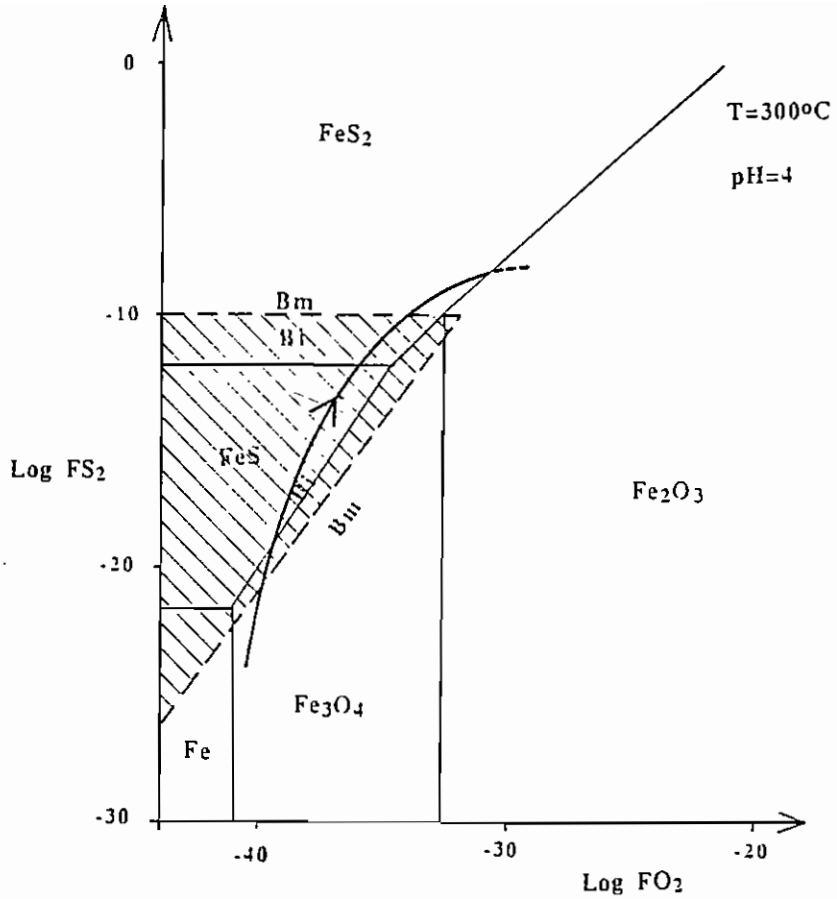


**FIGURE 16:** Log $FS_2$ vs log $FO_2$ diagram of the stabilities of the native element, oxide and sulphide opaque minerals at 300°C and pH = 4. Arrow indicates the probable evolutionary path of the mineralising fluid at Stormont, based on the observed paragenesis. Bi = native bismuth, Bm = bismuthinite. Modified from Brown and Nesbitt (1987, p. 2370); additional calculations are shown in Appendix B.

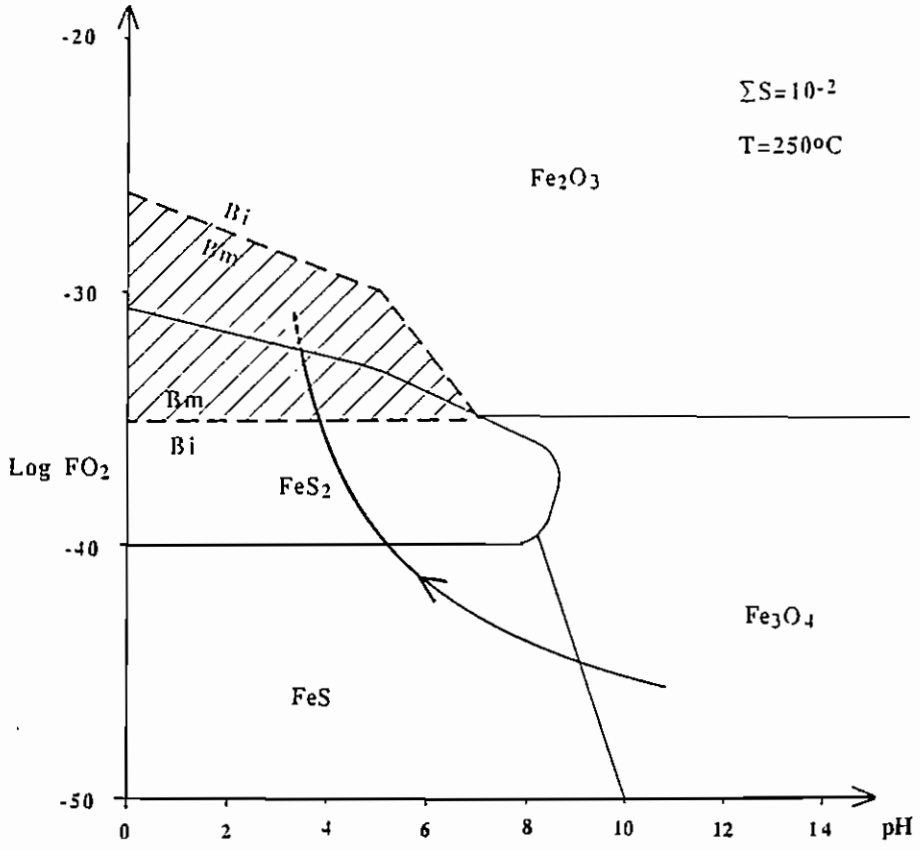


**FIGURE 17:** Log $FO_2$ Vs pH diagram of the stabilities of the native element, oxide and sulphide opaque minerals at 250°C and $\Sigma S = 10^{-2}$. Arrow indicates the probable evolutionary path of the mineralising fluid at Stormont, based on the observed paragenesis. Bi = native bismuth, Bm = bismuthinite. Iron species stabilities taken from Large (1977, p. 557), additional calculations required involving the bismuth species are shown in Appendix B.

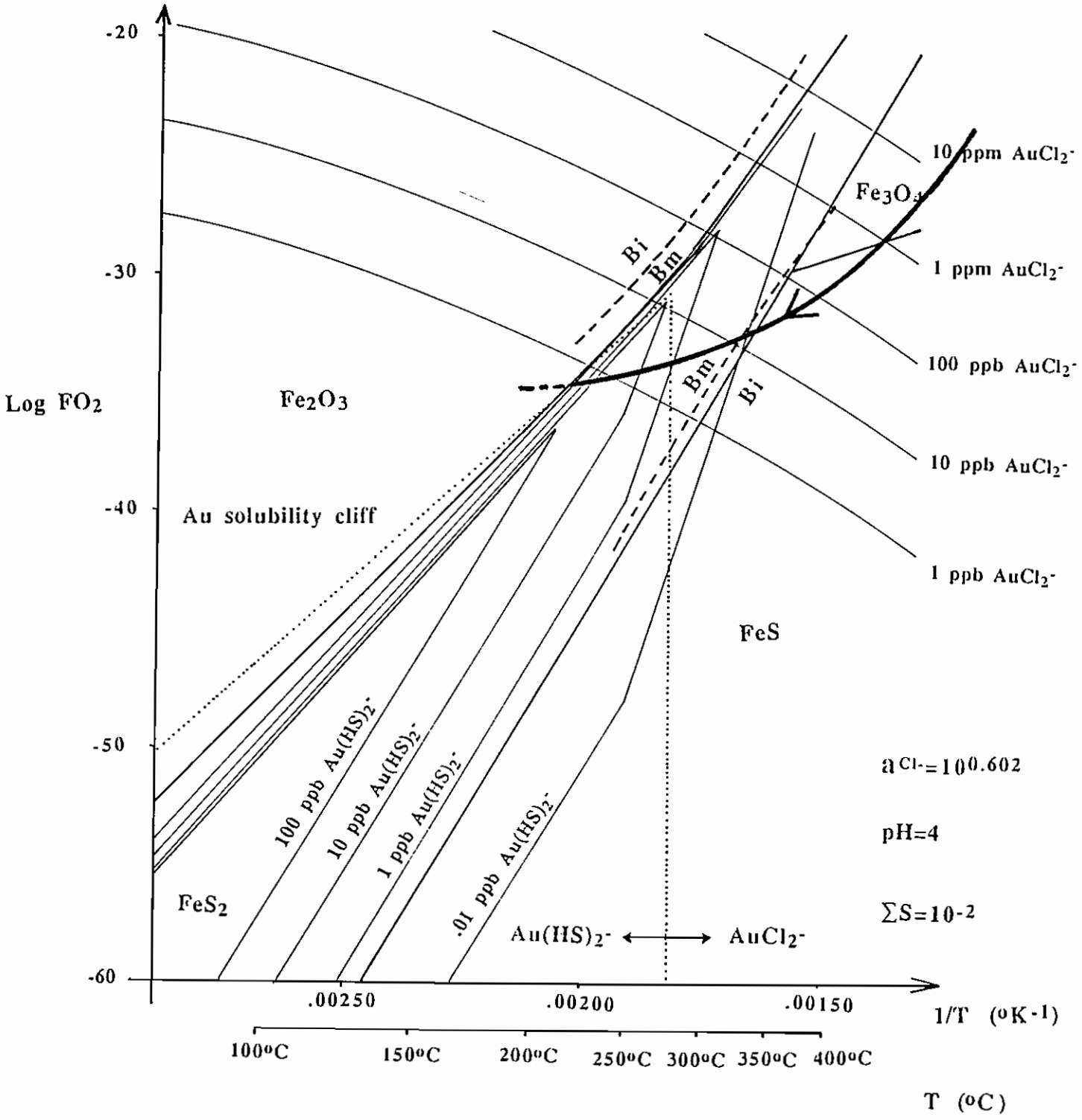


**FIGURE 18:** Log $FO_2$ vs temperature diagram of the stabilities of the native element, oxide and sulphide opaque minerals at $a^{CL^-} = 10^{0.602}$, pH = 4, and $\Sigma S = 10^{-2}$. Arrow indicates the probable evolutionary path of the mineralising fluid at Stormont, based on the observed paragenesis. Bi = native bismuth, Bm = bismuthinite. Dotted line indicates the position where both gold complexes are equally efficient at transporting gold ("switch-over line"). Thin continuous lines are gold solubility contours for both gold complexes. All calculations required for the construction of this diagram are shown in Appendix B.

# CHAPTER 8

# METAL ASSOCIATIONS AND SPATIAL VARIATIONS

## 8.1 INTRODUCTION

R.G.C. drill-holes FD 1-FD 9 (Fletcher's Adit) and SD 1-SD 6 (Stormont) have been assayed for Au, Cu, Pb, Zn, Ag, As, Bi, Mo, Sn, and W. This chapter this data is presented as "down-hole" stratigraphic metal variations, metal correlation plots and metal correlation coefficient matrices for both Stormont and Fletcher's Adit. The stratigraphic variation diagrams from representative drill-holes are accompanied by schematic stratigraphic columns which indicate how metal abundance varies with each stratigraphic unit and skarn assemblage. The horizontal scale of some of these plots (e.g. SD 3) include only the upper portion of the footwall clastics, which allows more detail to be observed in the skarn region. Plots from other drill-holes (e.g. SD 1) include assay data from the skarn to the base of the Moina Sandstone, allowing the metal variations in the footwall rocks to be best observed.

Metal correlation plots and correlation coefficient matrices are calculated for assays from skarn lithologies only, and assays below detection limits are recorded as zero values. Each assay represents the average metal content over one metre. No mineral exploration company drill-holes exist in the Ti Tree Creek area.

## 8.2 STRATIGRAPHIC VARIATIONS

### 8.2.1 STORMONT

Figure 19 displays the stratigraphic variation of metal abundance in SD 1 (SD 3 is included in Appendix D). This type of plot shows where each metal has been deposited with respect to the different lithologies.

Gold, Bi and Pb have a similar stratigraphic distribution pattern (Figure 19) and existing predominantly in the middle and basal portions of the skarn. No elevated grades occur in the footwall. The Au, Bi and Pb association is a strong feature of mineralization at both Stormont and Fletcher's Adit.

Zinc shows a more erratic variation with high grades consistently occurring in the skarn, with two elevated concentrations occurring at approximately 75 and 110 m. These

secondary peaks in Zn grade correspond to zones of intense jointing and minor faulting, respectively.

Copper shows a distinct peak which corresponds to a fault zone hosting greisen veins (with chalcopyrite mineralization) at approximately 110 m. Copper grades in the skarn are similar to those in the footwall rocks.

Silver occurs in consistently low amounts, with only minor peaks corresponding to the fault zone at approximately 105-110 m and at the middle portion of the skarn.

Molybdenum is usually in very low abundances in the metasomatised calcareous units, but commonly occurs in greater amounts in the middle to lower portions of the arenite sequence and grades generally increase with depth. Molybdenum is indicative of high temperatures so that this decrease "up-hole" is possibly a function of decreasing temperature.

Tin grades display an unusual trend. There are generally elevated grades in the skarn, but a distinct peak in grade occurs at the top of the shale horizon. This peak may be due to Sn-silicates such as malayaite (although no such minerals were identified) and therefore elevated grades occur in the more silicious units.

Tungsten grades vary greatly throughout the stratigraphic section in SD 1. They are being generally elevated in the skarn and irregular in the footwall. The footwall grade elevations represent wolframite hosted in veins.

Arsenic grades are generally below the detection limit in the skarn, peak at the hornfelsic shale/calcarenite's upper contact with the skarn and are elevated in fractured areas in the footwall arenites.

The metal variations with rock type in SD 3 are shown in Appendix D. In SD 3, the top of the skarn is extremely leached and the effects of supergene enrichment on the metal abundance is visible.

Additional information for Stormont can be attained from SD 3. Here, Au, Bi, Pb, Cu, Zn and As show some degree of supergene enrichment. Zinc grades display a remarkably constant trend of increased values up the stratigraphic section, with a slight depression in concentration at the base of the silicious zone, a slight rise in concentration at approximately 32 m corresponding to a minor fault and a increase in concentration in the leached skarn due to

supergene enrichment. Copper grades also show a distinct increase in grade in the leached skarn, as well as elevated values in the silicious zone, but have a broad area of low values over the majority of the skarn unit.

### 8.2.2 FLETCHER'S ADIT

At Fletcher's Adit FD 6 is the deepest drill-hole, Figure 20 displays the variation in metal grades through the stratigraphy.

A slight peak in gold grade is present at the top of the hematitic pebble conglomerate, which may be a result of a decrease in $fO_2$ as the fluid passed through the intensely hematitic unit into the quartz arenites above. Slightly elevated gold concentrations also occur at the 50 m level, which correspond to a fault. Gold grades are on average much lower than in the Stormont drill holes, but show similar elevated values in the middle to basal portion of the skarn.

Except for one assay, Bi grades are only elevated in the skarn horizon. Assays from the basal silicious zone and the unsilicified skarn are similary high grade.

Lead grades are consistently high throughout the ≈ 200 m of stratigraphy at Fletcher's Adit, only marginally rising in the skarn unit and therfore displays a very different stratigraphic variation of Pb compared to Stormont. There is a general rise in values up through the arenites and then a sudden drop on contact with the hornfelsic shale/calcarenite unit. The Pb-bearing fluids may have had difficulty penetrating the hornfelsic shale/calcarenite sequence due to its high impermeability and because there were only a small number of fractures that could act as conduits for the hydrothermal fluids. While these fluids paused at the base of the shales, the higher grades of Pb may have been deposited in the upper arenites due to a temperature drop in the fluid.

Copper is predominantly confined to the skarn and the silicified base of the skarn (unlike Stormont). Minor Cu concentration elevations in the footwall arenites coincide with silicified areas.

Silver occurs as a few elevated grades in the skarn rocks. Generally, silver is lower in concentration at Fletcher's Adit in comparison to the Stormont assay data.

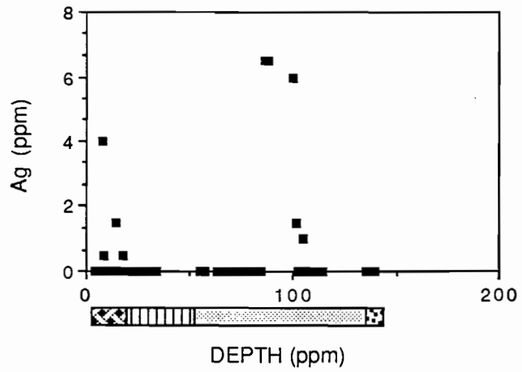


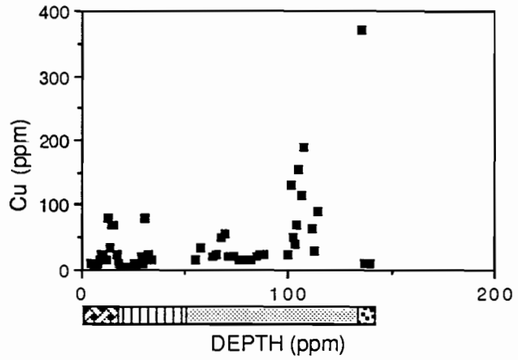


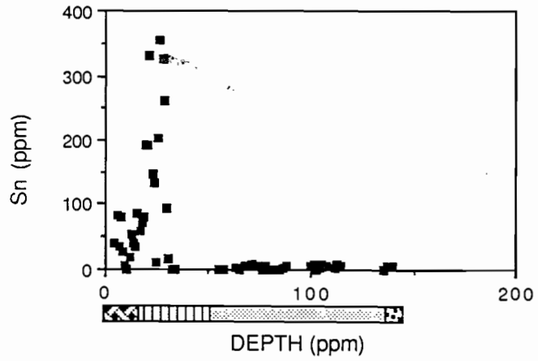


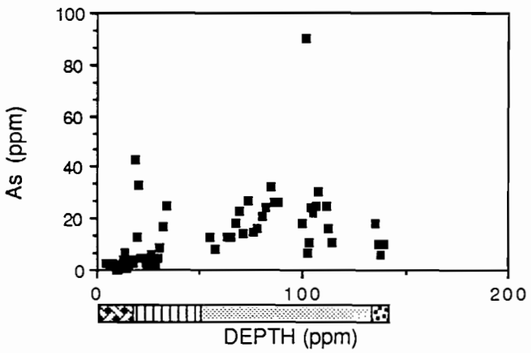


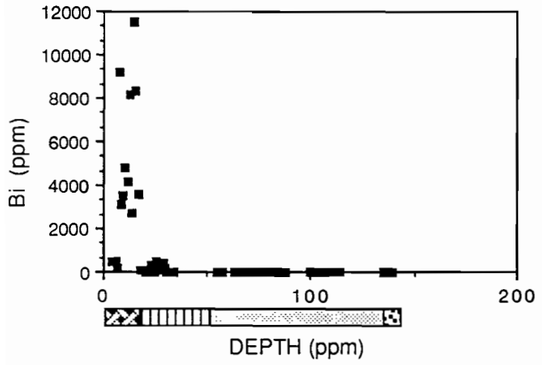


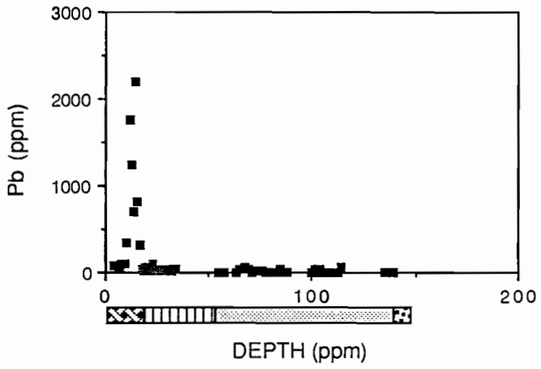


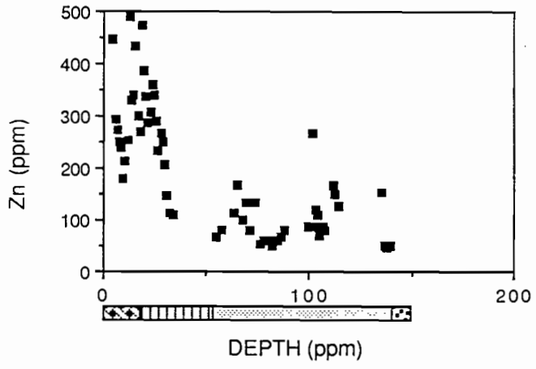


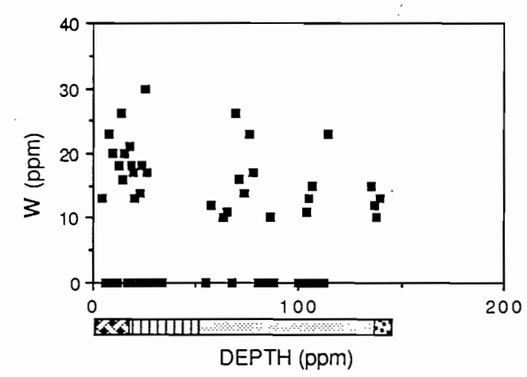


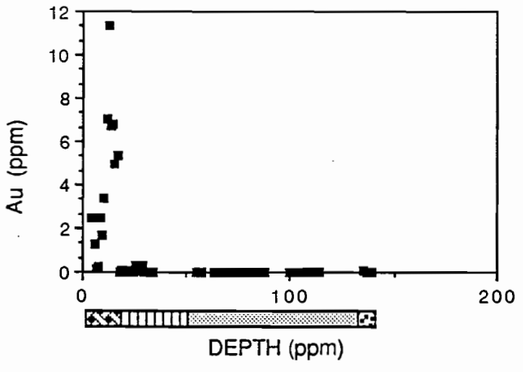


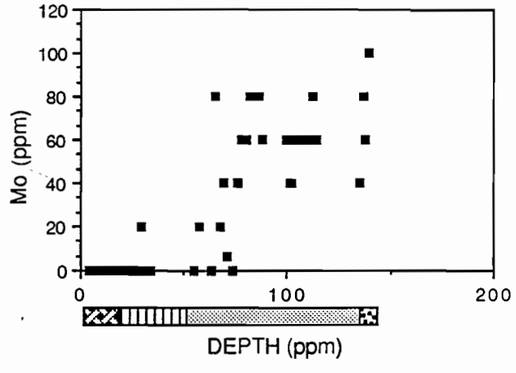


## LEGEND

- Limestone
- Weathered and leached skarn
- Skarn
- Quartzite
- Shale (predominantly)
- Sandstone (predominantly)
- Hematitic sandstone and pebble conglomerate
- No core recovered

**FIGURE 19:** Stratigraphic variations in metal content in the SD 1 drill-hole at Stormont.

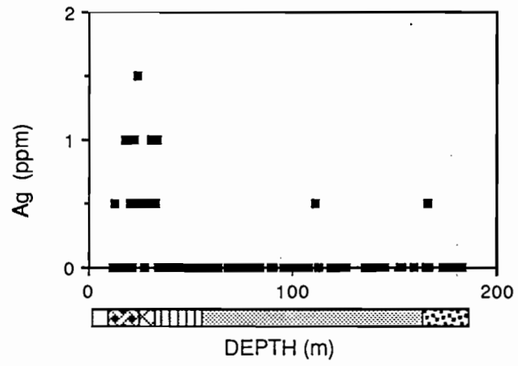


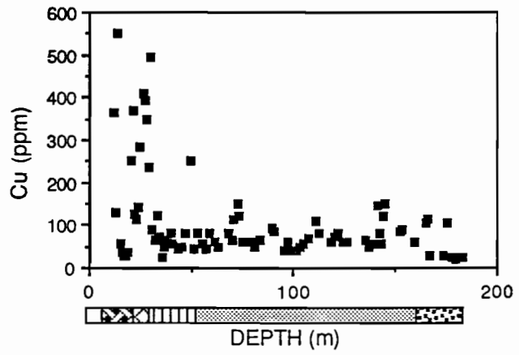


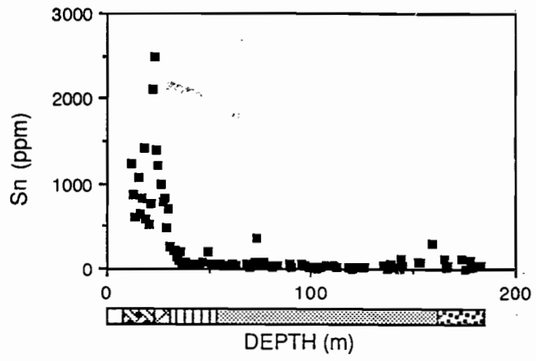


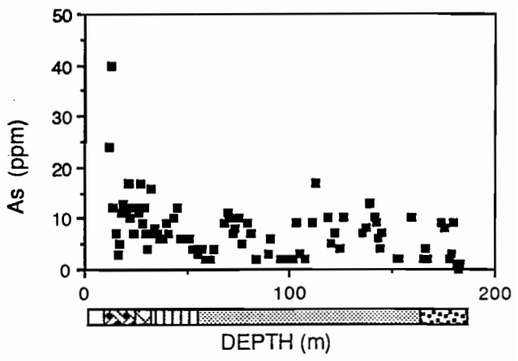


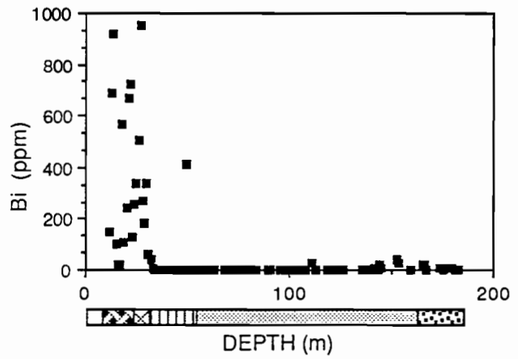


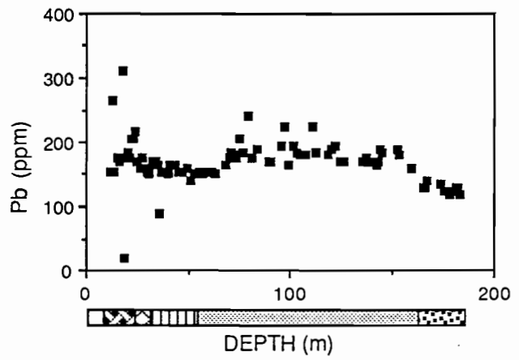


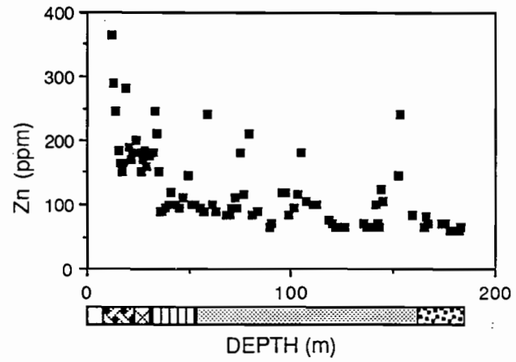


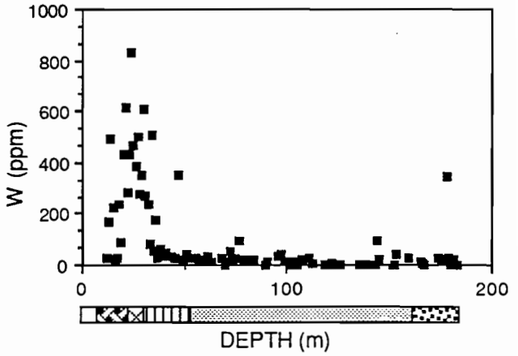


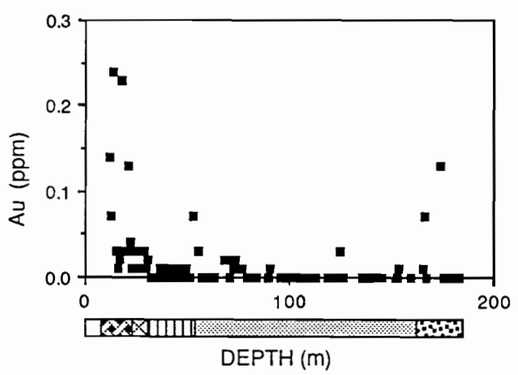


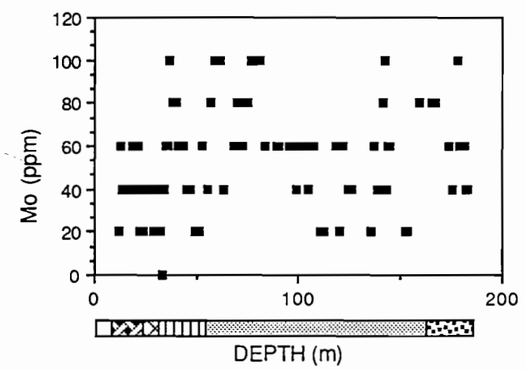


## LEGEND

- Limestone
- Weathered and leached skarn
- Skarn
- Quartzite
- Shale (predominantly)
- Sandstone (predominantly)
- Hematitic sandstone and pebble conglomerate
- No core recovered

**FIGURE 20:** Stratigraphic variations in metal content in the FD 6 drill-hole at Fletcher's Adit.

Zinc is more abundant in the skarn unit and is enriched in a number of small fault zones and their associated veins present in the footwall. This data follows a similar distribution trend to the Stormont assay data.

Molybdenum grades show an erratic trend appearing to be unaffected by changes in stratigraphy, fracture abundance or permeability. This trend is unlike those seen at Stormont which is erratic up to the top of the arenite sequence, but then virtually lacking Mo above this horizon. Temperatures during the deposition of Mo at Fletcher's Adit would probably have been higher than at Stormont due to the decreased granite-to-prospect distance. As a result the molybdenum may have been deposited continuously (unlike Stormont where deposition stops at the base of the skarn) as the mineralizing fluids moved up the stratigraphy.

Tin in FD 6 is strictly confined to the skarn, with the highest concentration of Sn occuring in the siliceous zone at the base of the skarn. This assay trend is unlike SD 1 where the distinct Sn peak in grade coincided with the top of the hornfelsic shale/calcarenite. Tungsten shows a very similar trend to Sn, indicating an association between the two elements. Arsenic grades are consistently low, show a slight elevation in the skarn, but like SD 1 vary greatly in the footwall.

Appendix D contains similar stratigraphy-metal plots for FD 7 and FD 8. These plots provide the additional information on the spatial variations of metals at Fletcher's Adit. In FD 7 Cu variation is very similar to SD 3 and unlike SD 1 and FD 6, with Cu grades at FD 7 being depressed in the middle and lower portions of the skarn. The Mo grade trend in FD 7 is totally unlike the erratic variation of this metal seen in other holes from Stormont and Fletcher's Adit. At FD 7, Mo concentrations display an exceptionally well-defined trend of a gradual decrease to the top of the arenites, then a gradual increase to the top of the hornfelsic shale/calcarenites, then a peak at the silicious base of the skarn and finally, consistently low grades in the middle to upper portions of the skarn.

In FD 8, Bi, Cu, As, Zn, W and especially Sn grades show supergene enrichment trends in the upper, leached portions of the skarn. Gold seems unaffected by the intense weathering of the skarn. Copper, Pb and Zn show a distinct enrichment peak corresponding to the base of the hornfelsic shale/calcarenites, probably due to the fluid's progress up the

stratigraphic section being retarded by this relatively impermeable unit, and metal deposition being aided by the "pooling" and cooling of the mineralizing fluids as they paused to penetrate this unit.

## 8.3 METAL ASSOCIATIONS

The stratigraphic variation diagrams indicate that strong similarities exist, at least spatially, between some metals. Gold, Pb and Bi are good examples of metals that have a similar spatial concentration distribution "down-hole". In this chapter, metal associations are reviewed through the use of metal grade-metal grade plots and correlation coefficient matrices.

### 8.3.1 METAL-METAL PLOTS

#### 8.3.1.1 Stormont

Appendix E contains a plethora of metal-metal correlation diagrams for all assay data from skarn lithologies at Stormont. Seventy-five one metre assays are involved. Gold and bismuth have been plotted against the other nine metals assayed, and some other combinations have been added where the stratigraphic variation suggests there may be an association (e.g. Sn-W).

Visually, the Au-Bi, Au-Pb, Bi-Pb and Sn-W plots display good to excellent correlations. The Au-Cu, Au-Ag, Au-As, Ag-As, Bi-Ag, Au-Sn, Au-W, Bi-Sn, Bi-W, Bi-Cu, and Bi-As show very poor correlations.

The poor Au-Cu and Au-Ag visual correlations and excellent Au-Bi visual correlation are important, as these correlations are characteristic of gold skarns (Chapter 11). The Au/Bi/Pb relationship seen in the stratigraphic variations of metal content is reinforced in these plots.

One interesting feature of these plots is the similarity between Bi-Sn, Bi-W and Bi-Cu (Appendix E). These three plots all have two distinct regions, the first includes assays that are low in Bi (generally less than 1000 ppm) and high in Sn, W and Cu. The second region, which is clearly separated from the first, is characterised by very high Bi grades (2000-12000 ppm) and very low Sn, W and Cu grades. These regions indicate two episodes of Bi

deposition, the first being low grade and associated with Sn, W and Cu, and the second being high grade (and being associated with Au and Pb). This late stage, Bi/Au/Pb-rich phase of mineralization is not present at Fletcher's Adit!

#### 8.3.1.2 Fletcher's Adit

A similar collection of metal correlation plots is given in Appendix E for 165 assays (over a one-metre intervals) from skarn lithologies at Fletcher's Adit.

The Au-Bi, Bi-Pb, and Au-Pb display very good visual correlations, while Bi-W, Bi-Cu, Bi-Sn, and Cu-Sn show moderate visual correlations. The Bi-Mo, Bi-Ag, Bi-As, Cu-Ag, Au-Ag, Ag-As, Au-Mo, Mo-W, Bi-Zn, Pb-Zn, Sn-W, Au-W, Au-Sn, and Au-Zn plots show little or no visual correlation.

The Bi-Sn, Bi-W and Bi -Cu plots have a distribution of data within a single region of low Bi concentration, indicating a single Bi depositional episode (unlike Stormont which has two distinct populations of low and high grade Bi ). This single region is characterised by Bi grades that are identical to the low Bi grade region for Stormont (i.e. Bi<1000 ppm) but have Sn, W and Cu grades that reach grades ten times as great as those at Stormont. Nevertheless, the low grade Bi regions from Stormont and the complete data set from Fletcher's Adit are comparable and imply that both deposits experienced an (?)initial, low grade Bi (+ Cu, W and Sn) mineralization event, while only Stormont experienced a (?)later, high grade Bi (+ Au and Pb) mineralization event!

### 8.3.2 METAL CORRELATION COEFFICIENT MATRICES

#### 8.3.2.1 Stormont

The metal correlation coefficient matrix for all assays from skarn lithologies in SD 1-SD 6, is given in Table 7. The number of assays used for this matrix was 75, therefore any correlation coefficient greater than 0.296 can be considered (with 99% confidence) to represent a significant correlation (Freund, 1976).

The significant results attained from Table 7 include: the very strong correlations between Au/Bi, Au/Pb and Bi/Pb; the strong correlations between W/Cu, Sn/Cu, W/Sn, Au/As and As/Ag; and the good correlations between Au/Ag, As/Cu, As/Zn and W/As.

#### 8.3.2.2 Fletcher's Adit

Table 8 is the metal correlation coefficient matrix for Fletcher's Adit where there are 165 samples from skarn lithologies only. With 165 samples, the coefficient corresponding to a significant correlation (with 99% confidence) is any value greater than 0.265 (Freund, 1976).

The significant results attained from Table 8 include: the very strong correlations between Au/Bi, Au/Pb, Pb/Ag and Bi/Pb; the strong correlations between Bi/W; and the good correlations between Bi/Cu, As/Cu and Sn/Cu.

## 8.4 CONCLUSIONS

There is a very strong association, spatially and temporally between Au, Bi and Pb. This association has been confirmed by the recognition of ore minerals such as galenobismutite, bismuthinite, native bismuth and native gold occurring in similar paragenetic positions, and being spatially associated with one another. The good Au/Bi and poor Au/Cu and Au/Ag correlations at Stormont are important in the classification of this deposit as a "gold skarn" (Chapter 11).

The stratigraphic distribution of metals shows that the Au, Pb and Bi are restricted to the skarn units. Faults and jointed areas in the skarn and footwall contribute to locally high grades of As, W, Zn, Ag and Cu. Supergene enrichment in the upper regions of weathered skarn plays a role in concentrating Cu, Pb, As, Zn, Bi, Sn and W grades.

The bimodal distribution of Bi-Cu, Bi-Sn and Bi-W values at Stormont and the complete lack of the high grade Bi values at Fletcher's Adit is interesting. This disparity between the two deposits highlights very clearly Stormont's high grade Bi and Au mineralization is the result of a separate episode of late mineralization, which simply did not occur at Fletcher's Adit. The early phase of mineralization which is common to both deposits is a low grade Bi/Au/Pb/(and Ag at Fletcher's Adit) and a moderately high grade Sn/W/Cu mineralizing event (especially at Fletcher's Adit). The late phase of mineralization unique to Stormont is a high grade Au/Bi/Pb event with very minor amounts of Sn, W or Cu. The distinction between these two events is most clearly seen in Bi-Cu, Bi-W and Bi-Sn plots for

Stormont (Appendix E). The late mineralization phase of high grade Au/Bi/Pb at Stormont corresponds to deposition on the "gold solubility cliff" discussed in Chapter 6 (Figure 18).

| | Au | Cu | Pb | Zn | Ag | Bi | Mo | As | Sn | W |
|---|---|---|---|---|---|---|---|---|---|---|
| Au | 1 | | | | | | | | | |
| Cu | -0.005 | 1 | | | | | | | | |
| Pb | 0.545 | 0.053 | 1 | | | | | | | |
| Zn | 0.168 | -0.053 | 0.157 | 1 | | | | | | |
| Ag | 0.362 | -0.053 | -0.002 | 0.143 | 1 | | | | | |
| Bi | 0.676 | 0.153 | 0.749 | 0.102 | 0.232 | 1 | | | | |
| Mo | -0.082 | -0.007 | -0.079 | -0.238 | -0.092 | -0.097 | 1 | | | |
| As | 0.556 | 0.399 | -0.043 | 0.367 | 0.469 | 0.199 | -0.07 | 1 | | |
| Sn | -0.235 | 0.461 | -0.2 | -0.221 | -0.011 | -0.16 | -0.148 | 0.133 | 1 | |
| W | -0.095 | 0.766 | -0.008 | -0.026 | -0.023 | 0.079 | -0.022 | 0.357 | 0.51 | 1 |

**TABLE 7:** Correlation coefficient matrix for metals contained in skarn lithologies only from Stormont. Analyses below the detection limit for each metal are included as zero values. N= 75; therefore if a correlation coefficient is ≥0.302, then the correlation is significant with 99% confidence (Freund, 1976). Data from R.G.C. Exp. Pty. Ltd..

| | Au | Cu | Pb | Zn | Ag | Bi | Mo | As | Sn | W |
|---|---|---|---|---|---|---|---|---|---|---|
| Au | 1 | | | | | | | | | |
| Cu | 0.127 | 1 | | | | | | | | |
| Pb | 0.723 | -0.074 | 1 | | | | | | | |
| Zn | 0.158 | 0.055 | 0.061 | 1 | | | | | | |
| Ag | 0.211 | -0.079 | 0.555 | 0.009 | 1 | | | | | |
| Bi | 0.677 | 0.324 | 0.551 | 0.138 | 0.182 | 1 | | | | |
| Mo | -0.102 | -0.135 | 0.031 | -0.029 | -0.049 | -0.157 | 1 | | | |
| As | 0.023 | 0.319 | -0.047 | 0.176 | -0.057 | 0.16 | -0.024 | 1 | | |
| Sn | 0.008 | 0.329 | 0.023 | 0.082 | 0.051 | 0.119 | -0.211 | 0.126 | 1 | |
| W | -0.018 | 0.244 | 0.023 | -0.083 | -0.086 | 0.467 | -0.031 | 0.029 | 0.066 | 1 |

**TABLE 8:** Correlation coefficient matrix for metals contained in skarn lithologies only from Fletcher's Adit. Analyses below the detection limit for each metal are included as zero values. N= 165; therefore if a correlation coefficient is ≥0.267, then the correlation is significant with 99% confidence (Freund, 1976). Data from R.G.C. Exp. Pty. Ltd..

# CHAPTER 9

# CONTROLS ON MINERALIZATION

## 9.1 STRATIGRAPHIC CONTROLS

### 9.1.1 SHALE

The presence of a 10-20 m thick unit of hornfelsic shale interbedded with calcarenites beneath the Gordon Limestone is a factor that affects mineralization. Throughout the field area, this shale unit contains abundant evidence of lateral fluid flow. Evidence includes the laterally extensive metasomatism and pyrrhotite mineralization of the calcarenite beds (Plate 39) and worm burrows (Plates 4 and 33), as well as a high proportion of sub-horizontal greisen veins (Plate 7). There is no evidence to suggest that fluids permeated the hornfelsic shale horizons via inter-granular porosity.

The stratigraphic distribution of metals such as Zn, Cu and Pb often displays peaks at the base of the shale unit, possibly indicating that the mineralizing fluids may have cooled (and deposited metals) and that their progress up the stratigraphic column was retarded by the low permeability of the shale unit. As a result of the shale's low permeability, fluids likely to pass through into the limestone via fractures. This dependence on fracture permeability is evident in the stratigraphic metal distribution plots and the existence of high grade Au-Bi in fractures in the skarns.

The presence of the hornfelsic shale horizon below the limestone results in the lateral dispersion of hydrothermal fluids. This has the effect of producing laterally extensive, but thin, skarn bodies and possibly dispersing the mineralization over a wider area.

### 9.1.2 CAMBRIAN VOLCANICS

The Denison Group sediments have very low concentrations of gold beneath Fletcher's Adit and Stormont. Cambrian volcanics are therefore the most likely source for the gold at Stormont, and their sub-surface position may influence the intensity and location of the high grade gold mineralization. Cambrian volcanics in the Moina area occur unconformably beneath the Roland Conglomerate and the Moina Sandstone. A Comalco drill-hole on the northern boundary of the mapping area intersected Cambrian volcanics beneath the Moina Sandstone at

only ≈80 m depth. Drill-holes at Fletcher's Adit and Stormont have penetrated Roland Conglomerate at ≈180 m and ≈138 m respectively, and therefore the likelihood of the existence of volcanics between the prospects and the granite is extremely high, especially at Stormont. The probability that the thickness of these volcanics being greater below Stormont is also high, as the granite-to-prospect distance at Stormont is known to be greater (Leaman, 1988 and Leaman and Richardson, 1988) and the Roland Conglomerate is intersected at shallower depths than at Fletcher's Adit.

The position of the sub-surface volcanics is poorly constrained despite extensive geophysical exploration in the area. High resolution geophysical methods would be hindered by the laterally discontinuous nature of the alluvial fan conglomerates, the major unconformity between the Cambrian volcanics and the Denison Group and the irregular form of the roof of the batholith.

### 9.1.3 DOLCOATH GRANITE

The presence of cupolas on the westerly dipping granite ridge would strongly influence the placement and type of mineralization. At the Moina Sn-W mine to the east of the study area, a cupola extends to ≈200m below the skarn, and has intruded the structurally weak region around the NW trending Bismuth Creek Fault (Kwak and Askins, 1981a). Whether similar, but deeper, granite cupolas occur at Ti Tree Creek, Fletcher's Adit or Stormont is unknown.

The metasomatising and mineralizing fluids can be very well focused, as indicated by patchy skarn development in the Ti Tree Creek area where limestone only tens of metres nearby shows no evidence of hydrothermal alteration. Cupolas, in addition to fractures, may help to explain these localised areas of metasomatism. Leaman (1988) suggests that small cupolas could occur on the top of the flat topped granite ridge, but are more likely to occur at the intersection between the roof and the steep sides of the batholith, such as Dolcoath Hill.

## 9.2 STRUCTURAL CONTROLS

### 9.2.1 FOLDING

The Stormont and Fletcher's Adit skarn bodies lie in a broad, E-W trending syncline associated with the first phase of Middle Devonian deformation in the Moina area (Map 7, Appendix H). This large syncline has resulted in the two deposits being preserved from the processes of denudation.

The folding associated with the second phase of deformation also has helped to preserve the skarn at Fletcher's Adit in particular, as this deposit lies in a major NW-SE trending syncline. The folding during this phase involved substantial quantities of brittle failure which played an important role in hydrothermal fluid access.

### 9.2.2 FAULTING AND JOINTING

The presence of major faults and areas of intense jointing are the most important control on mineralization. Stormont is associated with a large SE dipping normal fault and Fletcher's Adit with a small thrust and two small SE dipping reverse faults. The normal fault at Stormont appears to be responsible for the bulk of the fluid access, but at Fletcher's Adit the jointing can be so intense (Plate 6) that the small faults may only play minor roles. Intense jointing occurs in the hinge regions of the tighter second phase folds. Textures such as "wrigglite" and stockwork veining, as well as the extensive overprinting of these textures, indicates that metasomatic and mineralizing fluids are permeating from a number of different fractures. The faults and joints also play a very important role in fracturing the hornfelsic shales which are potential stratigraphic fluid traps.

In an attempt to define the zonation of skarn characteristics with respect to the major faults at Stormont and Fletcher's Adit, each drill-hole (from each deposit) has been rated in the intensity of jointing and faulting, retrograde alteration and leaching, maximum Au grade (ppm), silica alteration and abundance of two types of vein assemblages (Table 9). These intensity ratings have then been contoured in Figures 24 and 25.

For Fletcher's Adit, faulting and jointing intensity, as well as the abundance of calcite $\pm$ chlorite, actinolite and quartz veins (vein assemblage B), increased towards the two

outcropping faults near the adit. The intensity of silica alteration and the abundance of quartz ± muscovite, K-feldspar and pyrite veins (vein assemblage A) decreased from SW to NE. The maximum gold grade and the intensity of retrograde alteration increases from SW to NE. Thus, for Fletcher's Adit, the highest gold grades occur in regions where faulting and jointing intensity is high, retrograde alteration is abundant and silica alteration and carbonate veins are absent.

At Stormont, jointing and faulting, retrograde alteration, maximum gold grade, and quartz ± muscovite, K-feldspar and pyrite veining (vein assemblage A) increases in intensity from SE to NW. Calcite ± chlorite, actinolite and quartz veining (vein assemblage B) deceases in intensity from SE to NW. Thus, there are spatial associations of gold grade with fracturing at Stormont, as well as there being an association between high gold grades, intense retrograde alteration and an absence of carbonate veining. These characteristics are consistent with those observed at Fletcher's Adit.

| HOLE No | R.A. + LEACHING | SiO2 ALT | MAX Au (ppm) | VEIN A | VEIN B | JOINTS+FAULTS |
|---|---|---|---|---|---|---|
| FD 1 | 2 | 3 | 0.24 | 2 | 2 | 2 |
| FD 3 | 1 | 2 | 0.09 | 2 | 2 | 2 |
| FD 4 | 1 | 2 | 0.56 | 2 | 0 | 1 |
| FD 6 | 1 | 2 | 0.24 | 3 | 1 | 1 |
| FD 7 | 3 | 0 | 2.6 | 0 | 1 | 2 |
| FD 8 | 3 | 0 | 0.66 | 1 | 0 | 2 |
| FD 9 | 2 | 0 | 0.18 | 1 | 2 | 3 |
| | | | | | | |
| SD1 | 3 | 0 | 11.4 | 1 | 2 | 2 |
| SD 3 | 3 | 0 | 21.2 | 1 | 2 | 2 |
| SD 5 | 1 | 0 | 0.24 | 2 | 1 | 1 |
| SD 6 | 1 | 0 | 0.04 | 3 | 0 | 1 |

**TABLE 9:** Categorised down-hole characteristics for the Fletcher's Adit and Stormont areas. See Appendix G for drill-hole locations.

KEY: 0 = Absent 2 = Moderate
1 = Weak 3 = Intense or abundant

R.A. + LEACHING = Abundant actinolite and iron oxides.
VEIN A = Quartz ± muscovite, K-feldspar, pyrite.
VEIN B = Calcite ± chlorite, actinolite, quartz.

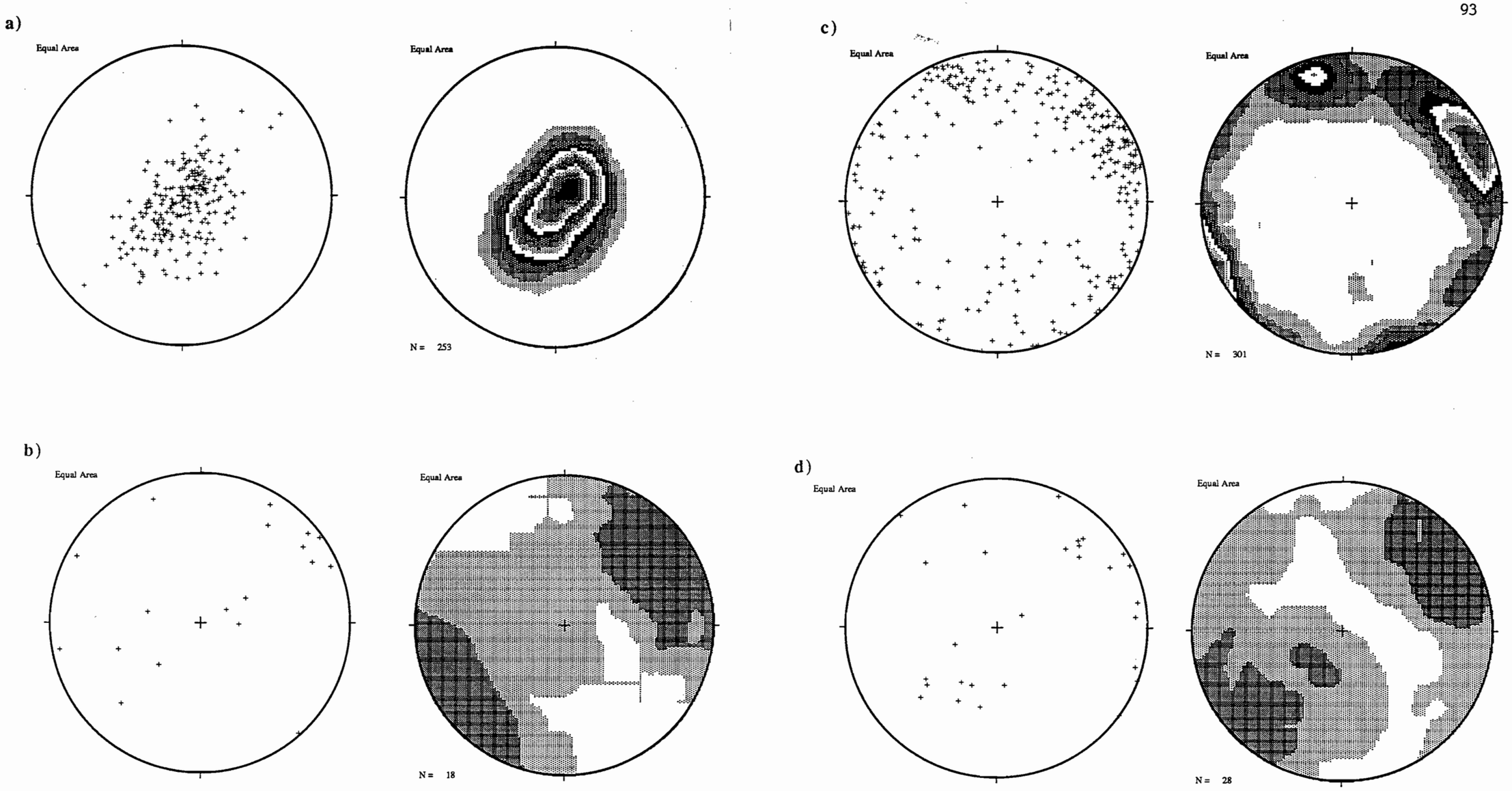


**FIGURE 21:** Poles to:

a) Bedding planes, from folded Ordovician lithologies.

b) Fault planes.

c) Joint surfaces.

d) Surfaces containing veins.

Contouring interval = $2\sigma$.

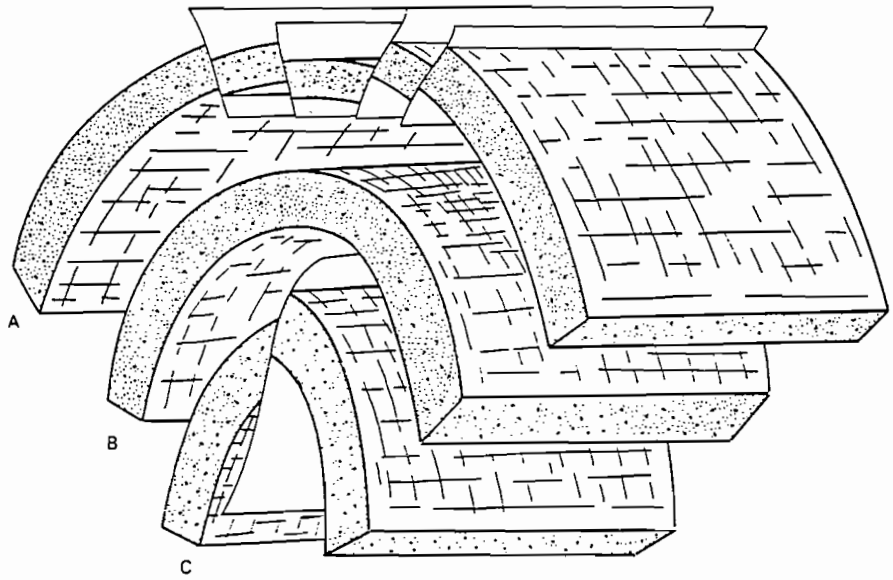


**FIGURE 22:** Block diagram showing the various regions within a concentrically folded sequence. Layer A has been folded so that there is normal faulting in the hinge. Layer B has been folded without faulting. Layer C in the core of the antiform has been folded and thrust-faulted.

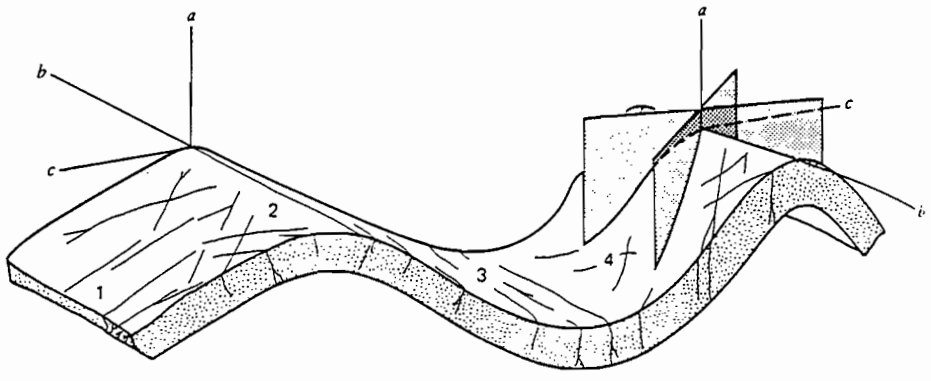


**FIGURE 23:** Joint sets commonly found in folded rocks: (1) *a-c* joints; (2) joints in paired sets symmetrically disposed about the *a-c* plane, intersecting in the pole to bedding; (3) radial joints; (4) joints in paired sets intersecting in *a* and inclined to *c*. From Hobbs et. al., 1976, p. 294.

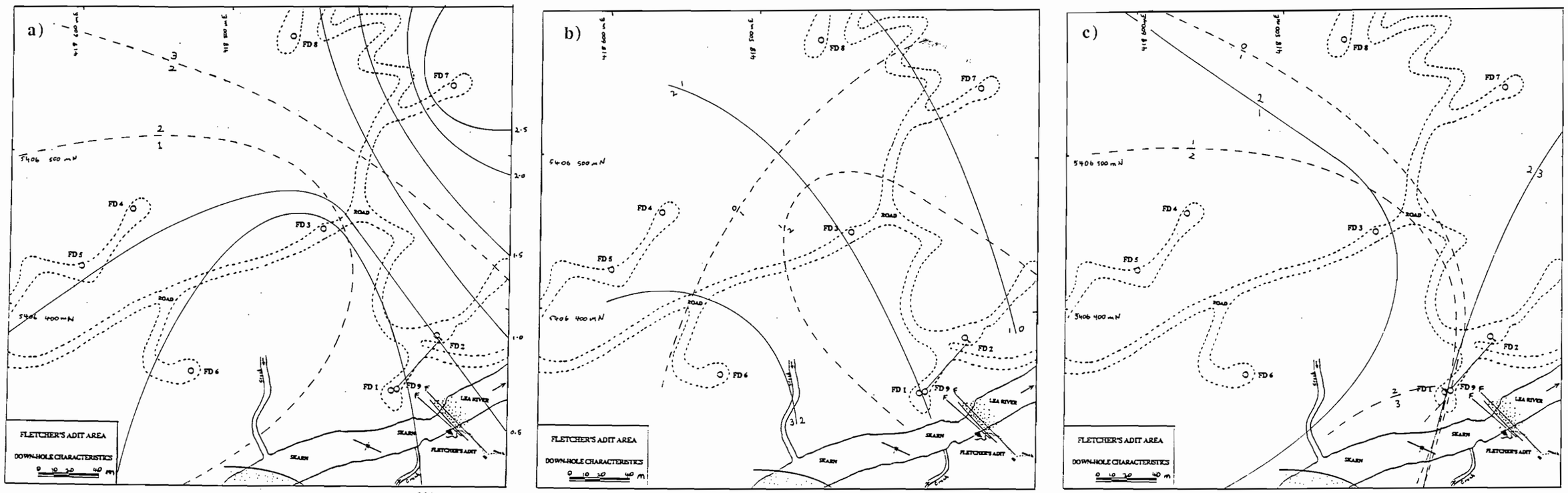


**FIGURE 24:** Spatial zonation of down-hole characteristics at Fletcher's Adit. Characteristics contoured here are ranked for each drill-hole in Table 9.

a) Retrograde alteration and leaching intensity (dotted contours) and maximum gold grade (continuous contours, in ppm).

b) Vein assemblage A (continuous contours) and B (dotted contours) abundance. See Table 9 for mineral assemblages.

c) Jointing and faulting intensity (continuous contours) and siliceous alteration intensity (dotted contours).

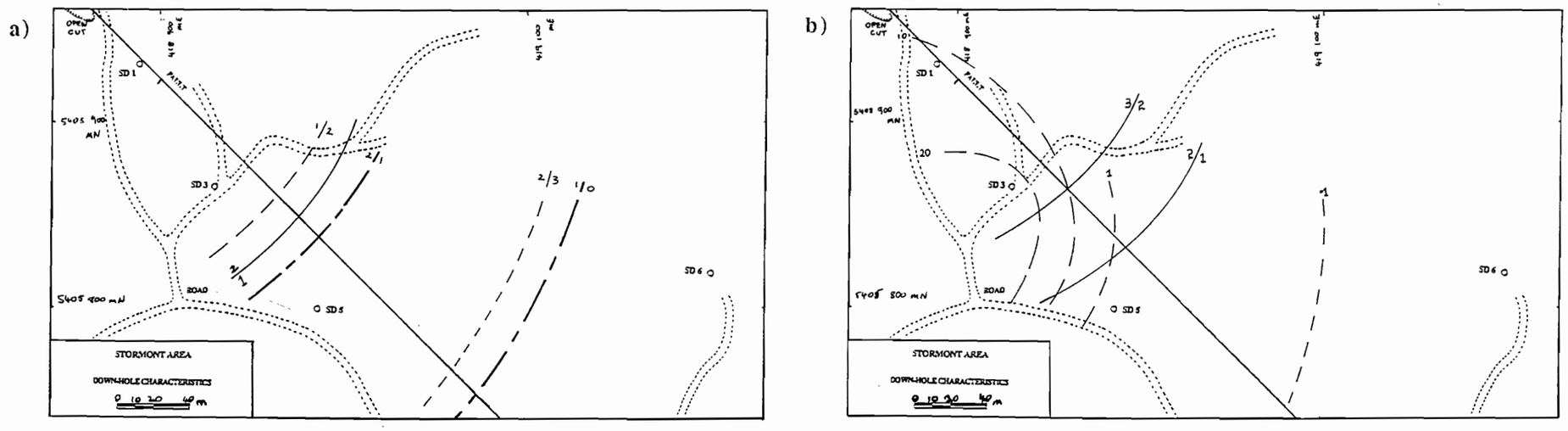


**FIGURE 25:** Spatial zonation of down-hole characteristics at Stormont. Characteristics contoured here are ranked for each drill-hole in Table 9.

a) Vein assemblage A (thin, dotted contours) and B (heavy, dotted contours) abundance, with jointing and faulting intensity (continuous contours). See Table 9 for mineral assemblages.

b) Retrograde alteration and leaching intensity (continuous contours) and maximum gold grade (dotted contours, in ppm).

# CHAPTER 10
# OXYGEN ISOTOPES

## 10.1 INTRODUCTION

The aim of the isotope study is to determine if the oxygen and hydrogen isotopes for the metasomatising/mineralizing fluids from skarn deposits in the Moina area display any trend consistent with the increasing granite-to-prospect distance to the west and, to determine the source and character of these fluids. It is proposed that the more distal skarn at Stormont may show a greater meteoric water component in its mineralizing fluids. A larger meteoric water component at Stormont may support the theory that, at Stormont, a convecting meteoric water cell was established which leached gold out of the underlying Cambrian volcanics, and deposited the gold late in the mineral paragenesis. Fletcher's Adit and Ti Tree Creek lack the late stage of intense retrograde alteration and high grade Au mineralization, and it is proposed that these two deposits would have fluids that were isotopically distinct from Stormont's, being dominantly magmatic.

Several problems hindered the testing of these hypothesese. Firstly, a mineral pair was needed that could be analysed for $\delta D$ and $\delta^{18}O$, and these phases had to be in quantities that enabled uncontaminated samples to be drilled out from hand specimens for each deposits. Magnetite and actinolite were the only phases that met this criterion, but these phases are stable over a large portion of the paragenesis (Tables 1, 2 and 3). To overcome this problem only areas of massive magnetite were sampled as this magnetite actinolite corresponds to the late actinolite replacement /early mineralization stage.

The second problem involves the calculation of the isotopic values of the mineralizing/metasomatising fluid in equilibrium with the mineral analysed. To do this the temperature of formation must be attained, using either fluid inclusion evidence (not applicable here) or an oxygen isotope mineral pair. For the samples analysed, the only suitable minerals were actinolite, magnetite and fluorite. Therefore the only oxygen isotope pair that could be used was actinolite-magnetite. Unfortunately there are no thermodynamic data available involving the oxygen isotope fractionation between actinolite and any other phase. Thus, estimates for the temperature had to be made. From the phase diagrams shown in Figures 13

and 18, the most likely temperature for the formation of this magnetite and actinolite is 350-400°C.

## 10.2 RESULTS

The $\delta^{18}O$ for the hydrothermal waters in equilibrium (at 350°C) with magnetite from Stormont, Fletcher's Adit, Ti Tree Creek and Shepherd and Murphy have been calculated and given in Table 10. The formula used, and its derivation is given in Appendix F. The results from Table 10 have been plotted in Figure 26.

## 10.3 CONCLUSIONS

The $\delta^{18}O$ of the hydrothermal waters in equilibrium with the sampled magnetite (at 350°C) are clustered around the metamorphic and primary magmatic water values, for all four deposits (Figure 26). The domination of metamorphic fluids indicates that these magnetites are positioned very early in the mineral paragenesis (Einaudi et. al., 1981). Thus, these samples are paragenetically much earlier than the late, high grade Au-Bi mineralization stage, and no conclusions can be drawn reguarding the influx of late meteoric waters at a late paragenetic stage!

The dominance of metamorphic water in isotopic equilibrium with many of the magnetite samples is an interesting result, especially in the case of the Shepherd and Murphy deposit, were wrigglitic magnetite (which comprises the majority of magnetite from this deposit) is thought to form from saline, boiling, fluorine-saturated fluids (Kwak and Askins, 1981a and b). Skarn-forming fluids are known to change in character from metamorphic to magmatic to meteoric with time (Einaudi et. al., 1981), so the results shown in Figure 26 most likely represent magnetites that were formed early in the paragenesis and in equilibrium with firstly metamorphic fluids, then metamorphic+magmatic fluids and then just magmatic fluids.

| SAMPLE | RUN | RESIDUAL | % YIELD | Sa. Vs Std. | Del O18 MAG | DEL O18 H2O at 350°C |
|---|---|---|---|---|---|---|
| STORMONT | | | | | | |
| 104 | 458 | 0.039 | 121.3 | -19.676 | 2.49 | 9.2 |
| 52 | 487 | 0.034 | 114.3* | -20.415 | 1.73 | 8.44* |
| 94 | 489 | 0.042 | 146 | -14.051 | 8.25 | 14.96 |
| | | | | | | |
| FLETCHER'S ... | | | | | | |
| 6 | 449 | 0.039 | 120 | -15.915 | 6.34 | 13.06 |
| 25 | 450 | 0.04 | 116.4 | -17.189 | 5.04 | 11.75 |
| 35 | 451 | 0.039 | 123.3 | -17.667 | 4.55 | 11.26 |
| 293 | 460 | 0.048 | 110 | -16.815 | 5.42 | 12.13 |
| | | | | | | |
| TI TREE CREEK | | | | | | |
| 307 | 461 | 0.043 | 117.4 | -18.921 | 3.26 | 9.97 |
| 312 | 462 | 0.042 | 121 | -18.054 | 4.15 | 10.86 |
| 311 | 496 | 0.064 | 129.4* | -21.623 | 0.49 | 7.20* |
| | | | | | | |
| SHEPHERD ... | | | | | | |
| 43 | 486 | 0.043 | 111.5 | -18.387 | 3.81 | 10.52 |
| 297 | 494 | 0.04 | 101.5* | -15.755 | 6.5 | 13.21* |
| 41 | 457 | 0.04 | 120.9 | -18.471 | 3.72 | 10.43 |
| 40 | 456 | 0.038 | 105.6 | -15.219 | 7.05 | 13.76 |

**TABLE 10:** Oxygen isotope results for magnetite samples taken from the Stormont, Fletcher's Adit, Ti Tree Creek and Shepherd and Murphy skarns. An asterisk denotes a suspect sample due to low or high % yields. The formula used to calculate the $\delta^{18}O$ $H_2O$ at 350°C is shown in Appendix F.

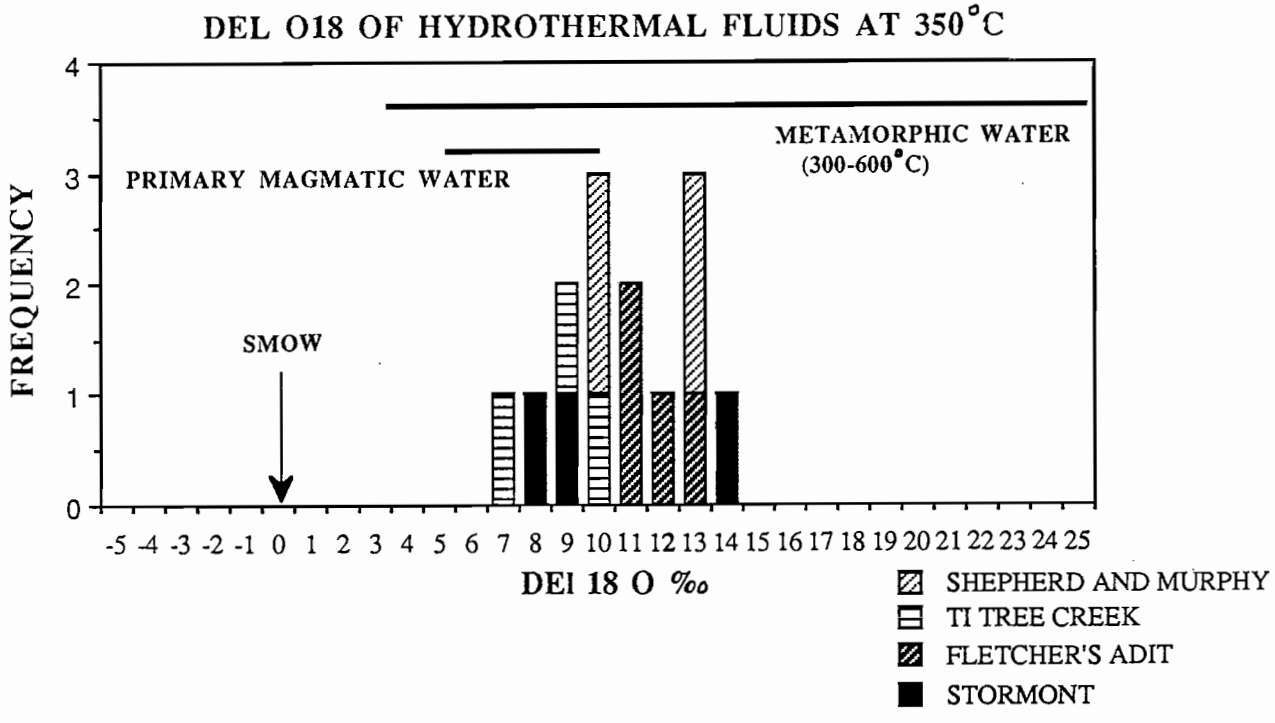


**FIGURE 26:** $\delta^{18}O$ of hydrothermal fluids in equilibrium with magnetites (at 350°C), from skarns in the Moina district. $\delta^{18}O$ values for metamorphic and primary magmatic water from Barnes, 1979.

# CHAPTER 11

# IS STORMONT A GOLD SKARN?

## 11.1 WHAT IS A GOLD SKARN?

Classification of skarns has been fraught with difficulty due to their extreme variability in metal content, texture, location, grade, mineralogy, as well as episodes and styles of mineralization (Meinert, 1983). Classification criteria have been based on geochemistry, tectonic setting and especially metal content, with variations within sub-classes being attributed to differences in magma type, environment of emplacement and host rock composition (Einaudi et. al., 1981). Before the late 1980's skarn deposits were divided into six categories based on metal content: iron, tungsten, copper, lead-zinc, molybdenum and tin, but it became evident that these classes could not be used to describe high grade auriferous skarns (Meinert, 1989).

The total quantity of gold obtained from skarn deposits is in the order of $10^6$ kg, and comes from five major skarn classes: gold, iron, copper, porphyry copper and lead-zinc (Meinert, 1987; 1989). Relatively recent discoveries of high grade skarns that are economic to mine for their gold content, has led to significant research in the field of gold skarns (Meinert, 1989). A summary of his findings on gold skarns is findings on this type of skarn is given below.

Gold skarns can be mined for their gold content alone and only contain minor amounts of Cu, Pb and Zn (Table 11). Gold grades are generally in the range of 5-15 ppm (Table 11) and Au (ppm)/Cu (%) ratios are in the order of 5 to 200, in comparison with other major skarn classes which are less than 5 (Figure 27). They contain anomalous amounts of arsenic, bismuth and/or tellurium, in comparison to other skarn classes.

Host rocks for gold skarns generally contain a significant clastic or volcaniclastic component. The mineralizing plutons are generally relatively mafic equigranular diorites and granodiorites, although they range from diorite (such as Hedley, B.C.) to rhyolite porphyry (such as Red Dome, Qld.).

Pyroxenes range from diopside to hedenbergite and are aluminous. Higher grade deposits tend to have pyroxenes with a hedenbergite mole percentage that is greater than 50%

and are often pure hedenbergites (Figure 8) and pyroxene usually is more abundant than garnet. Amphiboles are usually actinolites, but contain some aluminium. Garnets tend to belong to the grandite series (grossular-andradite), and are more aluminous than other classes (Figure 7). Ferrous/ferric ratios in the pyroxenes and garnets are high, which indicates reducing conditions in the skarn-forming fluids, or in the wall rocks.

Common metasomatic phases include scapolite, vesuvianite, K-feldspar, biotite, prehnite, apatite, sphene, ferrobustamite, albite, and cuspidine. The dominant sulphide minerals are usually arsenopyrite, marcasite and pyrrhotite. Bismuth minerals are abundant and include native bismuth, bismuthinite, maldonite, wittichinite, joseite and hedleyite. Tellurium mineralogies have been reported.

Garnet is more common in areas that are proximal to the igneous contact, while pyroxene abundance (and hedenbergite mole percent) increases in the more distal regions. An increase in the mole percentage of johannsenite ($CaMnSi_2O_6$) in pyroxene composition can occur in the distal portions of the skarn (Myers and Meinert, 1988). Gold, arsenic, bismuth and tellurium grades are generally higher in distal areas, while copper is concentrated in the areas closest to the mineralizing pluton. A "genetic continuum" may exist between gold skarns and gold-rich copper skarns (such as the Whitehorse Copper District, B.C.).

Mineralizing fluids are reduced, indicated by the mineralizing plutons having low $Fe_2O_3/FeO$ ratios, the calc-silicate's iron content being dominantly ferrous and the common occurrence of arsenopyrite, loellingite and native bismuth.

There is an intimate association between gold and bismuth in hand specimens, thin sections and assay data. Gold is transported dominantly as a bisulphide complex, at temperatures less than 300°C, unlike copper and other base metals. Thus the following metal correlations are typical:

1) Au/Bi = strong and positive .
2) Cu/Ag = strong and positive .
3) Au/Cu and Au/Ag = strong and negative.

[Meinert 1987, 1988a and 1989]

| SKARN TYPE | % OF TOTAL GOLD | SIZE (mt) | Au (g/t) | Ag (g/t) | Cu (%) | Au/Cu | Au (kg) | Ag (kg) | Cu (tons) |
|---|---|---|---|---|---|---|---|---|---|
| GOLD | 34.9 | 90.94 | 4.5 | 6.1 | 0.3 | 16.6 | 382678 | 502462 | 236412 |
| IRON | 3.1 | 29.84 | 1.1 | 5.7 | 0.5 | 2.3 | 33646 | 168996 | 147460 |
| COPPER | 9.1 | 74.05 | 1.4 | 15.2 | 1.4 | 1.0 | 100083 | 850763 | 1031631 |
| PORPHYRY Cu | 51.9 | 2138.60 | 0.3 | 7.2 | 1.0 | 0.3 | 568230 | 12589800 | 22287000 |
| Pb-Zn | 1.0 | 30.53 | 0.4 | 176.9 | 0.4 | 0.9 | 10857 | 4692850 | 102980 |
| WEIGHTED AV-TOTAL | | 2363.97 | 0.5 | 9.6 | 1.0 | 0.5 | 1095464 | 18804870 | 23805483 |

**TABLE 11:** The statistics involving gold in five major classes of skarn deposits (modified from Meinert, 1989, p. 540).

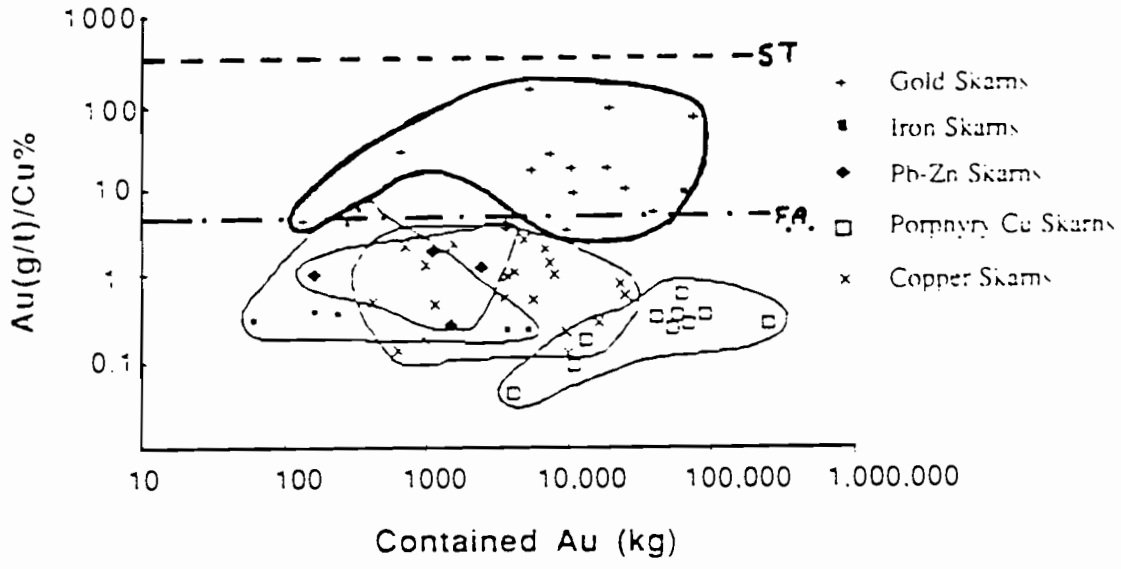


**FIGURE 27:** Au(g/t)/Cu(%) vs contained gold from six major skarn classes. Au(g/t)/Cu(%) values for Stormont and Fletcher's Adit have been superimposed on the original graph from Meinert, 1989, p. 544.

## 11.2 ARGUMENTS FOR STORMONT BEING A GOLD SKARN

### 11.2.1 HOST SEQUENCE

Gold skarns are often hosted in clastic or volcaniclastic-rich strata, which is the case for skarns in the Moina area. The skarn is hosted in the base of the Gordon Limestone (which has a moderate to high clastic content) and the very upper part of the Moina Sandstone (generally being ≈180 m of marine clastics). Additionally, the Gordon Limestone in the Moina area can be seen to contain cherty bands of clastic material (Plate 8). However, the above features are not unique to the Stormont prospect and therefore cannot alone account for the high gold grades.

The reason for the clastic or volcaniclastic host rock association with gold skarns is presently an enigma. Meinert (1989) has suggested the following explanations as possibilities:

1) A protolith gold contribution (at Stormont Au may be leached from the footwall clastics or Cambrian volcanics).
2) A compositional control on metasomatic reactions, and the precipitation of gold.
3) A permeability control on mineralization.
4) A continental scale tectonic control on sedimentation, volcanic activity, igneous petrogenesis and therefore skarn mineralization.

Points 3 and 4 above are not unique to Stormont as these features also occur in the Moina area, but the presence of sub-surface Cambrian volcanics underlying the Moina Sandstone and the Roland Conglomerate is a variable that could possibly be unique to (or more of an influence to) the Stormont prospect.

### 11.2.2 METALS

Stormont's metal abundances are summarised in Table 4. Gold averages 1.08 ppm and bismuth 0.103%, while copper, lead, zinc, silver, tin, tungsten and molybdenum are in very low abundances.

Stormont's Au (ppm)/Cu (%) ratio is ≈284 (averaged from all skarn assays), which is even greater than in the gold skarn field (Figure 27). In comparison, the Au (ppm)/Cu (%) ratio at Fletcher's Adit averages ≈5.37, which is just under that of the gold skarn field (Figure 27).

Stormont's statistical correlation matrix is shown in Table 7. There is a very strong positive Au/Bi correlation, a negative Au/Cu correlation , and a good Au/Pb correlation.

Gold grades reach values up to 21.2 ppm at SD 3, and at SD 1 bismuth reaches 1.15%, which are typical values of moderate grade gold skarns.

### 11.2.3 OPAQUE MINERALOGY

Stormont's opaque mineralogies dominantly consist of magnetite, pyrrhotite, native bismuth, native gold (which has an average fineness of 823) and bismuthinite, with only traces of base metal sulphides. This is consistent with gold skarns in general. Although only native bismuth and bismuthinite were found at Stormont, it is extremely likely that similar Bi-Te-Pb-S mineralogies to those found in Fletcher's Adit and Ti Tree Creek exist at Stormont. Justification for this statement comes from the strong Bi/Pb, Au/Pb and Au/Bi metal correlations (similar to those at Fletcher's Adit) and the complete absence of galena. To effectively assess Stormont's bismuth mineralogies many more samples would have to be analysed, as it is common for gold skarns to have six or seven Bi-Te-Au-Pb-Cu-S phases (Ewers and Sun, 1989).

Pyrrhotite is the dominant iron sulphide at Stormont which is typical of gold skarn mineralization involving reduced fluids. The extremely low quantities of sphalerite, galena and to a lesser extent chalcopyrite is also typical.

### 11.2.4 SILICATE MINERALOGY

The high intensity and extent of retrograde alteration at Stormont is typical of gold skarns. The increased permeability resulting from such pervasive alteration is important to allow the easy penetration of late auriferous fluids (Einaudi et. al., 1981), and implies that this class of deposit is characterised by high water-to-rock ratios in the middle to late paragenetic stages.

Garnet-to-pyroxene ratios are difficult to assess at Stormont, due to the near total retrograde alteration of clinopyroxene to actinolite. If one considers areas that are now actinolite $\pm$ quartz, calcite and magnetite representing areas that were once mostly pyroxene, garnet/pyroxene ratios would have been in the order of 60:40 to 30:70, which is consistent

with typical gold skarns. This is in contrast to Fletcher's Adit where garnet/pyroxene ratios are in the order of 90:10 to 60:40 and are not consistent with gold skarns (Meinert, 1988b).

Vesuvianite, sphene, K-feldspar, rutile and biotite are metasomatic phases that are common to both Stormont and typical gold skarns. Sphene and rutile were not identified at Fletcher's Adit or Ti Tree Creek.

Garnet compositions from all three deposits have been plotted on a pyralspite-grossular-andradite ternary diagram (Figure 7). Six garnets from Stormont (Appendix A) plot well within the gold skarn field defined by Meinert (1989). However they also plot in the Cu and Zn skarn field, but these metals are in such low abundances that there is no justification for attempting to classifying Stormont as a copper or zinc skarn. Four of the six garnets from Stormont represent a traverse across a zoned grandite. Such zonation does not affect the ternary diagram's classification scheme as the core-rim trend parallels the gold skarn field's direction of elongation.

In comparison with Stormont, the garnets from Fletcher's Adit are more iron-rich, and plot outside the gold skarn field (Figure 7). Those at Ti Tree Creek show a broader range in composition (from almost pure andradite to compositions closely approximating the garnets from Stormont), but importantly, plot consistently within the Cu skarn field, while only occasionally within the gold skarn field.

Clinopyroxene compositions for the three skarns are shown in Figure 8, on a johannsenite-diopside-hedenbergite ternary diagram. Out of five analyses from Stormont, three plot within the gold skarn field, one is borderline and one is totally uncharacteristic (being extremely Mn-rich). The weight percentages of $Al_2O_3$ in clinopyroxenes from the three deposits have been plotted against their hedenbergite mole percentages in Figure 28. Clinopyroxenes from all three deposits plot within the broad gold skarn field, but this area is not exclusive to gold skarns.

There are a lack of accumulated data on amphibole compositions in gold skarns, however the three deposits plotted in Figures 9 and 10 show no resemblance to amphiboles from the Whitehorse copper belt (a gold-rich copper skarn district).

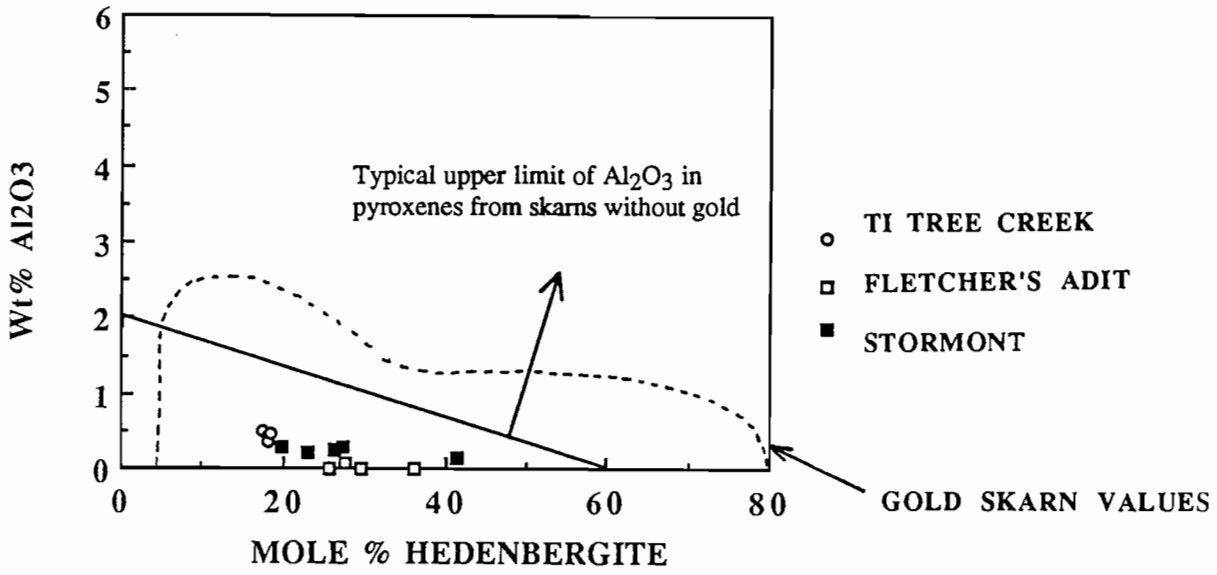


**FIGURE 28:** Iron and aluminium content from pyroxenes from Stormont, Fletcher's Adit, Ti Tree Creek, and gold skarns in general. Gold skarn field from Meinert, 1989, p. 545.

## 11.3 ARGUMENTS AGAINST STORMONT BEING A GOLD SKARN

### 11.3.1 MINERALIZING PLUTON

The Dolcoath Granite is a typical tin/tungsten-bearing ilmenite series granitoid (based on Ishihara's [1981] classification scheme for granitoids). The Dolcoath Granite's only similarity with granitoids associated with gold skarns world-wide is that it is equigranular. Meinert (1988b) concluded that the Dolcoath Granite is too reduced, its water content too low and it lacks a large vertically zoned magma chamber, which are requirements needed to form large, high grade gold skarns.

Figure 29 contains plots of $Na_2O$-$K_2O$, $Na_2O+K_2O$-$SiO_2$ and $Fe_2O_3+FeO$-$SiO_2$ for compositional data from the Dolcoath Granite, a granitoid associated with a Sumatran gold skarn (the Maura Sipongi deposit) and a granitoid associated with copper skarns which exhibit anomalously high gold grades (Whitehorse district, Yukon).

The rationale for including data from the Whitehorse district is that there may be a genetic continuum between gold skarns and auriferous copper skarns (Meinert, 1989). Additionally, the Whitehorse copper belt has been studied in detail (unlike most gold skarns), giving confidence in the quoted average granitoid composition for this district.

By comparison with fields defined by Meinert (1983) for the six major skarn types the composition of the Dolcoath Granite consistently falls within the tin skarn field (Figure 29). However for the $\Sigma Fe$-$SiO_2$ plot, there is some overlap between the Dolcoath Granite's field and the molybdenum skarn field (Figure 29).

In comparison with gold skarns and auriferous copper skarns in Figure 29, the Dolcoath Granite shows:

1) enrichment in silica, having on average ≈15 wt% more $SiO_2$ than the Sumatran gold skarn, and ≈20 wt% more $SiO_2$ than the Whitehorse granitoids.
2) a broad spread of $K_2O$ and $Na_2O$ values, with $Na_2O$ being lower and $K_2O$ being on average marginally higher than the two reference granitoids.
3) depletion is $\Sigma Fe$, having on average ≈2-3 wt% less $\Sigma Fe$ than the two reference granitoids.

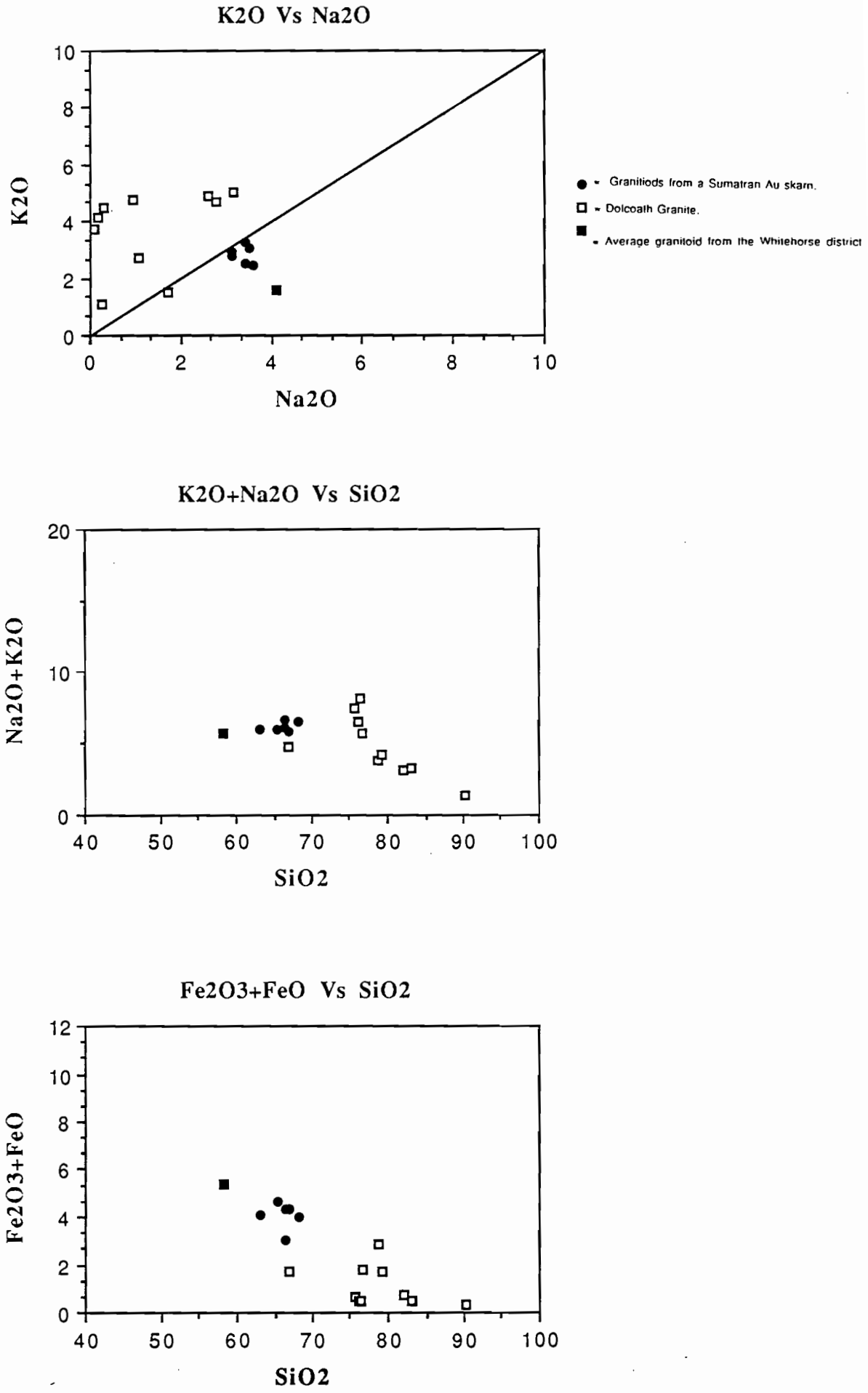


**FIGURE 29:** Major element trends for granitoids associated with the Moina skarns (Dolcoath Granite), a Sumatran gold skarn (at Muara Sipongi), and Au-rich copper skarns from the Whitehorse district, Southern Yukon. Data from Webb, 1974; Beddoe-Stephens et. al., 1987; Meinert, 1986.

It is noticeable from the three plots shown in Figure 29 that the granitoid compositions from the Sumatran gold skarn lie between the Dolcoath Granite's and the Whitehorse granitoid's major element compositions. This observation may be significant in understanding the igneous petrogenetic control on metalliferous skarn formation, and whether a genetic continuum exists between gold-bearing skarns and the other major skarn classes.

In summary, the Dolcoath Granite is a granitoid typically associated with Sn skarns, and its major composition does not mirror that of gold skarns or auriferous copper skarns. Thus, from the igneous petrology perspective, the skarn at Stormont should not be gold-bearing. Stormont's footwall lithologies must help to modify skarn-forming fluids, so that the fluids approach (but do not fully reach) those that mineralize and metasomatise gold skarns. The Dolcoath Granite's chemistry remains as the most crucial factor in explaining why Stormont's gold grades are low.

### 11.3.2 METALS

Arsenic is not abundant at Stormont, averaging only 14.2 ppm for all skarn assays. Gold grades are on average low in comparison to typical gold skarns, as all skarn assays (including zero values) average only 1.08 ppm. Accurate comparisons of gold grades are difficult however, due to quoted resource gold grades only including assays from a specific area defined by "cut-off grades".

The correlation coefficient for Au and Cu is -0.005 (Table 7). The Au/Ag correlation coefficient at Stormont of 0.362 is a statistically significant correlation, which is contrary to gold skarn characteristics.

### 11.3.3 OPAQUE MINERALOGY

Although pyrrhotite is present, it is not abundant. Additionally no marcasite, arsenopyrite or loellingite have been identified at Stormont. Although Stormont has the lowest quantity of magnetite of the three skarns, magnetite is locally abundant (usually spatially separated from the zones containing Bi, Au and Pb) which is rare in gold skarns formed from reduced fluids.

### 11.3.4 SILICATE MINERALOGY

One of the five salitic clinopyroxenes analysed from Stormont plots well outside the gold skarn field in Figure 8, being extremely enriched in Mn (≈8.93 mole % johannsenite). In comparison with samples from Stormont, pyroxenes from Ti Creek Creek are very consistent in composition plotting in the centre of the copper skarn field, while those from Fletcher's Adit are Mn-enriched, but just plot within the gold skarn field.

Meinert (1989) uses the graph shown in Figure 28 as another exploration tool for quickly identifying potential high grade gold skarns. Although Stormont has clinopyroxene compositions that plot within the broad gold skarn field, none plot within the high aluminium portion (an area exclusive to clinopyroxene compositions from gold skarns). This diagram also shows a trend of decreasing mol% hedenbergite and increasing wt% $Al_2O_3$ from Fletcher's Adit to Stormont to Ti Tree Creek, which probably reflects differences in the protolith's dolomite and clastic content.

Figure 10 indicates there is very little difference in $Al_2O_3$ wt% between amphiboles from Stormont and those from the Whitehorse district, which is known to have less $Al_2O_3$ than typical gold skarns.

Cuspidine ($Ca_4Si_2O_7F$) is not present at Stormont, with fluorine being mostly contained in the mineral fluorite which is not usually associated with gold skarns. Other particularly important mineralogies in typical gold skarns that do not occur in abundance (or at all) at Stormont include prehnite, scapolite and apatite.

## 11.4 CONCLUSIONS

From the data given above for and against Stormont's status as a gold skarn, the question arises: Why does Stormont have gold skarn characteristics, given the petrological nature of the Dolcoath Granite? It seems that Stormont represents a skarn that has been metasomatised and mineralized by fluids that have been strongly modified by their movements through the footwall lithologies, and also may have had pre-existing metamorphic and metasomatically derived phases influencing later reactions in the forming skarn. This modification of granitic fluids can be most effectively achieved when the skarn is at a greater

distance from the underlying granitic source, which explains the tendency for gold grades and the Mn content of clinopyroxenes to increase towards the west.

The formation of Stormont represents the partial evolution of tin skarn-forming fluids to potential gold skarn-forming fluids. The characteristics which argue against a gold skarn status for Stormont can be attributed primarily to the metasomatising/mineralizing Dolcoath Granite simply having the wrong chemistry. In addition, but to a lesser extent, the composition of the host and footwall lithologies may have hindered the development of a high grade deposit, in that they were not sufficiently auriferous.

Despite Stormont being associated with a granite of the wrong series (ilmenite instead of magnetite) and composition, the most fundamental gold skarn characteristics are fulfilled. The host rocks, metal correlations, metal abundances and Au(ppm)/Cu(%) ratios at Stormont are typical of high grade North American gold skarns. The garnet/pyroxene ratios, the opaque mineralogies, the style of mineralization, the degree of retrograde alteration and minor silicate mineralogies are definitely comparable to the North American examples.

Analysis of garnet and pyroxene compositions is quickly becoming the most definitive classification and exploration technique in skarn research. The garnet compositions at Stormont strongly support its classification as a gold skarn. The clinopyroxene compositions indicate that Stormont is a gold skarn, but is unlike the high grade gold skarns in that the $Al_2O_3$ content of the clinopyroxenes is low and the clinopyroxenes occasionally contain anomalous amounts of Mn .

The amphibole compositions at Stormont are unlike amphiboles from gold-rich copper skarns, but are lower in $Al_2O_3$ than the high grade gold skarns.

Thus, the compositions of the dominant calc-silicates also indicate that Stormont is a "gold skarn" albeit a lower grade and more distal deposit than the North American examples.

# CHAPTER 12
# DISCUSSION AND CONCLUSIONS

The Stormont Au-Bi skarn can be classified as a gold skarn based on the garnet and clinopyroxene composition classification scheme, host rock composition, metal associations, the degree of retrograde alteration, associated mineralogies and metal ratios from this deposit in comparison with those from major gold skarns defined by Meinert (1987; 1989). The unusual feature of this skarn is that it is associated with an ilmenite series granitoid (the Dolcoath Granite), which chemically is a typical Sn-W skarn-forming granite. High grade gold skarns throughout the world are generally mineralized by magnetite series granitoids (Meinert, 1988b).

Typically, gold skarns are associated with oxidised plutons, but are generally distal to the granitoid and are mineralized by fluids that have become relatively reducing (i.e. pyrrhotite and arsenopyrite are common). The fluids responsible for mineralizing these deposits are initially oxidised and are therefore capable of transporting large quantities of gold as a chloride complex. Additionally, the oxidised granitoids are the source for the majority of the gold. As the fluids move to more distal areas in the contact aureole, they drop in temperature and $fO_2$ and deposit reduced iron sulphides and then gold.

At Moina however, the ilmenite series Dolcoath Granite produces fluids that are more reducing and less efficient at transporting gold. Additionally, the granite is a typical Sn-W skarn-forming granitoid and therefore contributes very little gold. At the distal position of Stormont, the late mineralizing fluids are very similar in chemistry to those of typical gold skarn fluids, but have not been as oxidised initially (and therefore have not transported much gold), and the granitoid has not contributed much gold. It is likely that at Stormont the majority of the gold has originated from the Cambrian volcanics in the footwall, and not from the granite. This fundamental difference between Stormont and typical gold skarns helps to explain why gold grades are very patchy at Stormont, instead of being uniformly high such as the classic gold skarns of the world.

Despite the fundamentally limiting factor on gold mineralization at Stormont mentioned above, the late stage fluids that mineralized this deposit were chemically similar to those from

typical gold skarns. Given that the mineralizing fluids emanating from the Dolcoath Granite initially had a non-ideal chemistry, potential gold skarn-forming fluids were modified by passing through the thick footwall sequence of rudites (with abundant disseminated hematite), arenites and argillites, as well as underlying volcanics. Modification of Sn-W skarn-forming fluids into Au skarn-forming fluids is best achieved when the granite-to-prospect distance is at a maximum. Thus Stormont, being the most westerly and more distal deposit (0.5-1 km), bears the greatest similarity to the classic North American gold skarns.

Given that the Cambrian volcanics are the most likely source of gold in the Moina district, the extraction of moderately large amounts of gold would have been best achieved by the establishment of a convecting cell of meteoric and magmatic fluids. The gold-leaching fluids are hypothesized to have been dominantly meteoric in character, as the gold is paragenetically very late and skarn-forming fluids are known to change from dominantly metamorphic to magmatic to meteoric with time (Einaudi et. al., 1981). The channelling of mineralizing fluids up a discrete conduits would not have resulted in significant leaching of gold from the surrounding volcanics.

During the mineralization stage at Stormont, the paragenesis indicates that the hydrothermal fluids were dropping in temperature, $fO_2$ and pH, while rising in $fS_2$. The drop in $fO_2$ with time may indicate that the footwall sedimentary sequence was no longer acting as an oxidising agent to the granitic fluids, or that the Cambrian volcanics were starting to act as a reducing agent as a late stage meteoric (+ magmatic) water convection cell was initiated. This drop in $fO_2$ and temperature coincides well with thermodynamic modelling involving iron sulphides, oxides, native bismuth and bismuthinite.

The rate of decline of $fO_2$ with temperature decreases with time, which may be a result of the gradual establishment of a convecting meteoric (+ magmatic) water cell. Deposition of Au on the "gold solubility cliff" from a $Au(HS)_2^-$ species is strongly supported by the observed paragenesis and thermodynamic modelling using reasonable values for pH, T, $fO_2$, $\Sigma S$ and $a^{CL-}$.

The metal-metal plots for skarn lithologies at Stormont reveal that there exists a population of metal grades that are very high in Au and Bi while low in Cu, W and Sn, that is

unique to Stormont. This population is distinct from a low grade Au and Bi population which is common to both Fletcher's Adit and Stormont. The high grade, late stage Au and Bi population may be the result of the establishment of a convecting water cell, during the late retrograde alteration phase at Stormont.

The intensity of retrograde fluid activity at Stormont was very high (in comparison to other skarns in the Moina area), as indicated by the pervasive alteration of salitic clinopyroxene to actinolitic amphibole. The paragenesis also continues to lower temperatures at Stormont. Thus, during the middle and late stages of skarn development at Stormont, water/rock ratios were very high, retrograde alteration of the early calc-silicates was intense, and leaching of gold from Cambrian volcanics in the footwall was taking place. The greater granite-to-prospect distance, the increased fracture/fault controlled permeability, and abundance of late retrograde fluids at Stormont all contributed to the development of a late stage convection cell that was large, active, and effective at leaching gold from the underlying volcanics.

Textural and mineralogical differences between the three skarns involved in this study can be attributed mainly to the differing granite-to-prospect distances, amounts of dolomite, Al, and Si in the protoliths, intensity of retrograde alteration, degree of fracture controlled permeability, and possibly the sub-surface presence and thickness of the Cambrian volcanics.